2009-01-01

Analysis Of Shallow Seismicity And Stress Fields In Southeastern Alaska

Hugo Rodriguez
University of Texas at El Paso, hugor@miners.utep.edu

ANALYSIS OF SHALLOW SEISMICITY AND STRESS FIELDS

IN SOUTHEASTERN ALASKA

HUGO RODRIGUEZ, B.S.

Department of Geological Sciences

APPROVED:

_____
Diane I. Doser, Ph.D.

_____
Aaron A. Velasco, Ph.D.

_____
Leticia Velazquez, Ph.D.

_____
Patricia D. Witherspoon, Ph.D.
Dean of the Graduate School

ANALYSIS OF SHALLOW SEISMICITY AND STRESS FIELDS IN SOUTHEASTERN ALASKA

by

HUGO RODRIGUEZ, B.S.

THESIS

Presented to the Faculty of the Graduate School of

The University of Texas at El Paso

in Partial Fulfillment

of the Requirements

for the Degree of

MASTER OF SCIENCE

Department of Geological Sciences

THE UNIVERSITY OF TEXAS AT EL PASO

December 2009

ACKNOWLEDGEMENTS

First and foremost, I have to thank my advisor Dr. Diane I. Doser. Her knowledge and wisdom was the key to my success as a student and now as a professional geophysicist. Her patience is simply humbling. I also must give great thanks to Dr. Aaron A. Velasco who consistently nudged me in the right direction whenever I was having trouble advancing with my research. And to Dr. Leticia Velazquez who was able to accommodate my difficult schedule.

I must also mention Dr. Randy Keller, who along with Tina Carrick accepted the challenge of bringing me into the field of Geophysics. A profound thank you to the UTEP Department of Geosciences staff, who at times had to turn on a dime to meet my needs.

And last, but certainly not least, to my family and friends. In the end, it was to them that I turned to for support and they were rock solid… no pun intended.

This manuscript is submitted to the Supervising Committee on November 23, 2009.

ABSTRACT

Southeastern Alaska is dominated by strike-slip motion along the Queen Charlotte-southern Fairweather fault system (QCFS) in the south and transitions to oblique convergent motion partitioned between strike-slip motion along the Denali and northern Fairweather fault systems and thrusting along faults of the St. Elias region. Geologic complications are further increased by the subduction of the Yakutat microplate beneath North America and glacial processes. By studying regional background seismicity we intend to better determine the current state of stress of southeastern Alaska from the Dixon Entrance to Yakutat Bay. Phase data was gathered for over 4000 earthquakes of depths <20 km and magnitude <5 that occurred from 1973-2005 from Alaskan and Canadian databases. We relocated these earthquakes using the Double-Difference joint hypocenter method. Two areas of interest were identified with high concentrations of seismicity after relocation calculations for the entire southeast Alaska region; Glacier Bay through Yakutat (GBY) and the area surrounding Mt. Ogden (MOG). Earthquake locations in GBY are diffuse with some isolated clusters. The MOG subregion is dominated by a large northeast to southwest trending cluster that trends along the Speel River. We used these relocations and first motion data to estimate the stress fields for earthquake clusters that formed. Only a few of the calculated stress tensors were successful in representing the region's overall tectonic signature. We combined the calculated stress information with GPS, magnetic and gravity data in order determine how plate motion is partitioned in this region and to identify other potentially active faults.

TABLE OF CONTENTS

Page

LIST OF TABLES

LIST OF FIGURES

CHAPTER 1

INTRODUCTION

This study focuses on background seismicity in southeast Alaska and its influence on regional stress development. Relocated small (M<5.0) earthquakes at shallow (<20 km) depths and stress calculations from first motion data are used to delineate suspected structures which could help to better understand how plate motion is accommodated during the transition from strike-slip motion to reverse-oblique motion from south to north of the study region. The region has been the site of a number of large (M>6.5) earthquakes whose stress interactions are poorly understood due to the lack of an integrated study of the region's entire seismic catalog.

Southeast Alaska (Figure 1-1) is located on the eastern boundary of the Pacific plate where it interacts with the North American plate. The Pacific plate is estimated to be moving at a rate of ~6 cm/yr relative to North America (DeMets *et al.*, 1990; 1994). Caught between these two plates is the Yakutat microplate, which moves at ~5.1 cm/yr relative to North America (DeMets and Dixon, 1999). This tectonic interaction has resulted in the formation of approximately 135,000 km^2 of heavily glaciated and mountainous terrane assemblages that are cut and displaced by a series of splay faults that connect two major seismogenic structures, the Queen Charlotte-Fairweather fault system and the Denali fault system (Richter and Matson, 1971; Gehrels and Berg, 1992). Slip rates on these major faults do not account for the total relative plate motion (Fletcher and Freymueller, 1999), which is a cause for great concern in the overall understanding of seismic hazards present in the region. Fletcher and Freymueller (1999) suggested that a major component of the absent slip could be occurring at the Transition Fault Zone, which defines the contact between the Pacific plate and Yakutat block (Figure 1-1).

Throughout the last 250 years, the region has experienced significant thinning of icefields and glaciers, which has resulted in isostatic rebound of the Earth's crust (Arendt *et al.*, 2002; Motyka *et al.*, 2007). The consequence of ice melting is unloading of the crust and a drop in the amount of stress accumulation needed to cause earthquakes along reverse faults (Sauber and Ruppert, 2008). The inherent danger behind unloading pre-existing aseismic/low seismicity zones is that regional fault kinematics can be altered (Morner, 1979; Johnston, 1987; Stewart *et al*., 2000).

The combined population of southeastern Alaska's major cities is 47,000, including the capital city of Juneau. Its major forms of revenue are tourism, fishing and timber industries that rely heavily on sea ports and airports. Within the next couple of years, the Alaska Gas Pipeline is scheduled to begin construction in the northwest of the study region. The effects of a major earthquake could easily disrupt the region's fragile economy. By supplementing past studies of large earthquakes in the region (Doser and Lomas, 2000; Ruppert, 2008) with a detailed analysis of background seismicity our understanding of seismic hazards will be improved.

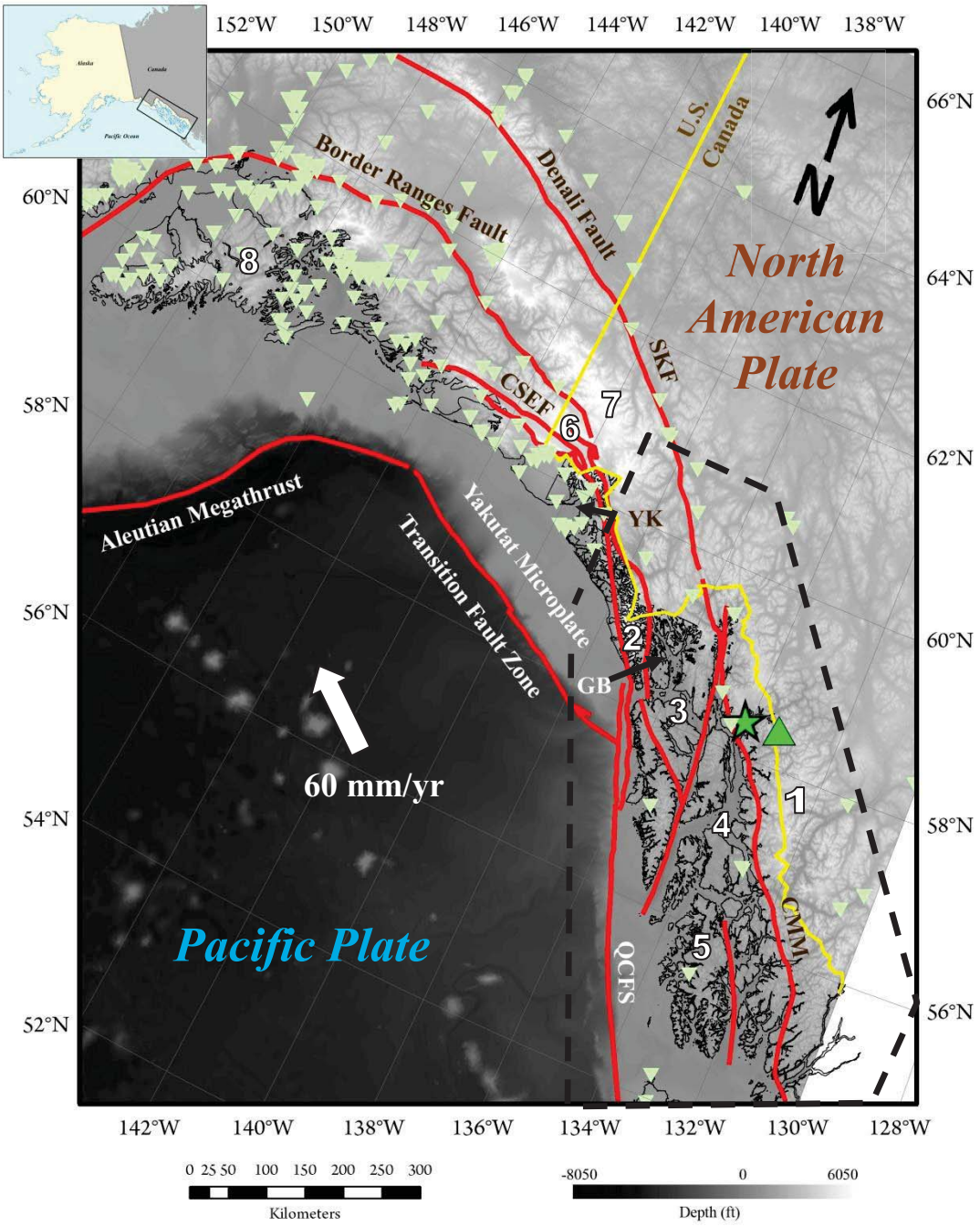

Figure 1-1. Tectonic setting of southeast Alaska. Major faults are red lines; national boundary is yellow, study region in dashed outline; green triangles are seismic stations; green star is Juneau; green triangle is Mt. Ogden; GB is Glacier Bay; YK is Yakutat; SKF is Shakwak fault; CSEF is Chugach-St. Elias Fault; CMM is Coast Mtns. Megalineament; QCFS is Queen Charlotte-Fairweather Fault system; 1 is Coast Mtns; 2 is Fairweather Range; 3 is Chilkat-Baranof Range; 4 is Kupreanof Lowlands; 5 is Prince of Wales Mtns; 6 is Chugach Mtns; 7 is Wrangell Mtns; 8 is Kenai Mtns. Faults from Plafker et al. (1994).

CHAPTER 2

PREVIOUS STUDIES

2.1 Tectonics, faults and seismicity

Southeastern Alaska is a complex geological region with an elaborate system of seismically active strike-slip faults whose history is heavily influenced by previous episodes of tectonism. In general, the region is an archipelago whose major terrane assemblages were accreted from convergence of the Pacific, Kula, and Farallon plates into the North American plate (Burchfiel and Davis, 1972; Oldow *et al*., 1989). The current position of these is attributed to the oblique westward subduction of the Farallon and Kula plates into North America 230 Ma, with a gradual shift to northwest convergence of the Pacific plate with present day Alaska dragging various tectonic assemblages to their present day position and causing internal deformation (Oldow *et al*., 1989; Plafker *et al*., 1989, 1994).

The study region, 54N-61N to 130E-139E, is dominated by two large transform systems; the Queen Charlotte-Fairweather fault system (QCFS) and the Denali fault system (DFS) (Figure 1-1). The QCFS represents the boundary between the Pacific and North American plates (Tobin and Sykes, 1968; Page, 1973; Plafker et al, 1978; Page, 1991). The Pacific plate is moving at a rate of 60 mm/yr to the northwest relative to a stable North American plate and parallel to the QCFS (DeMets *et al.*, 1990, 1994). Combined, the northern QCFS and southern DFS characterize the kinematic transition from dextral strike-slip motion to reverse oblique convergence in the Yakutat Bay area (Doser, 2003). The seismic history of each system is poorly understood due to the incompleteness of earthquake catalogs. In addition, most previous studies have focused only on the larger magnitude earthquakes of these fault systems (Figure 2-1).

Both fault systems combined do not account for the large slip deficit of relative tectonic movement at convergence. Fletcher and Freymueller (2003) compiled GPS and EDM survey data in the region surrounding the Yakutat microplate and reported a slip rate of 45.6 ± 2.0 mm/yr along the Fairweather fault and 3.8 ± 1.4 mm/yr on the Denali fault relative to a stable North America with a locking depth of 9.0 ± 0.8 km using the DeMets and Dixon (1999) plate model (Figure 2-2). Velocity measurements of the Yakutat microplate show that it is moving independently of the Pacific plate at ~51mm/yr relative to North America and parallel to the QCFS. The result is a large slip deficit when compared to the 60 mm/yr motion of the Pacific plate (DeMets *et al.*, 1990, 1994). Fletcher and Freynueller (1999) argue that the Transition Fault Zone accommodates most of the remainder of slip, in conjunction with other minor faults in the area.

The present day accretion of the Yakutat microplate, located in the northeastern portion of the study area, is of great interest because it sits on the transition between strike-slip and convergent motion. At the surface, it is bounded to the south by the Transition Fault Zone and the north by the steep topography of the St. Elias Mountains. It has undergone 600 km of subduction and can be observed up to 140 km in depth beneath the North American plate with the northeastern-most corner located approximately 150 km southwest of the Totschunda fault (Figure 1-1) (Plafker, 1994; Ferris *et al*., 2003; Eberhart-Phillips, 2006). Recent studies describe the Yakutat microplate as a 15-20 km thick oceanic plateau that is promoting flat-slab subduction (Ferris *et al*., 2003; Pavlis *et al*., 2004) due to its buoyancy and independence from the North American and Pacific plates. Gulik *et al.* (2007) combined bathymetry and USGS seismic data (from Bruns, 1985) to accurately map the suspected Transition fault zone scarp and also found an inactive backthrust fault located 10 km to the north (Figure 2-3). The vertical profile of the

Transition fault alongside the thrust feature confirmed Plafker's (1987) and later Fletcher and Freymueller's (2003) suspicions that the Transition Fault Zone represents a transformation from strike-slip behavior as the Transition Fault Zone splays westward from the Fairweather fault and converts into possibly oblique-slip convergence as it enters the Pamplona Zone to the northwest. Anomalous crustal behavior surrounding the Yakutat microplate is further complicated by western Cross Sound earthquake slip vector orientations that are moderately rotated in a counterclockwise direction from relative plate motion (Figure 2-2). This observation indicates that the Cross Sound region is tectonically seismogenic and accommodates the most variable changes in stress directions (Doser and Lomas, 2000).

The QCFS lies just offshore and runs parallel to the Canada – Alaska coastline. Lanphere (1978) and later Nokleberg (1985) estimated QCFS total displacement around 350 km. Five large earthquakes have been associated with dextral strike-slip motion along this fault system; the 1927 Sitka of M 7.1, the 1949 Queen Charlotte of M 8.1, the 1958 Fairweather of M 7.9, the 1972 Sitka of M 7.4, and the 2004 Queen Charlotte of M 6.8. Bird (1997) reported consistent patterns in the distribution of earthquake occurrences along the QCFS near Graham Island. She found significant fluctuations in the total number of earthquakes throughout the 1980's and that the events were consistently of low magnitudes ($\leq$ M 5.3) and strike-slip (Figure 2-4). An elaborate system of strike slip, thrust and normal faults branch eastward from the QCFS. The most significant are two relatively aseismic right-lateral strike slip faults, the Clarence Strait fault and the Chatham Strait fault (Figure 2-5). Lithology and structures constrain movement along the Clarence Strait fault to 15 km of displacement which occurred no later than the upper-Triassic (Lanphere, 1978; Gehrels *et al.*, 1987). The Chatham Strait fault, although considered inactive, is believed to be associated with a M_w 5.3 earthquake in 1987 (Page, 1991) and has an

estimated dextral displacement of 205 km which occurred over two periods; 100 km before the late-Triassic time and 50-100 km since the early to mid-Tertiary (Overshine & Brew, 1972; Lanphere, 1978). Other estimates suggest dislocation distances as large as 600 km with several kilometers of vertical displacement since the Early Eocene (Loney *et al.*, 1967; Plafker, 1994).

The Chatham Strait and the Peril Strait faults appear to connect the QCFS to the DFS. The Denali fault is mostly strike slip with transpressional components that accommodate the aforementioned tectonic convergence. Seismicity that can be directly attributed to the DFS includes a M 7.2 in 1912, a M 6.2 in 1958 and in 2002 two earthquakes of M 6.7 and M 7.9. The Fairweather fault can arguably be extrapolated to the Totschunda fault which merges with the Denali fault (Richter, 1971). Power (1988) conducted a microearthquake study near the Totschunda fault and concluded that a fault connection between the Fairweather and the Totschunda faults is not likely due to the lack of seismicity in the connecting gap.

2.2 Geology

Geologically, southeast Alaska has been described as an archipelago made up of ten major assemblages; five terranes and five lithic assemblages with distinct geologic records shown on Figure 2-5 (Gehrels and Berg, 1994). Some of these have been altered by metamorphism or cross cut by the region's transpressive/dextral slip fault systems creating a landscape with narrow southeast-northwest trending geologic exposures. The earliest of these assemblages, and most dominant in the Alaskan panhandle, is the Alexander terrane which is a mixture of stratified, metamorphic, and plutonic rocks that range in age between the Proterozoic-Early Cambrian through Mid-Jurassic. It was originally an oceanic arc that completely accreted to North America during the early Tertiary.

To the west are the Wrangellia terrane and the Chugach terrane (Figure 2-5). Wrangellia is found on Vancouver Island and is truncated at Queen Charlotte Island, except for some small exposures in islands just south of Glacier Bay (Plafker *et al*., 1976, Berg *et al*., 1978). Its composition includes three key stratigraphic layers that range from Middle Triassic to Jurassic; thick basalt flows, shallow to deep marine carbonates, and fine grained clastics punctuated by tonalitic plutons overlying a complex upper Paleozoic mafic conglomerate of volcanic, pyroclastic and clastic rocks (Gehrels and Berg, 1994). The Chugach terrane is an arrangement of two structural components that range from upper Paleozoic to early Cretaceous (Plafker, 1977; Gehrels and Berg, 1992). Both components are deformed but carry distinct lithologies; one is composed of flysch, greywacke, argillite and slate, while the other has volcanic rocks, chert, limestone, and plutonic rocks. Greenschist, amphibolite and a small amount of scattered blue schist outcrop can also be found in this terrane.

East of the Alexander terrane are the Taku and Stikinia terranes. Formation of the Taku could have occurred as early as the lower Paleozoic and continued through the mid-Cretaceous (Gehrels and Berg, 1994). It is largely made up of metamorphosed basalts, pillow basalts, gneiss, granites, greenschists, low grade metawacke and fine grained sedimentary rocks. The Stikinia terrane is a Devonian to Middle Jurassic assemblage of arc-type volcanics, basinal strata and carbonate rocks (Gehrels and Berg, 1994).

The most significant of the lithic assemblages in southeastern Alaska is the Gravina Belt. It is an Upper Jurassic to mid-Creataceous thin, continuous assemblage of marine sediments, interbedded volcanics and polymictic conglomerates with interspersed tonalitic and peridotite plutons (Gehrels & Berg, 1992). It is the geographic transition between the Alexander and Taku terranes and separates the high grade greenschist facies metamorphic zone next to the Coast

Mountains from the lower grade amphibolites facies to its east (Gehrels and Berg, 1994). Other minor lithologic units found in the region include Quaternary and Tertiary sediments and plutons and metamorphic structures related to the Coast Mountains batholith.

2.3 Potential Fields

To compliment surface geology, gravity and magnetic data were gathered from USGS and Canadian data sources to characterize geophysical potential field sources at depth. Little work has been conducted in the study region to establish a link between surface exposures and regional crustal anomalies (Saltus, written communication 2008). Of the two geophysical datasets, aeromagnetic surveys were more densely spaced and therefore more appropriate for this study. The northeastern corner of the study region, the area northwest of Glacier Bay, and a thin segment that follows the 57th parallel have magnetic readings that were taken at intervals >9.6 km. The rest of the study area has readings at intervals <1.6 km mile (Saltus et al., 1999). Blank areas contained no data or had data that were omitted due to unrealistic or null values. Gravity measurements were generally limited to shorelines, streams and areas that were easily accessible. All data were mapped with Oasis montaj software using default gridding parameters and shaded relief with illumination from the northwest.

Figure 2-6 illustrates the region's magnetic anomalies which clearly define known fault patterns. The most distinct magnetic anomalies are two high amplitude, short wavelength southeast-northwest striking magnetic bands that correspond with crystalline assemblages of the Chilkat-Baranof Range and the Coast Mountains batholith. Chilkat-Baranof Range magnetic highs, which are bounded to the south by the Peril Straight fault and to the east by the Chatham Strait fault, are likely associated with Craig subterrane metamorphic and plutonic rocks. The

Coast Mountains batholith is neatly paired with a near vertical, dextral fault known as the megalineament which merges with the Denali Fault to the north (Gehrels and Berg, 1994 after Brew and Ford, 1978) and separates it from the Taku and Chugach terranes.

The extent of the Taku terrane and Gravina belt is geographically associated with the Coastal Foothills which are bounded to the east by the Coast Mountains megalineament and the west by the Clarence Strait and Chatham Strait faults. Although heavily speckled with granodioritic/tonalitic plutonic outcrops, few onshore magnetic anomalies were detected in this terrane. It is represented on the magnetic map as a continuously low amplitude body not unlike those that typically characterize sedimentary filled basins.

West of the Clarence Strait fault are the Prince of Wales Mountains and Kupreanof Lowlands. The majority of this area is composed of the Craig the subterrane with some Quaternary and Tertiary strata on the western half of Kupreanof Island. The Prince of Wales Mountains are defined with sharp, short high amplitude anomalies that continue as far west as the QCFS. The sharp anomalies appear to be separated by a complex fault system until a large anomaly appears on Kupreanof Island to the north. Interestingly, this large anomaly could represent the extent of the granite and gabbro outcrops that are interspersed within the mapped Quaternary and Tertiary strata.

Considering large spacings in magnetic survey readings in the northwest, few details are apparentin the Fairweather Mountains. A strip made up of moderate amplitudes with short wavelengths that follows the QCFS along the Fairweather Mountains is likely associated with Chugach terrane volcanic rocks.

The most distinct regional characteristic of the Bouguer gravity anomaly map (Figure 2-7) is that it shows a continuous gradient from positive to negative values between the Gulf of Alaska

into the North American continent. This density gradient is typical as the crustal rocks change from dense, thin oceanic crust into a thickening, less dense continental crust. Further examination reveals interspersed gravity highs and lows within the archipelago's western islands that appear to be directly related to plutonic and volcanic assemblages as mapped by Gehrels and Berg (1994) within the Chugach, Wrangellia and Alexander terranes. The lows are suspected to be pieces of continental crust that have been accreted and continually cut and deformed throughout the region's tectonic history.

2.4 Glacier activity

High latitudes and a mountainous landscape in proximity to the Pacific Ocean and Gulf of Alaska have contributed to southeastern Alaska's glacial systems. The greater portion of the panhandle was covered by the inland glaciers that fused with mountain ice caps during the Wisconsinan maximum of the last glacial period (Hamilton, 1994 after Mann, 1986). Only areas located in rain shadows and on large islands were spared glaciation. Regional geomorphology is, in large part, due to large scale glacial erosion of crustal assemblages. Fjords connected by an intricate system of waterways presently make up the post-glacial geomorphology. Over time ongoing tectonism has caused the offset and destruction of glacial features (Hamilton, 1994).

Arendt *et al.* (2002) have estimated that over the last 250 years glacial ice mass loss has occurred at increasing rates. They reported that between the mid-1950s and the mid-1990s Alaskan glaciers had a change in thickness of -0.52 m/year which corresponds to an annual volume change of -52 ± 15 km^3/year (water equivalent). They estimated an increase to -1.8 m/year in thickness, equivalent to -96 ± 35 km^3/year, between the mid-1990s and 2001. The southeastern Alaska region was the most affected by the ice mass loss (Figure 2-8).

Larsen *et al.* (2002) calculated isostatic rebound of the earth's crust as a response to the ice volume lost in the Glacier Bay region. They found that the highest rates of rebound were occurring near Yakutat and Glacier Bay. Studies found uplift rates of 30 mm/year in Glacier Bay and 32 mm/year in the Yakutat Icefield and 10 mm/yr throughout the transitional coastal region (Motyka *et al.*, 2007; Larsen *et al.*, 2002, 2004; Freymueller, 2008). The effect on horizontal motions can be as much as 5 mm/yr (Elliot *et al.*, 2008 cited in Freymueller**,** 2008). Approximately 42% of the earthquakes in this study occur in the Glacier Bay region. Their signature is a combination of tectonics and seasonal glacial activity (Rogers, 1976; Horner, 1983; Sauber and Ruppert, 2008).

2.5 Regional stresses

Ongoing deformation in southeastern Alaska can be attributed to a variety of processes: active tectonics, postseismic relaxation from large earthquakes (magnitude >7), glacial isostatic rebound, and inflation of volcanoes (Freymueller, 2008). These processes all influence the region's complex stress field and define zones where seismicity is more prone to occur**.** Seismic hazard evaluation for any region is largely dependent on the available data. Southeastern Alaska's seismic network is a fairly recent development and does not provide adequate coverage over a large part of the study region (see section 3.1 and Figure 1-1). For this reason, most of the earthquake studies that have calculated the state of stress in the panhandle region, or Alaska in general, have concentrated on frequent moderate to large magnitude earthquakes ($M > 3$).

Ristau *et al.* (2007) compiled a regional stress map for western Canada from a collection of catalog moment tensor solutions of earthquakes with $M \geq 4$ since the mid-1990s. They found that at the scale of their work the principal stress axis (σ_1) orientation along the QCFS north of

53° latitude has a trend of 18.2° plunging 10.1° and with σ_3 trending 108.3° and plunging at 1.3°. The stress ratio, Φ, which shows the relative sizes of the principle stress (Angelier, 1979) was calculated to be 0.48. South of 53°N, Ristau *et al.* (2007) calculated σ_1 with a trend of 216.3° and plunge of 0.10, σ_3 plunges at 85.0° and trends 316.0. Here Φ is 0.10. Errors for these calculations vary between 10° and 20°. These calculations are consistent with the deviation from mostly strike slip behavior that dominates the system north of 53°N and a convergent segment to the south. Ristau *et al* (2007). associate the high plunge angle of σ_3 south of 53°N with deformation of the North American plate and a lack of Pacific plate subduction. These calculations are in agreement with Bird's (1997) focal mechanism solutions. Although most of the earthquakes in the Ristau *et al.* (2007) study were not located directly on the QCFS, they still provide a useful insight for plate interaction in the southern parts of my study region.

Ristau *et al.* (2007) divided the Yakutat microplate region into an east and west portion to calculate stress orientations (Figure 2-9). They found a σ_1 azimuth of 175 ± 10° with a σ_3 plunge of 68° in the western region, which is nearly perpendicular to the direction of Pacific plate convergence. The orientation of σ_1 in the eastern region is ~31° counterclockwise of that of the western region and σ_3 has a shallower plunge of 52°. This is consistent with Doser and Lomas (2000) who found that a transition from strike-slip to oblique convergence was in agreement with focal mechanisms in the area. The increase in large earthquakes in this region was also consistent with an increase of coupling forces from strike-slip to convergence going from east to west; the two largest earthquakes recorded during the study time frame were M 6.4 and M 7.5, respectively.

Ruppert (2008) conducted a similar study of stress orientations with a focus on the Yakutat area and followed major seismic trends northward throughout the entire Alaska region with the

exception of the panhandle. She used focal mechanisms of $M \geq 3$ earthquakes from previous studies in order to create a detailed map of stress orientations (Figure 2-10). In the southeastern portion of her study area, the Yakutat microplate region, her dataset's maximum horizontal stress orientations also agreed with Doser and Lomas (2000), further confirming the tectonic environment. Ruppert (2008) calculated two stress tensors within my study region. Like Ristau *et al.* (2007), she divided the Yakutat convergent zone into eastern and western halves; results for the western half were σ_1 trending 179° and plunging 19°, σ_3 trends at 290° and plunges 45°. Φ is 0.32 and the variance is 0.17. In the eastern half σ_1 trends at 216°, plunges 10° and σ_3 trends at 328° with a plunge of 64°. Φ is 0.32 and the variance is 0.16. These results are very similar to those of Ristau *et al.* (2007). Differences in the orientations are due to earthquake magnitude selection and Ruppert's (2008) calculation included slightly more area to the north.

Considering that historically Alaska has always lacked an appreciable earthquake monitoring network (this will be further discussed in section 3.1), little could be done at the scale of Ristau and Ruppert's studies to delineate crustal seismic behavior not associated with major tectonic features. Earlier studies that used microearthquake surveys have had some success in evaluating the region's overall seismic behavior. Two of these studies include Rogers (1976) and Horner (1983). Both reported that the region was very active with thousands of low magnitude earthquakes along the QCFS, the DFS and centered in densely glaciated areas. Only a few of these earthquakes could be located and had large margins of error, up to 1° of latitude.

The Rogers (1976) study found that the Chatham Strait fault region and to the east of it is a relatively aseismic zone and that earthquake activity is generally restricted to the major strike-slip systems to the west. Interestingly, Rogers (1976) observed in some areas, like Glacier Bay and the Coastal Range batholiths, that microearthquake activity had a tendency to not follow the

region's large earthquake patterns. He deduced that strain release is not restricted to major fault motion and that these microearthquake concentrations had a tendency to occur in heavily glaciated regions.

Horner (1983) derived a composite P-nodal solution to evaluate fault plane behavior from first motions gathered during a 1979 microearthquake survey near the Shakwak segment of the Denali fault (Figure 1-1). He found that fault plane movement was at a high angle relative to the Denali fault. He speculated that this was due to readjustments of tectonic stresses. A similar microearthquake study conducted by Wolf *et al.* (1997) east of Juneau, near Mt. Ogden (Figure 1-1), found a correlation between the seasonal water cycle and increased levels of seismicity that were clearly independent of a tectonic signature. But neither study gave definitive insight into the stress regime of minor fault systems that appear to contribute to these perturbations in stress distribution.

Leonard *et al.* (2008) calculated deformation rates from earthquake catalog data and compared them to those derived from GPS measurements. They determined a rate of 27.3 ± 16.65 mm/yr with a 68% confidence interval for the QCFS. Fletcher and Freymueller (2003) gauged the long term slip rate along the QCFS to be 45.6 ± 2 mm/yr from GPS data. The best fit for the earthquake catalog derived model, considering the maximum uncertainty of this estimate, gives a value of 43.95 mm/yr, which overlaps with the minimum GPS slip rate of the northern QCFS estimated by Fletcher and Freymueller (2003) at 44 mm/yr.

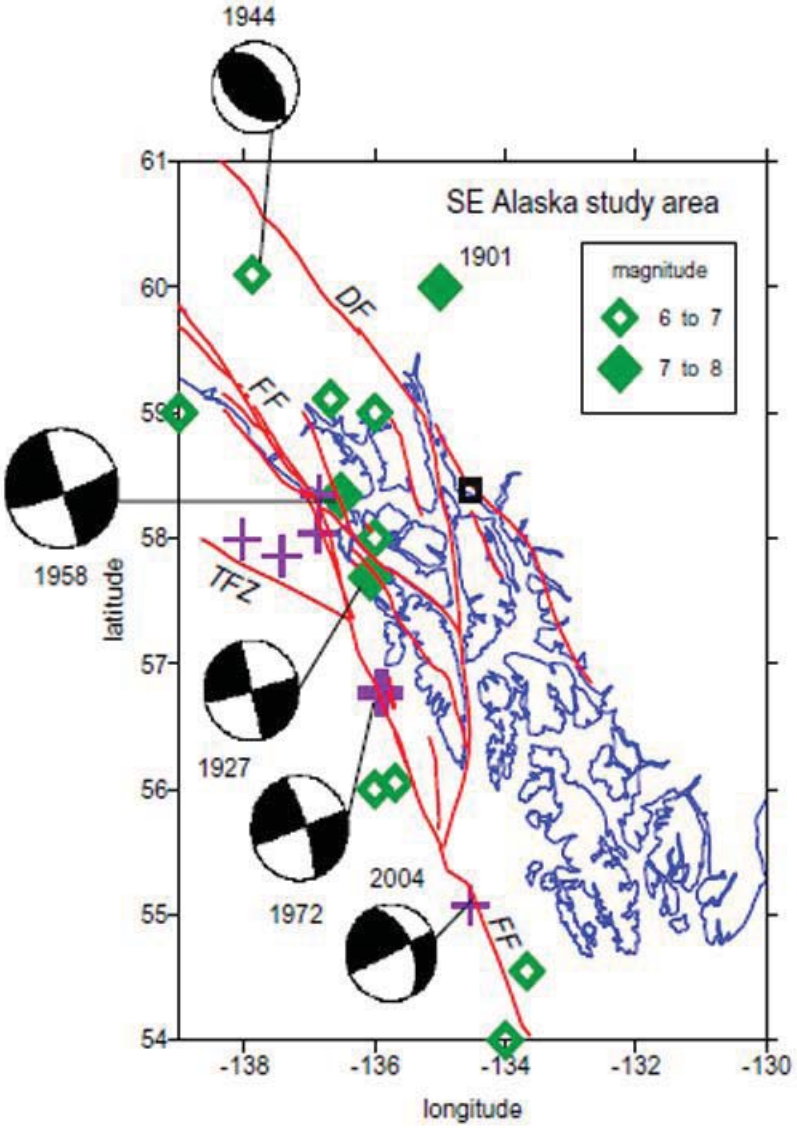

Figure 2-1. Large magnitude (>6) earthquakes in study region. Green diamonds are events that occurred before 1971, purple crosses are events that occurred after 1971. DF is Denali fault, FF is Fairweather fault, TFZ is Transition zone fault. Box is Juneau. From Doser (2007).

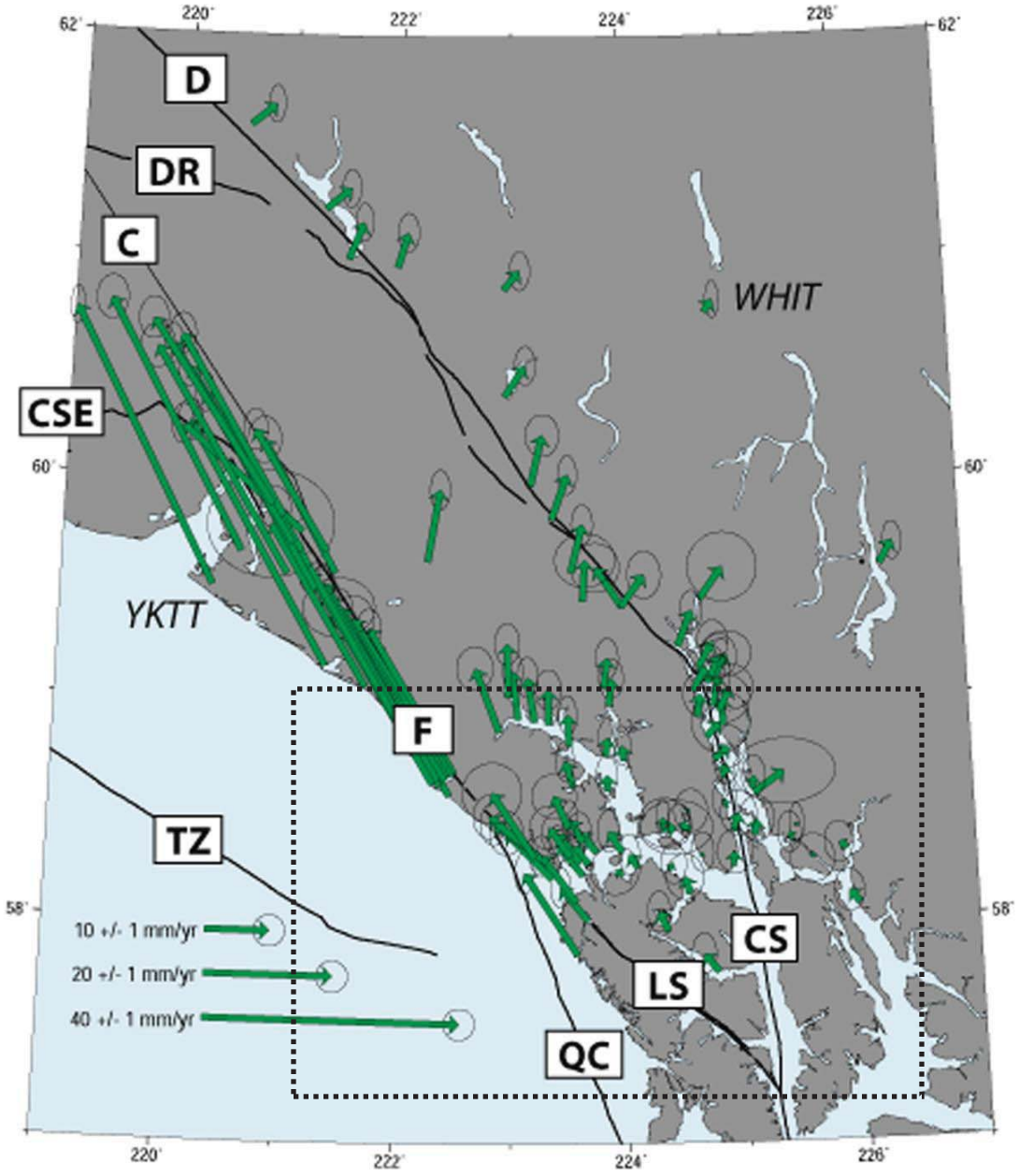

Figure 2-2. Calculated horizontal velocities from GPS measurements in southeastern Alaska relative to Whitehorse (WHIT). Dotted line represents Cross Sound Region. Major faults are marked with letters inside boxes: D, Denali Fault; DR, Duke River Fault; C, Connector Fault; CSE, Chugach-St. Elias Fault; F, Fairweather Fault; TZ, Transition Zone; QC, Queen Charlotte Fault; LS, Lisianski Strait Fault; CS, Chatham Strait Fault; YKTT, Yakutat. Modified from Freymueller et al. (2008).

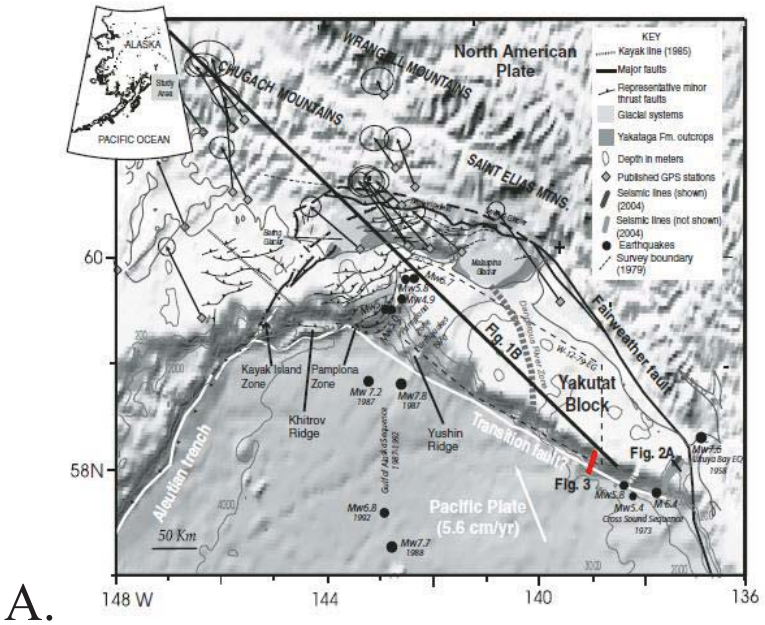

A.

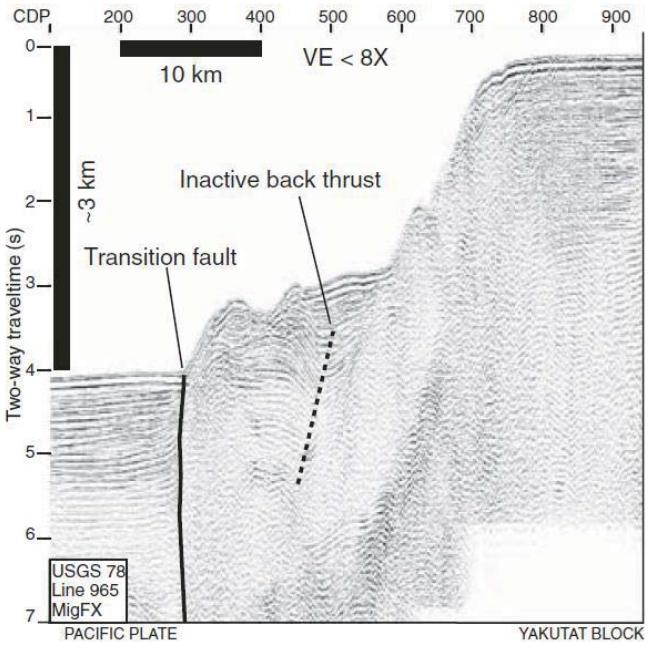

B.

Figure 2-3. A. Red line is location of U.S. Geological Survey reprocessed seismic line. B. Interpreted fault structures. The near vertical behavior of the Transition fault is characteristic of strike slip systems. To the north is an inactive thrust fault. From Gulick, (2007).

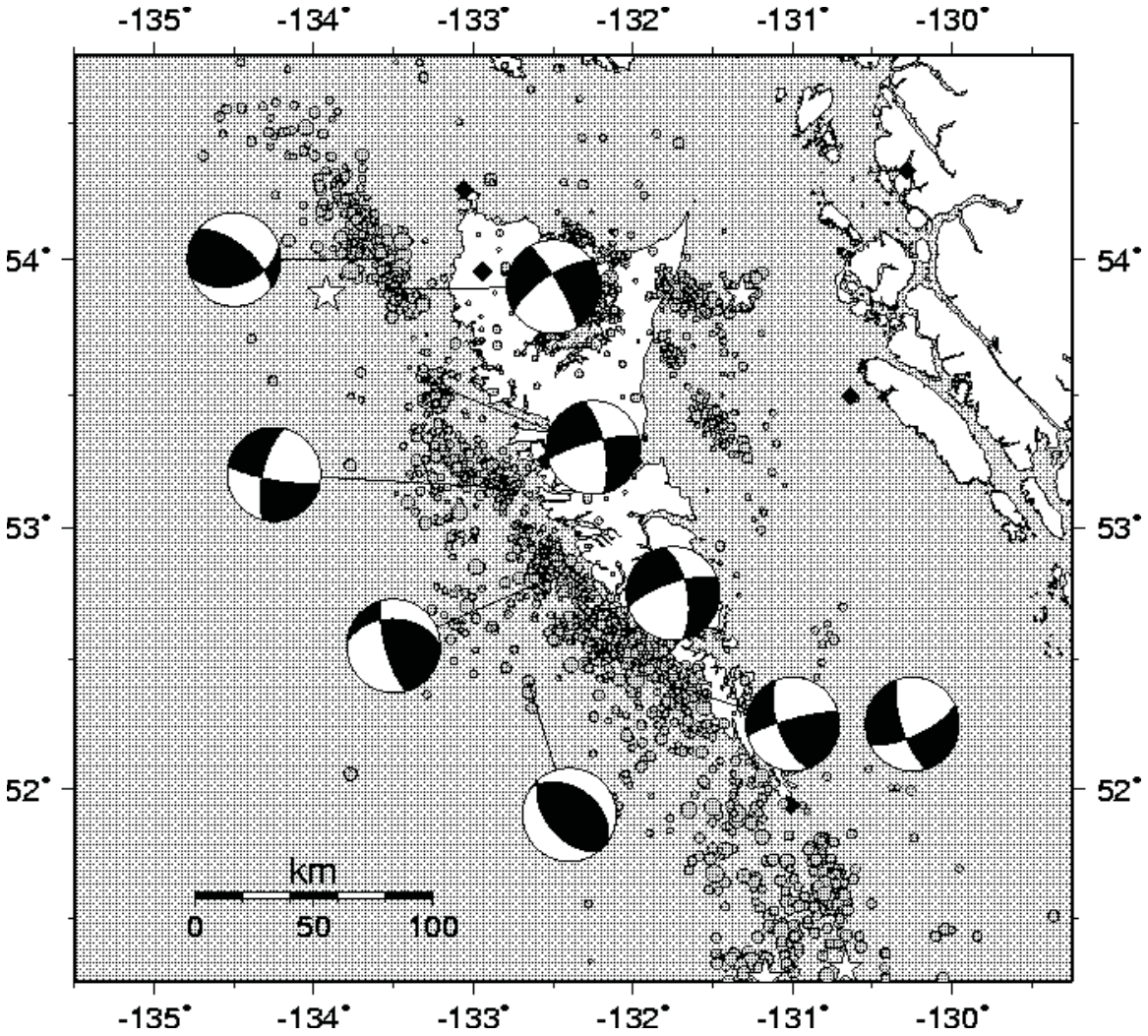

Figure 2-4. Focal mechanisms in the Graham Island area located in the southern section of the study region along the Queen Charlotte-Fairweather fault system. Faults are mostly strike-slip with slight thrust components. Pure thrust events occur on subsidiary faults. From Bird (1997).

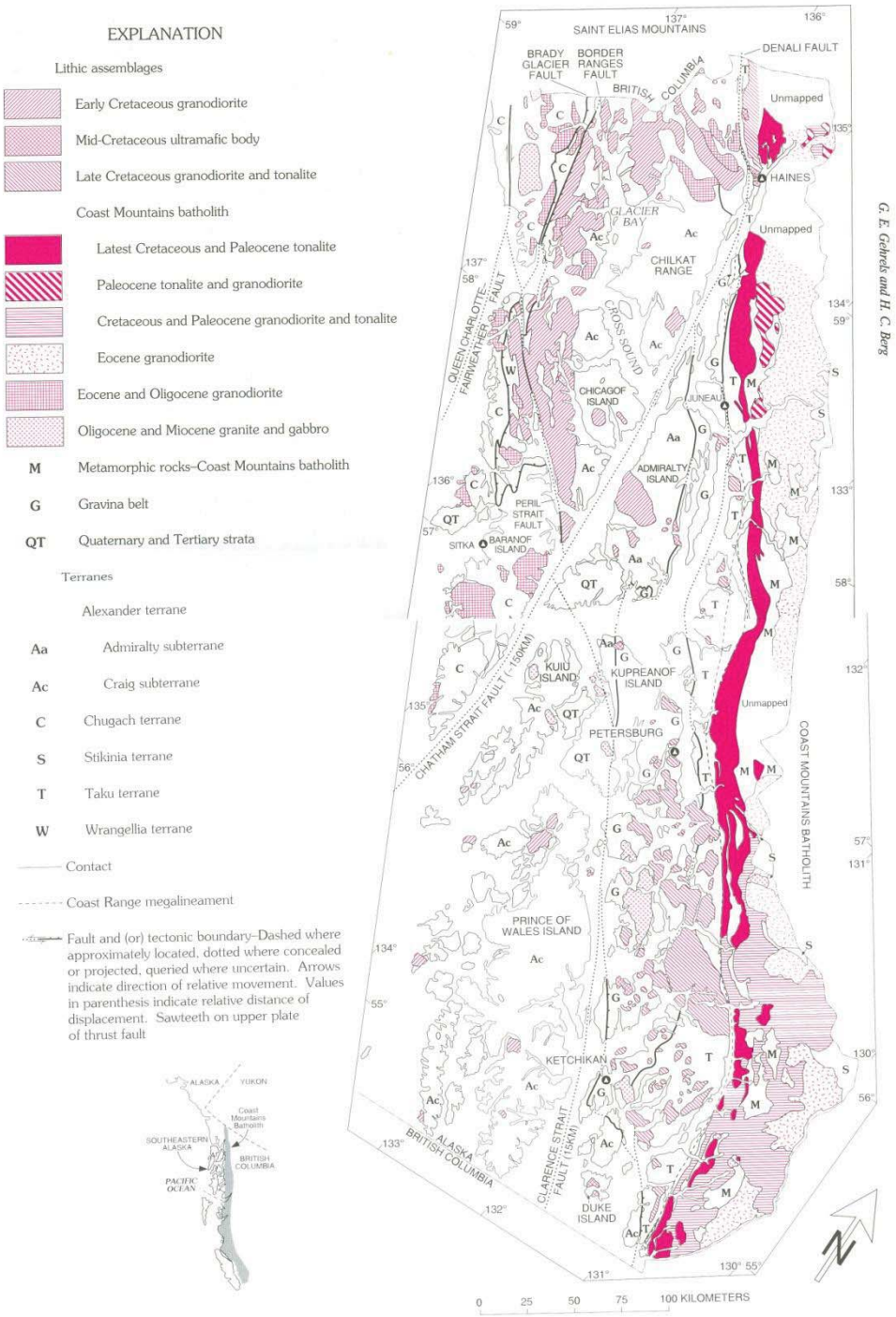

Figure 2-5. Map of terranes, lithic assemblages, and major faults in southeastern Alaska. From Gehrels and Berg (1994).

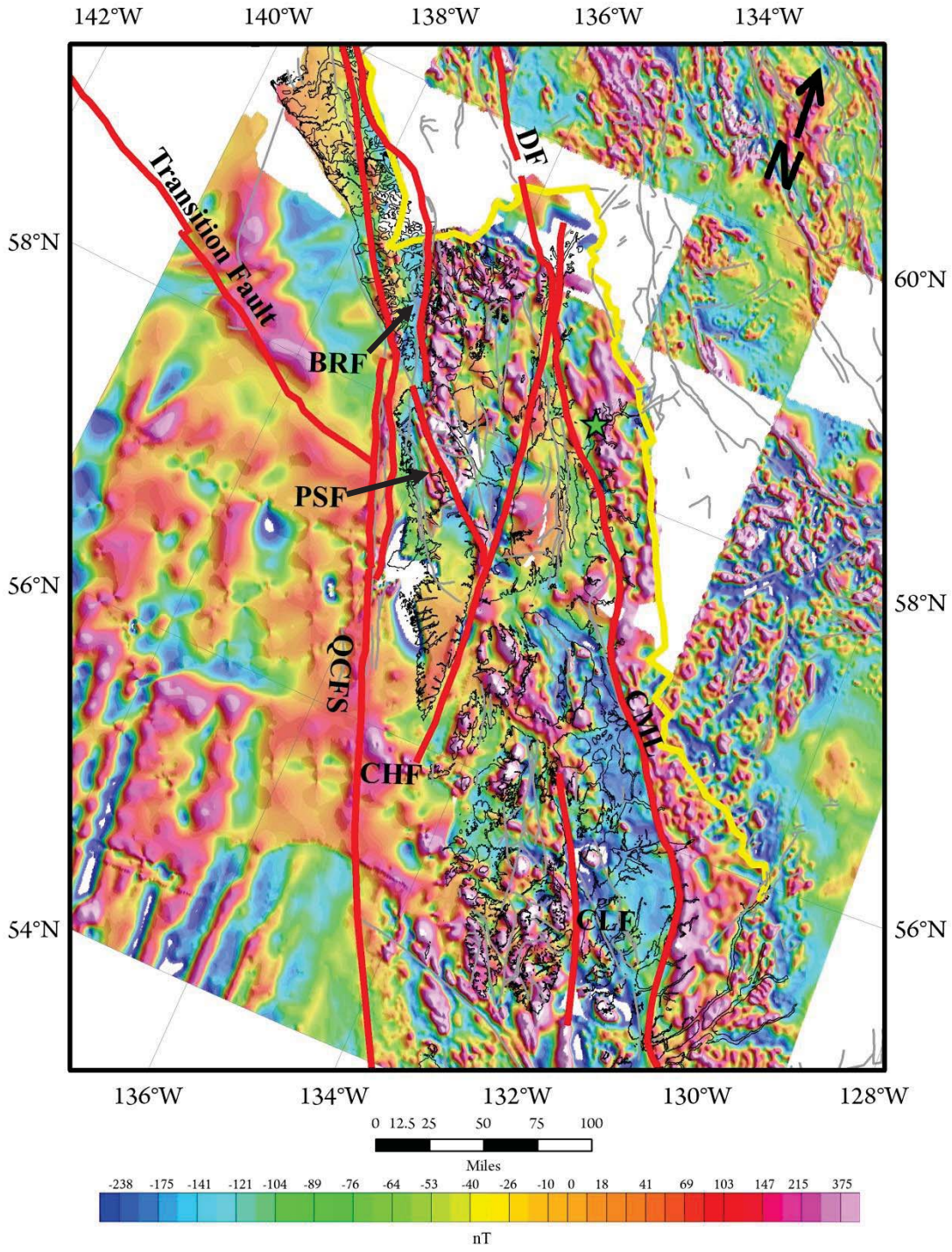

Figure 2-6. Magnetic map of southeast Alaska. Gray lines are minor faults. DF is Denali fault; CML is Coast Mtns Megalineament; CLF is Clarence Strait fault; CHF is Chatham Strait fault; BRF is Border Ranges fault; PSF is Peril Strait fault. Blank areas indicate where no data is available. Other symbols same as Figure 1-1.

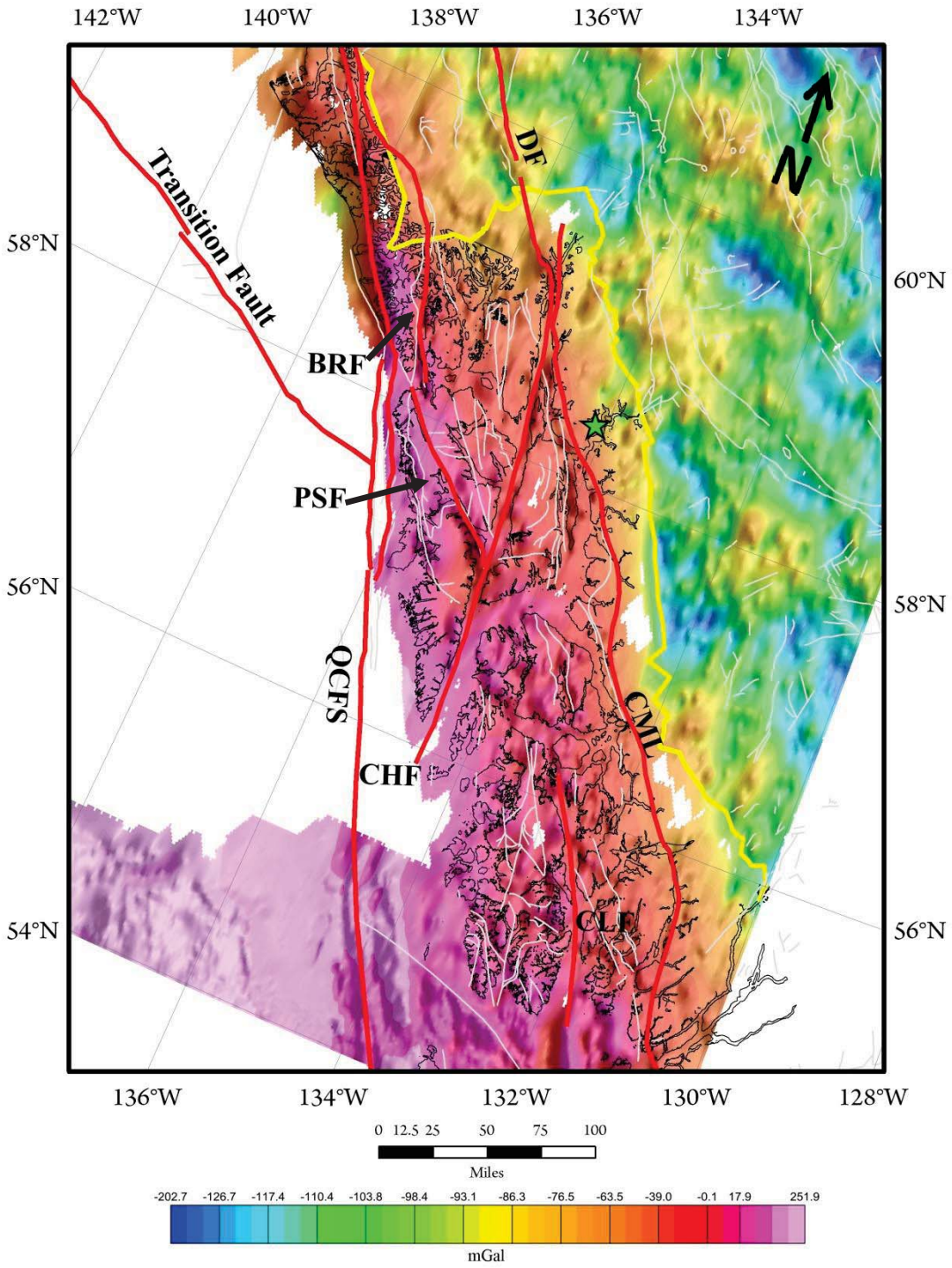

Figure 2-7. Bouguer gravity map of southeast Alaska. Symbols are same as Figure 2-6.

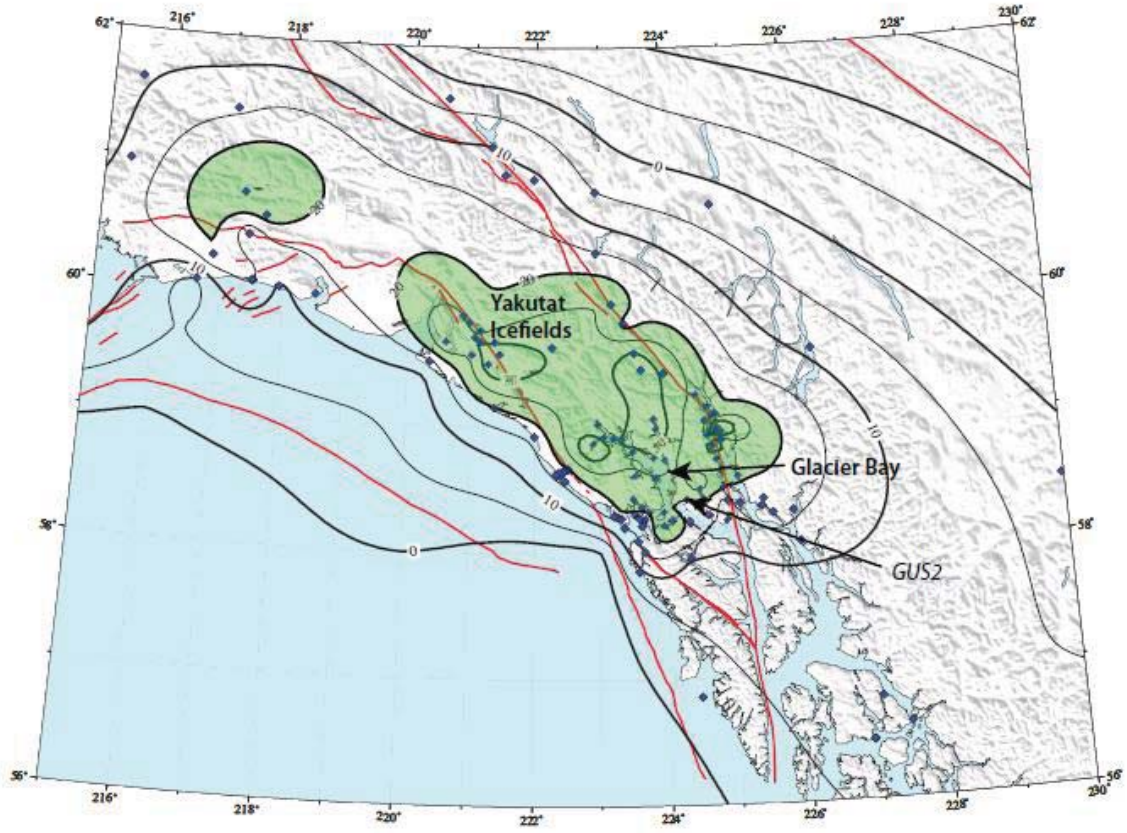

Figure 2-8. Uplift rates in southeastern Alaska due to crustal relaxation after ice mass loss. Green shaded regions indicate uplift rates greater than 20 mm/yr. Diamonds are measurement sites; contours at 5mm/yr intervals. From Freymueller et al. (2008).

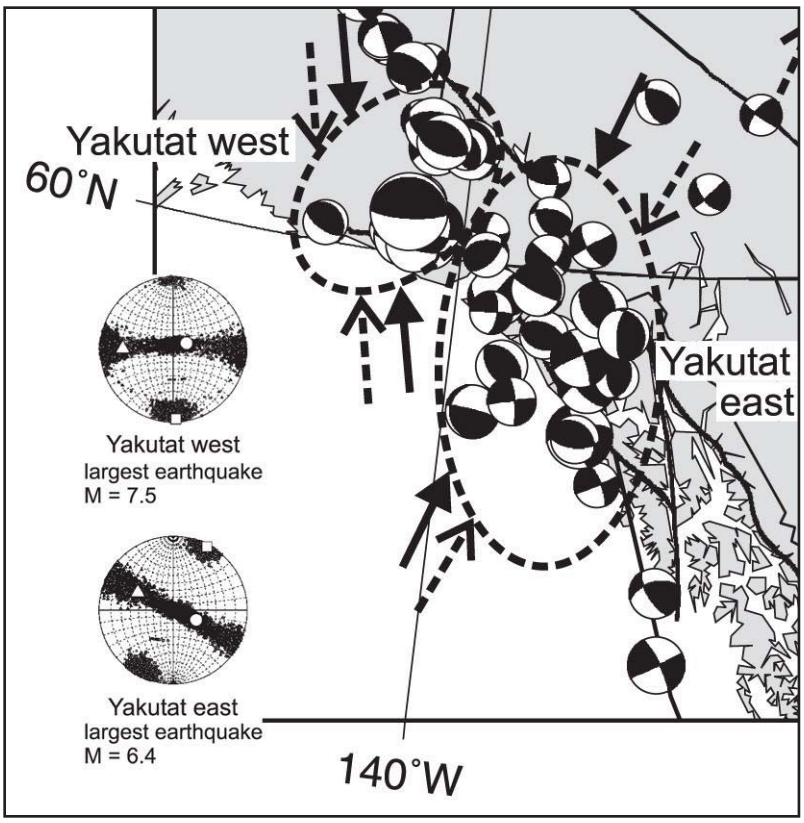

Figure 2-9. Stress orientation results for the Yakutat East and Yakutat West areas modified from Ristua et al. (2007). Beach balls are moment tensor solutions; dashed ellipses show selected region for stress calculation; solid arrows are stress direction; dashed arrows are P-axis direction. On stereonets: square is maximum compressive stress (σ1); triangle is intermediate compressive stress (σ2); circle is minimum compressive stress (σ3).

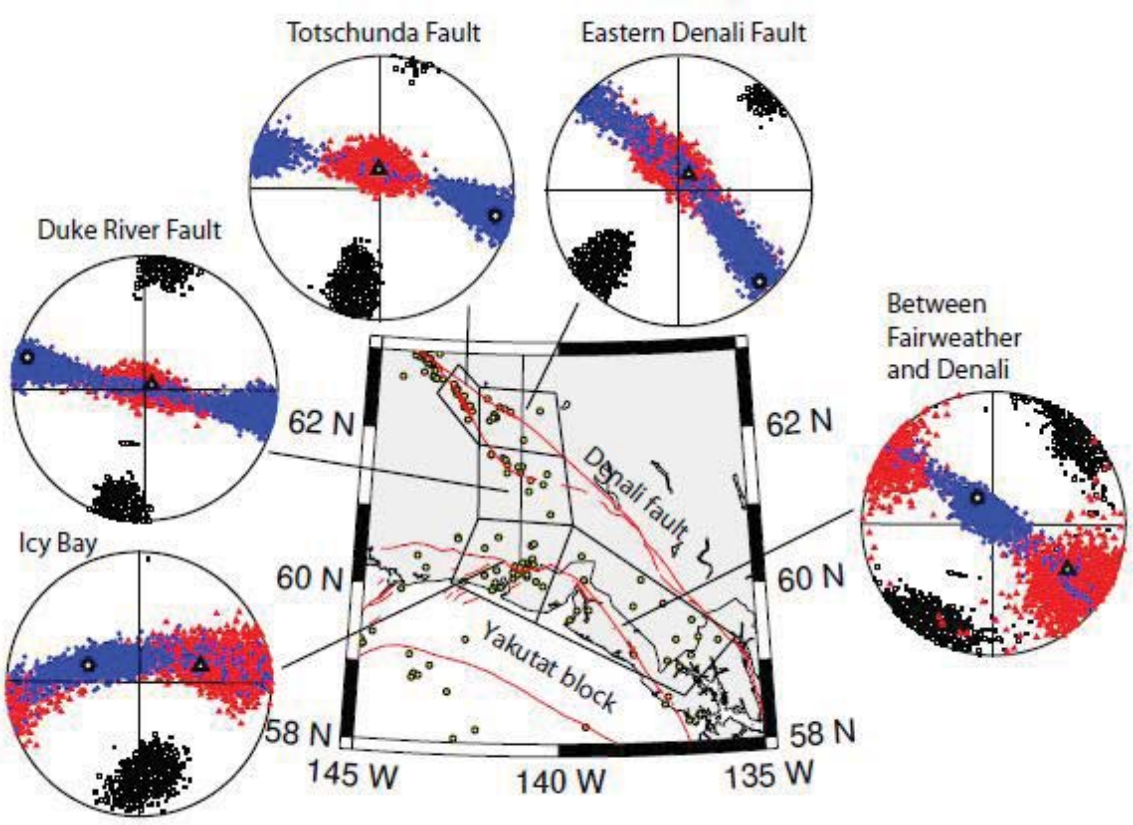

Figure 2-10. Stress tensor solutions in the Yakutat region and nearby areas from Ruppert (2008). Rectangles on map show area extents of calculations. Red are major regional faults; yellow dots are earthquakes. On stereonets: square is maximum compressive stress (σ1) with black uncertainty levels; triangle is intermediate compressive stress (σ2) with red uncertainty levels; circle is minimum compressive stress (σ3) with blue uncertainty levels.

CHAPTER 3

DATA AND METHODS

3.1 Data

Two earthquake data catalogs were used in this study, that of the Alaska Earthquake Information Center (AEIC) and the Canadian National Data Centre for Earthquake Seismology and Nuclear Explosion Monitoring (CNDC). From the AEIC a total of 1,524 earthquakes were obtained from 1/10/1973 through 12/29/2005 and 3,558 earthquakes were gathered from the CNDC from 1/3/1985 through 12/29/2005 (Figure 3-1). The starting dates reflect differences in the establishment of the seismic networks in the two regions. The large difference in total earthquakes between the two catalogs since 1985 is likely due to a couple of factors. The first is that the AEIC runs a declustering algorithm developed by Reasenberg (1985) to eliminate dependent seismicity which greatly reduces the number of earthquakes available in the catalog (Wyss, 1999). I could not verify if the CNDC declusters their catalog as well. Second, ongoing efforts by the AEIC are being made to include events occurring immediately after the 2002 Denali M 7.9 earthquake.

Redundant earthquakes between catalogs were identified with an algorithm that found CNDC hypocenters that occurred within a given time range of earthquakes that were registered in the AEIC catalog. As shown in Figure 3-2 a time range of ±5 seconds captures the maximum number of redundant earthquakes before a dramatic drop off occurs in events detected over increasing time ranges. A total of 465 earthquakes were identified as redundant and removed from the dataset. It is important to note that a range of ±5 seconds, which corresponds to a radius of approximately 31 km between hypocenters in a homogenous earth model, is geophysically realistic. A range of ten seconds also increases

the possibility of misidentifying true separate events as redundant and removing them from the dataset. Effects that redundant earthquakes can have on a system will be further discussed in the Section 3.2.

Over time, the AEIC has changed weighting methods for its phase arrivals and each method is different from that of the CNDC. Data attained from the AEIC had a combination of pick weights ranging from 0 to 1 provided by a data analyst between 1973 through 1998. Post-1998, AEIC weighting is done with the combination of a program called dbloc2 along with hypocenter location parameters and this weighting scheme gives values from 0 to 63. The CNDC had a convention similar to that of the early AEIC catalog but used integers between 0 and 4. This lack of consistency between weighting schemes would have caused gross miscalculations during relocation. Additional data provided by each catalog was insufficient to derive a consistent weighting method from a numerical ratio. For these reasons, and to allow error propagation during relocation calculations, a weight of 1.000 was applied to all P arrivals and 0.500 to all S arrivals.

The CNDC catalog included a multitude of additional phase arrivals, including Pg, Pn, P, Sg, Sn, S and Lg. Only the first P and S phase arrivals were chosen for each station as the hypoDD relocation scheme does not allow for multiple P and S phases from a single station to be used in the relocation process. For the purpose of calculating the best possible earthquake relocations from the inversion all available earthquake data were used and later were trimmed to focus on earthquakes with magnitudes <5 and depths no greater than 20 km. The final dataset consisted of 4,617 earthquakes with 46,615 phases recorded at 731 stations (Figure 3-3).

3.2 HypoDD Program

In order to study seismogenic structures in southeast Alaska from a large number of hypocenters precise relocations are absolutely necessary. Event locations provided by catalogs, such as the AEIC and CNDC, use single event location algorithms and an accepted regional velocity model. These methods succumb to changes in crustal structure that the ray paths travel through before reaching the receiving station which can produce large residual errors. This is of great concern in southeast Alaska where the velocity structure contains significant lateral variations that have a great effect on relocation calculations (Page *et al*, 1986; Fogleman, 1993). For these reasons the Double Difference method introduced by Waldhauser and Ellsworth (2000) (hypoDD) was chosen for this study.

The hypoDD program uses the double difference algorithm which is based on the Joint Hypocenter Determination method (JHD) (Waldhauser, 2000). The logic behind the double difference algorithm is that by simultaneously solving for the location of at least two earthquakes relative to each other the effects of velocity structures can be reduced. This holds true as long as some geophysically meaningful parameters are applied; that is if the relative distance between two earthquakes is smaller than the distance from the earthquakes to the recording station and no larger than the heterogeneous velocity components in the crust. Such constraints allow for the ray path of both earthquakes to travel through the same medium from source to station therefore reducing errors caused by un-modeled velocity changes.

To prepare data for use in hypoDD a program called ph2dt must first be used. This program filters out events that are not to be considered in the hypoDD calculation due to a lack of station information or if they are unable to meet nearest neighbor requirements. In

order to establish a neighbor, a search radius is set that permits hypocenters to be paired. These pairs are linked to other pairs to create clusters that share phase inputs from similar stations whose distances from the events are limited by a distance parameter. The number of phases recorded at each station for each event pair determines if a pair is weak or strong. To establish a strong pair, the minimum number of phases recorded at a station must be at least eight in order to satisfy the number degrees of freedom for each pair: latitude, longitude, depth and time. If the minimum degrees of freedom are not met at a station the system becomes ill-conditioned. Weak links are common in earthquake location studies and are, consequently, still used. In order to reduce the effects that a weak link(s) can have on a system a damping factor is introduced to limit excessive hypocentral adjustments. The magnitude of the damping factor largely depends on the condition number (CND) that is produced after each iteration. The CND is the ratio between the largest to smallest eigenvalue of the iteration results. Waldhauser (2001) suggests a damping factor within the range of 1-100 to produce a CND within 40-80. Because CNDs are calculated, multiple hypoDD calculations are recommended in order to adequately observe the system's behavior and choose appropriate damping factors.

The size of the catalog and number of earthquakes to be relocated dictate which inversion method is used in hypoDD. The Conjugate Gradient Least Squares Method (LSQR) is optimal for datasets that are large with a considerable number of clusters spread over large distances. This method also solves the damped least squares problem, but consequently underestimates errors resulting in moderately reliable epicenter locations and poor depth resolution (Paige & Saunders, 1982; Waldhauser and Ellsworth, 2000).

SVD (Singular Value Decomposition) is optimal for smaller, more robust datasets within a smaller area. This method requires that the system is well-determined; hence tight spacing between sources relative to a nearby station is necessary. This method provides reliable solutions, but is limited to the number of events the computational algorithm can handle.

HypoDD functions in two essential loops after an initial location is established with a given set of parameters. The first loop is the power behind hypoDD; it takes partial derivatives of event travel times with respect to their locations and origin times. The changes in location, residuals, and partial derivatives calculated by the inversion are then looped into the inversion matrix to achieve a better fit between the model and the data. During calculations, the data are continually reweighted to control observations with large residuals. If an event falls out of the specified distance range during calculations it is deleted. In general, the result after each iteration is a shift of residuals toward convergence. Convergence is usually achieved in 5 iterations with LSQR and in 3 with SVD. Positive residuals indicate that low velocity zones are not accounted for in the velocity model, whereas negative residuals are an indication of high velocity zones (Waldhauser, 2001).

Overall, hypoDD is very effective in locating large quantities of earthquakes of all magnitudes. This being said, there are limitations that the algorithm cannot account for. The most common is the availability of stations and their distribution. The availability of stations and their geometry can cause large variations in hypocenter location. Picking errors are also of great concern when working with low magnitude earthquakes considering that phase arrivals are more difficult to discern.

If a redundant earthquake(s) was not filtered out from the dataset it will act as a pair with itself causing a significant reduction in the residual output after each iteration and causing the

system to converge earlier. In this case, both the LSQR and SVD solutions will be erroneous. For this reason, spherical distances between catalog epicenters were checked with a spherical coordinate program. Distances between the AEIC and redundant CNDC epicenters ranged from 0 to 388 km. Large location differences between hypocenters are due to variations between chosen catalog velocity models or that the earthquakes were not redundant; they simply occurred in the range of ±5 seconds of the AEIC earthquake within the study region. Although hypoDD minimizes the effects of changes in velocity structures it has been shown that if the velocity model does not sufficiently represent the study region a significant amount of error can propagate through calculations (Michelini & Lomax, 2004). If the initial or near surface velocity is high, hypocenters will be pushed up, which could cause shallow events to become airquakes and removed from further iterations. Low velocities push hypocenters down. Considering 1-D velocity models will never truly quantify lateral crustal variations a bias will always exist, but the inability to map the earth in three dimensions exists in all earthquake location methods (Thurber, 2004).

3.2 GetStress Program

Stress orientations were calculated using Robinson's (2001) GetStress program. This program offers a method to estimate the maximum compressive stress (σ_1) and the minimum compressive stress (σ_3) directions from a sparse dataset. By taking into account a number of earthquakes within a region the inversion clusters the best fit stress directions while plotting stress variability within the region as noise. This methodology is well suited for a region such as southeast Alaska where station coverage has been historically insufficient to determine focal mechanisms and consequently, stress tensors. Other advantages to GetStress

are that it bypasses the need to determine focal mechanisms therefore reducing noise and biases introduced by this intermediate step. Finally, the user is able to choose a desired confidence limit.

The theory behind the program assumes that small faults occur in many different directions in tectonically active regions and that small magnitude earthquakes (i.e. M <5) will occur on those faults that have orientations near optimal for Coulomb failure. Robinson refers to the failure criterion as:

$$\tau_{shear} \geq -\mu (\tau_{normal} + P)$$

Where τ_{shear} is the shear stress on the fault, μ is the coefficient of dry friction, τ_{normal} is the normal stress and P is pore pressure. Optimal orientation is referred to as

$$\tau_{shear} + \mu (\tau_{normal} + P)$$

being the maximum for a given orientation. Two optimal orientations are normally the result, therefore σ_1 is calculated with:

$$\beta = 0.5 \tan^{-1} (1/\mu).$$

Consequently, slip on an optimally oriented fault is thought to occur in the direction of maximum shear hence giving an optimal stress solution.

Data for GetStress is retrieved from an optional output file named *hypodd.src* that is activated in the hypoDD output parameter options. The *hypodd.src* file provides the take-off angle and azimuth information needed to model stresses with GetStress. Reformatting and combining *hypodd.src* with the corresponding earthquake phase data (compressive or dilation

P wave arrivals) was done using a set of three Fortran programs provided by Dr. Diane Doser: hugosort.f, srcsort2.f and finsort.f.

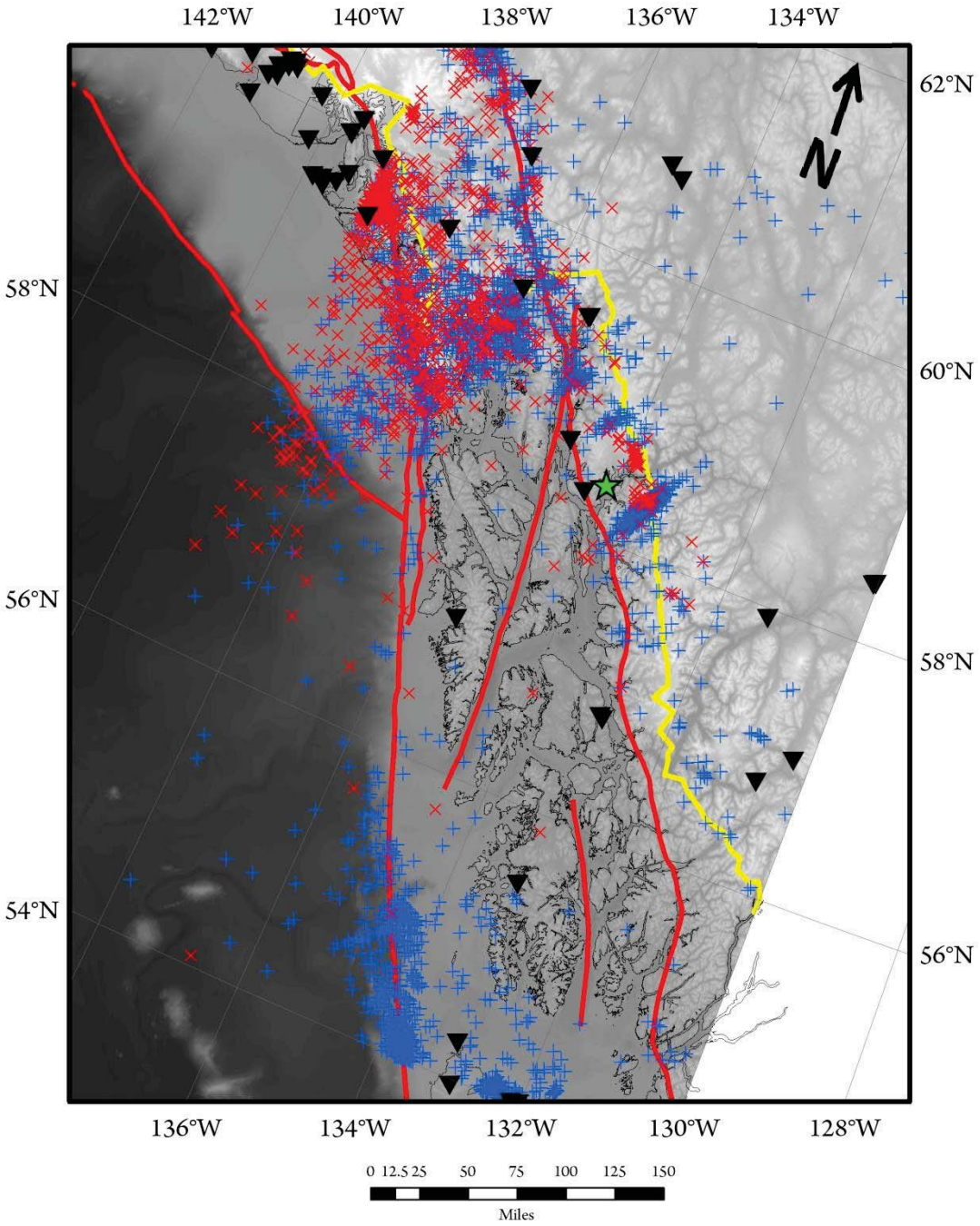

Figure 3-1. Map showing the difference in recorded events between the Alaska Earthquake Information Center (AEIC) and Canadian National Earthquake Database (CNED). Red crosses are from AEIC, blue Xs are CNED. All other symbols and labels are same as Figure 1.

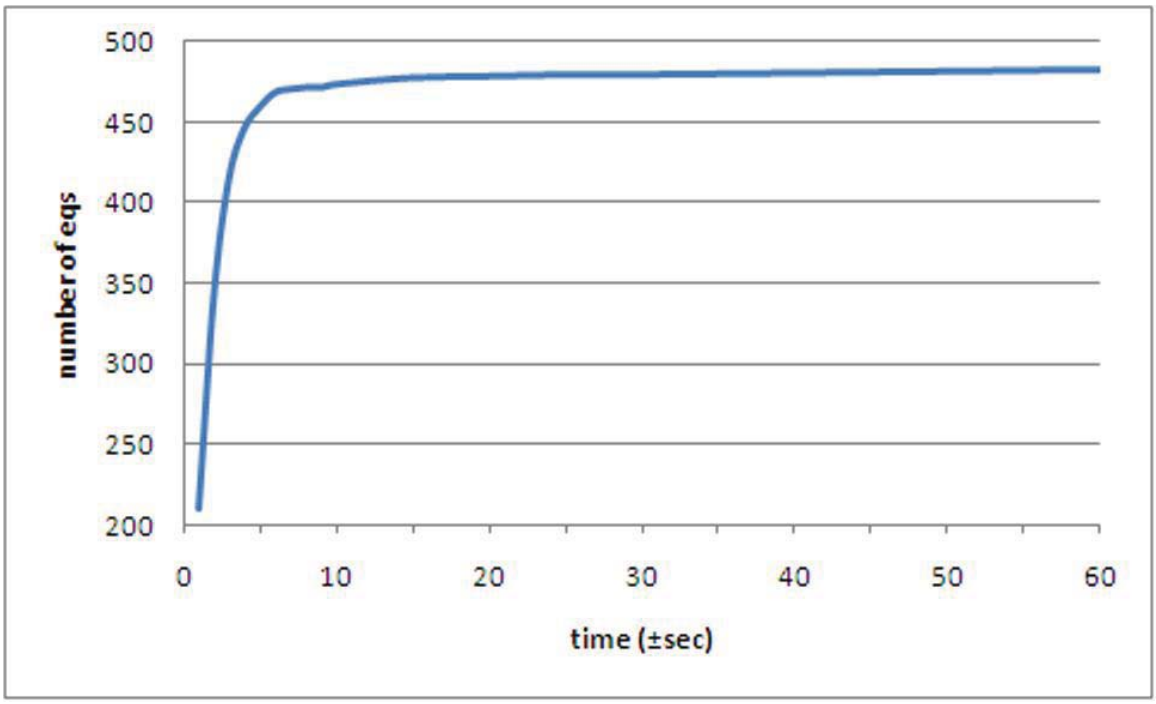

Figure 3-2. Number of duplicate earthquakes identified with increasing time range.

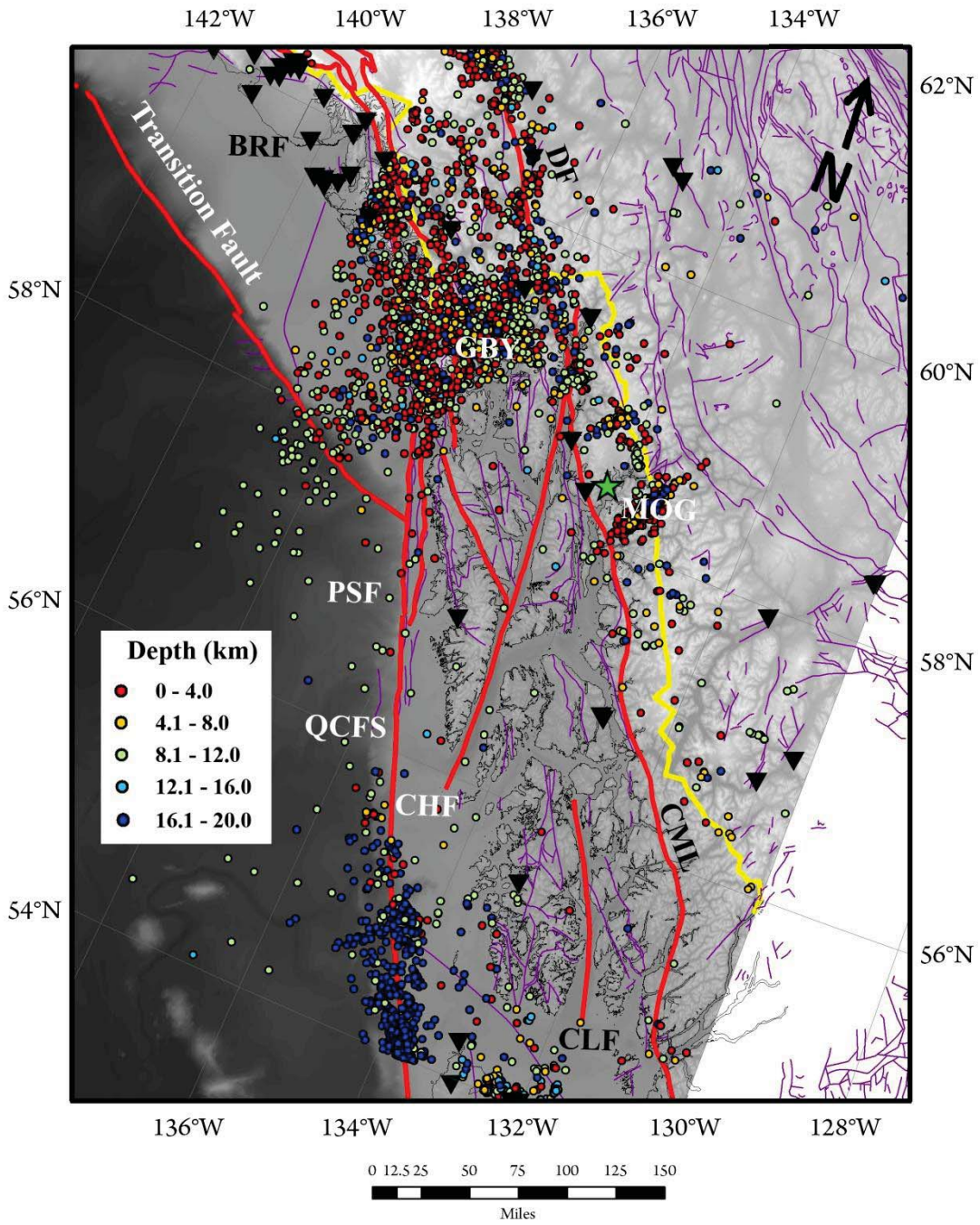

Figure 3-3. Seismicity map showing all earthquake catalog data without duplicates. Purple lines are minor faults. GBY is Glacier Bay – Yakutat; MOG is Mt. Ogden; DF is Denali fault; CML is Coast Mtns Megalineament; CLF is Clarence Strait fault; CHF is Chatham Strait fault; BRF is Border Ranges fault; PSF is Peril Strait fault. All other symbols same as Figure 1-1.

CHAPTER 4

DISCUSSION

4.1 Earthquake relocation results

Earthquake relocations were calculated for the entire study region (SEAK) and two subregions, Glacier Bay-Yakutat (GBY) and Mt. Ogden (MOG). The extents of the subsets were chosen by examining Figure 3-3 with the hope that by capturing areas where earthquakes were more densely located inversion parameters could be modified to better constrain the system and obtain higher confidence results. Due to the lack of available observation data obtained by seismic stations in the area, inversions were calculated with the minimum number of observations, 4, needed to maintain a well determined system. Also, the same input parameters consistently appeared to best decrease residuals (see Table 4-1 and Table 4-2). This was likely caused by the system being overwhelmed by the large number of earthquakes in GBY. The distance between clusters and stations was maximized to include all possible observation information. The most effective parameters to maintain optimal control over the solution while allowing the system to converge were the damping factor (DAMP) and the event separation distance (WDCT).

4.2 Southeast Alaska

Southeast Alaska (SEAK) earthquake relocations were computed seven times, of which *run07* produced the best results (see Table 4-3). The ph2dt program reduced the number of earthquakes to be calculated for this region to 2,025 of the original 4,617 events from the catalogs. From this new pool of earthquakes, 1,434 were able to meet the hypoDD input requirements. Figure 4-1 shows a comparison between catalog events, AEIC and CNED

combined, and those that were successfully relocated. Most of the earthquakes that occurred in the Pacific Ocean and in the mid-west portion of the study region were dropped because of the lack of phase data captured by seismic stations and the large distances between events, limiting connectivity to each other and to seismic stations.

Without question, the majority of clustering occurred in areas where large regional faults are in proximity to heavily glaciated areas, such as GBY and MOG (Figure 4-2 and Figure 4-3). At this scale, communication is apparent between the QCFS and the southern Denali fault. Moderate size ($2< M <4$) earthquakes at depths greater than 16 km appear to form a crude east-west line that bisects northern Glacier Bay. Numerous earthquakes of all depths and magnitudes <3 follow the strike of the northern the QCFS.

The contrast between these two areas is further revealed by examining the regions' magnetic and gravity map, Figures 4-4 and 4-5, respectively. Earthquakes in north Glacier Bay are interspersed within the Chilkat Range magnetic high and gravity low. QCFS earthquakes lie on the relatively lower intensity magnetic anomaly and gravity high of the southern Fairweather Range. The near orthogonal trend of seismicity in north Glacier Bay, compared to that along the QCFS, could be an indicator for inland stress transfer at depths not directly observable at the surface.

Pockets of localized earthquake activity appear throughout the northern areas of the study region. These pockets are generally in proximity to known fault intersections, with the exception of activity near Mt. Ogden, where some east-west lineations appear with lengths ranging from 15 to 60 km. A seismic gap is present near Cross Sound, where the Peril Strait fault meets the QCFS. The Cross Sound area is a place where numerous large magnitude ($M>5$) earthquakes have been reported (Doser and Lomas, 2000; Doser et al., 1997 after Perez and Jacob, 1980). A

seismic gap within a noticeably active seismic region points to stress loading on the Yakutat microplate-North American plate interface. Little more can be analyzed at this scale, for this reason two subregions were selected for further study.

4.3 Glacier Bay and Yakutat

Earthquake relocations for the area between Glacier Bay and Yakutat (GBY) were computed six times from which *run03* produced the best results (see Table 4-3). In this subset, 1,557 of 1,951 earthquakes met hypoDD input requirements. Figure 4-6 is a comparison between catalog and relocated earthquakes. As expected, outlying events were dropped from the relocation process and clusters became more isolated and dense. In this study, GBY has the most seismic stations available at wide angles from each other to record small magnitude seismic activity. As a result, convergence was achieved with fewer iterations and with a fairly small final RMS of 24 msec.

Figure 4-7 and Figure 4-8 show that, as a whole, earthquake patterns reflect those described for SEAK. Both the northern QCFS and the Denali fault have a favorable south to north outline of events. Closer examination reveals that the internal seismic behavior of GBY is populated with small, dense clusters that occasionally merge with one another. The lack of isolation between clusters reveals that this area is either structurally more complex at depth or that phase pick qualities varied enough to drag some events further away from the structure in which they nucleated. Localized internal seismicity does not appear to share the region's distinct north-south trend. Clusters instead tend to have indistinct patterns of earthquakes with varying depths and magnitudes. The lack of coherency in these clusters can possibly be attributed to crustal relaxation from ice mass loss (Freymueller et al., 2008, see Figure 2-8) reactivating dormant

paleofaults that do not mirror the modern geologic structures. Deeper indistinct patterns could be related to corner points of active subsurface faults.

This is further supported by the total magnetic intensity anomaly (TMI) map and Bouguer gravity anomaly map, Figures 4-9 and 4-10, respectively. Both show a complex subsurface made up of juxtaposed anomalies. This is more clear-cut in the magnetic anomaly map where the northern Glacier Bay area, between the Denali and Border Ranges faults, is riddled with high amplitude, short wavelength features associated with Cretaceous granodiorite and ultramafics that have no apparent dominant trend. Immediately to the west of the Border Ranges fault there is a basin-like feature followed by the high amplitude signature of the southern Fairweather Range which runs parallel to the QCFS and its associated seismicity. A north trending paired inflection, peak-trough-peak, occurs on both potential field maps at the exact location of the northern QCFS seismic gap.

From ten cross sections that were attempted in GBY (Figure 4-11), only two were successful in showing apparent seismic behavior for their associated clusters, *gby06* and *gby07*. *gby06* is located northeast of Glacier Bay. The bulk of seismic activity in this cross section occurs at a depth of 10km. From 10km and deeper events tend to be more localized and follow a near vertical pattern. *gby07* is a cross section of events that are distributed along the Denali fault. Looking along strike to the northwest reveals that events occur within a range of 20km. A small concentration of earthquakes, predominantly of M~2 and M~3, are located at near the locking a depth of 10km as reported by Fletcher and Freymeuller (2003).

4.4 Mount Ogden

Mount Ogden (MOG) earthquake relocations were computed eight times; of which *run07* produced the best results (see Table 4-3). In this subset, 688 of 1,098 earthquakes met hypoDD input requirements. Although good seismic station azimuthal control surrounds MOG, the stations are distant (Figure 1-1). For this reason, few earthquakes of $M \leq 2$ were successfully relocated. Figure 4-14 shows a comparison between catalog events and those that were successfully relocated. Earthquakes appear to have drifted closer together within the cluster, while most of the outlying earthquakes were dropped from the calculation.

A long, SW to NE densely populated cluster dominates MOG. Although a surface fault is not mapped, this cluster clearly delineates a seismically active structural feature that follows the Speel River, a drainage stream for the Wright Glacier (Wolf et al., 1997). Figure 4-15, clearly shows three stratified seismogenic zones. Figure 4-16 maps event distribution by magnitude and shows that events of $M \geq 3$ are more frequent near Mt. Ogden and gradually decrease with distance.

MOG crustal anomalies are best detailed with the TMI map, Figure 4-17. High amplitudes in this region can be attributed to Cenozoic dike swarms mapped at the surface by Ford and Brew (1987). The suspected fault is clearly traced by a linear magnetic feature that cuts high amplitude anomalies as it makes its way to the Speer River. A large, low amplitude anomaly is located north of the seismic cluster. This anomaly extends toward the seismic cluster with a pair of NW-SE trending, low amplitude limbs with a few scattered earthquakes on them. The northern limb is of particular interest because no catalog earthquakes were located over it prior to relocation. This suggests that both anomalies are fault related.

Figure 4-18 shows selected depth cross-sections for MOG. Of particular interest is that of *mog1* as shown in Figure 4-19. Laterally, the cluster is concentrated into a space 20 km in length along the Speel River and approximately 10 km wide. Three distinct clusters formed with depths centered at ~3 km, ~5 km, and ~18 km. Although these clusters are well defined, the result shows that hypocentral movement at depth between catalog and hypoDD relocated earthquakes was minimal. This is likely an effect caused by a lack of stations near the MOG clusters. The closest station is located just west of Juneau, approximately 50 km from the Mt. Ogden, well outside of the distance needed to accurately determine focal depths.

Wolf et al. (1997) concluded that the most likely cause for concentrated earthquake activity near Mt. Ogden is due to seasonal increases in pore pressure allowing faults or zones of weakness near failure to slip. Although Wolf et al. (1997) did not have earthquake depths associated with their locations, they mention that the extent of fluid percolation into the fault system near Mt. Ogden is unknown and therefore the effects are speculative at depths where pore pressure increases are questionable. Still, given the region's state of stress due to tectonic loading, the large number earthquake occurrences could be due to a triggering relationship between tectonically induced earthquakes at depths of ~18 km and those at shallower depths.

4.5 Stress tensor calculations and results

Regions for stress tensor computations were selected with two considerations; the amount of first motion data available in a region to enable a successful stress orientation calculation and the general fabric of the region's geologic make up. Overall, first motion data within any cluster is scarce. For this reason, the extent of selected stress regions in SEAK and GBY are large. Focal mechanisms from large magnitude earthquakes and centroid moment tensors (CMT) as reported

by Doser and Lomas (2000) and the Global CMT catalog were used to keep selected regions within an assumed regional stress regime.

A critical parameter in determining stress orientations is the coefficient of dry friction, μ. I selected a value of 0.6 based on the work of Smith and Sandwell (2003) on the southern San Andreas Fault. The logic behind using this number is that the QCFS is similar to the San Andreas Fault. It should be noted that Bufe (2005) used a reduced effective coefficient of friction, μ', of 0.4 and Bird (1996) used 0.17 for studies in Western Canada. The difference is that μ' takes pore pressure in account, while μ does not. Statistical sampling with a coarse resolution of 10° was set for the majority of calculations. Each calculation randomly resampled the data 1000 times and the confidence limit was set to 95%. Table 4-4 shows stress axis results for select stress regions.

4.6 SEAK stress calculations

The stress regions selected for SEAK are shown in Figure 4-20. The goal in selecting stress regions was to capture sufficient data in a small enough area to calculate stess tensors with a high degree of confidence. For SEAK, the amount of first motion data available within the selected stress regions varied between 4 and 136 observations.

Figures 4-21, 4-22, and 4-23 show GetStress output windows for *seak04*, *seak08* and *seak15*, respectively. *Seak04* produced the best result for this region. It shows isolation between σ1 and σ3, but has a low count of observations and wide confidence region for each axis. *Seak08* and *seak15* each had enough data to achieve a solution with high confidence, but neither produced reasonable results. *Seak08* produced a solution which indicates that normal faulting dominates the MOG region. Considering the region's tectonic setting, this result is highly unlikely.

Seak15, which combines stress regions *12* and *14*, had an inconclusive result. The best fit stress axis in this solution show that this stress region is compressive, which is a desirable result. Still, due to the consistent overlapping of confidence regions the solution was also dismissed.

To investigate the possible influence of different stress regimes at varying depths, *seak12* was divided into three different depths; shallow 0-6 km, intermediate 6-14 km, and deep 14-20 km. *Seak12* was chosen because of its proximity to the QCFS, a fault whose stress field has been documented in previous studies. The most promising result was the shallow stress calculation *seak_12_3_s*. As shown in Figure 4-24, this result has a resemblance to the dip-slip type focal mechanism *060688* as reported by Doser and Lomas (2000). Calculations for the deeper sections of *seak12* were both inconclusive due to mixing of stress fields. Overall, results at the SEAK scale show consistent overlapping of stress fields where sufficient data were available to allow variability during the stress inversion.

4.7 GBY subregion stress calcualtions

Stress regions selected for GBY are shown in Figure 4-26. The number of observations in the stress regions varied between 13 and 223. Figure 4-27 shows the GetStress output *gby01*. Although *gby01*only has 25 observations, σ1 and σ3 were well defined. The confidence regions for the each principle axis varies considerably, but remained isolated from one another. The GetStress result shows that both σ1 and σ3 are in a favorable position to represent a strike-slip dominated stress region for *gby01*. Recall Figures 2-9 and 2-10, where Ristau (2007) and Ruppert (2008) calculated stresses that included the *gby01*stress region. Both found that the dominant stress field was predominately compressive or thrust. Note that σ1 for *gby01*is in agreement with their calculations.

Figure 4-28 shows the result for stress region *gby05*. This region was purposely chosen to encapsulate earthquakes the spread through the Border Ranges fault. Some overlapping occurred between confidence regions, but the overall concentration of similar solutions surrounding their respective best fit stress axis allows an acceptable degree of confidence in the stress tensor. By observation of the number of earthquakes available in the stress region, the compressive stress environment that g*by05* represents is heavily weighted to the south. Doser and Lomas (2000) reported that a *M*6.0 strike slip event occurred within the *gby05* stress region. Although results vary between this study result in *gby05* and that of the Doser and Lomas (2000) earthquake, given southeast Alaska's complex stress transfer systems that accompany its tectonic setting, it is not beyond reason to consider the possibility that the fault mechanism varies by earthquake magnitude.

In an attempt to better resolve a stress solution in GBY, stress region *gby6* was divided into different depth intervals. Depth intervals were selected by observation, the more localized regions were isolated into three groups; shallow from 0-8 km, intermediate from 8-13 km and deep >13 km. None were successful in producing a high confidence stress tensor.

4.8 MOG subregion stress calcualtions

Figure 4-26 shows the two stress regions that were chosen in MOG. *Mog1* had 89 observations available, while *mog2* had 31. Despite having a large number of earthquakes within the stress region, the stress tensor solution varied little over iterations and resulted in an extensional stress region. *Mog1's* extensional stress tensor solution contradicts southeast Alaska's overall tectonic signature and the depth cross section, Figure 4-19, which suggests the

fault structure that produced the earthquakes has a near vertical profile indicating either vertical dip-slip or strike-slip movement.

Although *mog2* had fewer observations, the confidence region had a little more scatter and the stress tensor solution was considerably more favorable. The *mog2* stress tensor suggests that a thrust fault is present beneath the Wright Glacier. This result further dismissed the stress tensor solution for *mog1*. Neither region was able to produce higher confidence stress tensors by dividing the earthquakes into different depth intervals.

Table 4-1. HypoDD input parameters.

	SEAK	GBY	MOG
IDAT (data type: catalog data)	2	2	2
IPHA (pahse 1=P, 2=S, 3=P & S)	3	3	3
DIST (max. dist (km) event cluster-sta)	10000	10000	10000
OBSCT (# of obs per catalog data, 0=no min)	0	0	0
ISTART (intial location, 2=catalog)	2	2	2
ISOLV (1=SVD, 2=LSQR)	2	2	2

Table 4-2. HypoDD weighting input parameters.

	SEAK *run07*		GBY *run03*		MOG *run07*	
	set 1	set 2	set 1	set 2	set 1	set 2
NITER (number of iterations)	5	5	5	5	5	5
WTCTP (weight for P picks)	2.0	1.0	2.0	0.5	2.0	0.5
WTCTS (weight for S picks)	1.0	0.1	1.0	0.1	1.0	0.1
WRCT (cutoff threshold for outliers)	3.0	0.5	3.0	0.5	3.0	0.5
WDCT (max. event seperation dist)	10	10	10	10	10	5
DAMP (damping factor)	80	40	50	30	70	60
CID (cluster to relocate, 0=all)	0		0		0	
ID (ids of events, blank=all)	(all)		(all)		(all)	

Table 4-3. HypoDD output report from selected runs. Complete hypoDD reports listed in Appendix Table 4-1 *seak run07*, Table 4-2 *gby run03*, and Table 4-3 *ogden run07*. See Section 3.2 for CND explanation.

	SEAK *run07*		GBY *run03*		MOG *run07*	
	set 1	set 2	set 1	set 2	set 1	set 2
NITER (number of iterations)	5	5	5	5	5	5
RMSCT (ms)	35	44	22	29	88	97
DX (m)	41	31	45	23	87	44
DY (m)	48	35	36	22	120	60
DZ (m)	36	25	26	14	49	25
DT (ms)	3	2	2	1	5	3
CND (condition number)	25	54	35	61	41	39

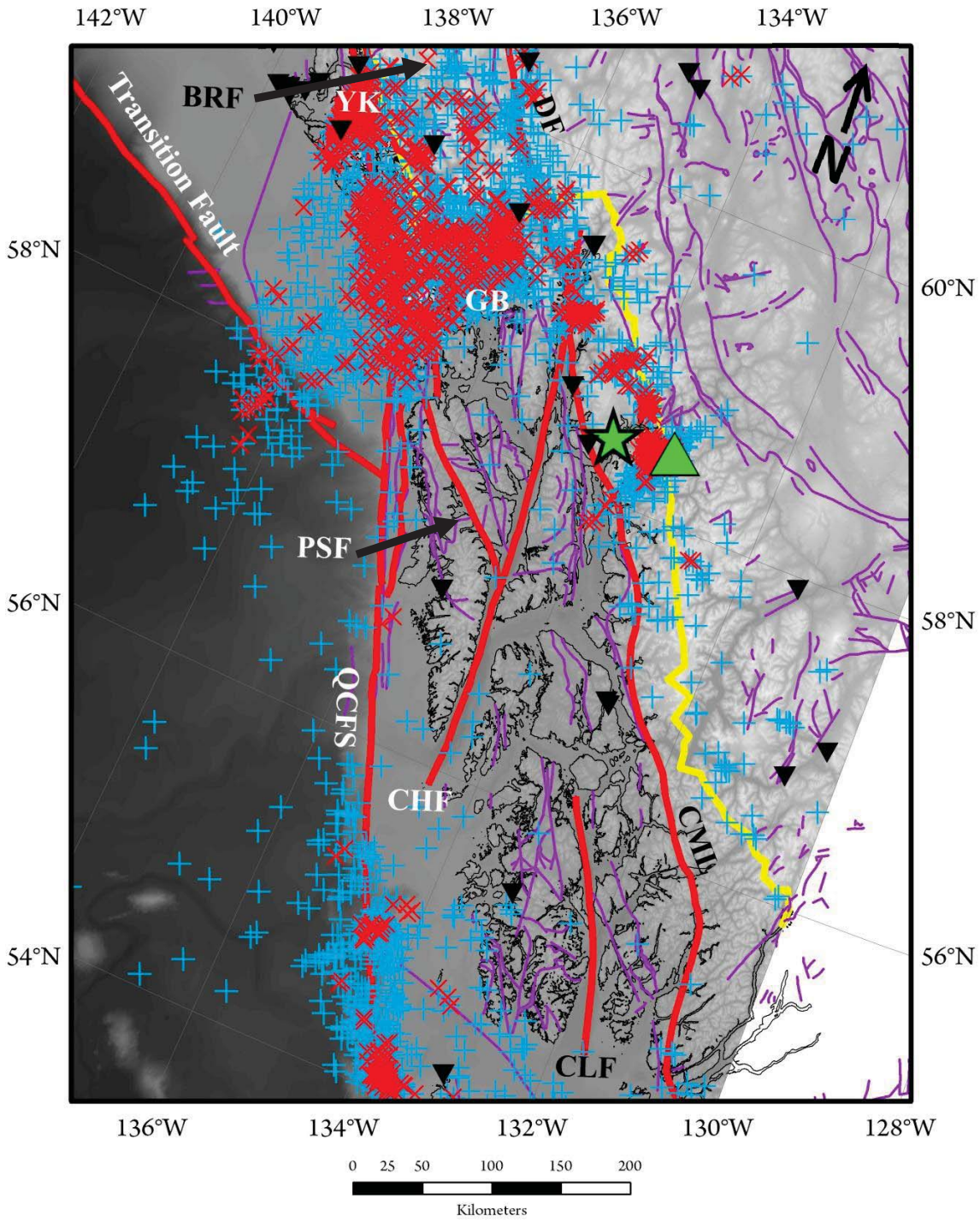

Figure 4-1. SEAK plot comparison of catalog and relocated earthquakes. Blue crosses are catalog earthquakes locations, red X's are relocated; major faults are red lines; national boundary is yellow, black triangles are seismic stations; green star is Juneau; green triangle is Mt. Ogden; GB is Glacier Bay; YK is Yakutat; PSF is Peril Strait Fault; CHF is Chatham Strait Fault; CLF is Clarence Strait Fault; BRF is Border Ranges Fault; CML is Coast Mtns. Megalineament; QCFS is Queen Charlotte-Fairweather Fault system. Faults from Plafker et al. (1994).

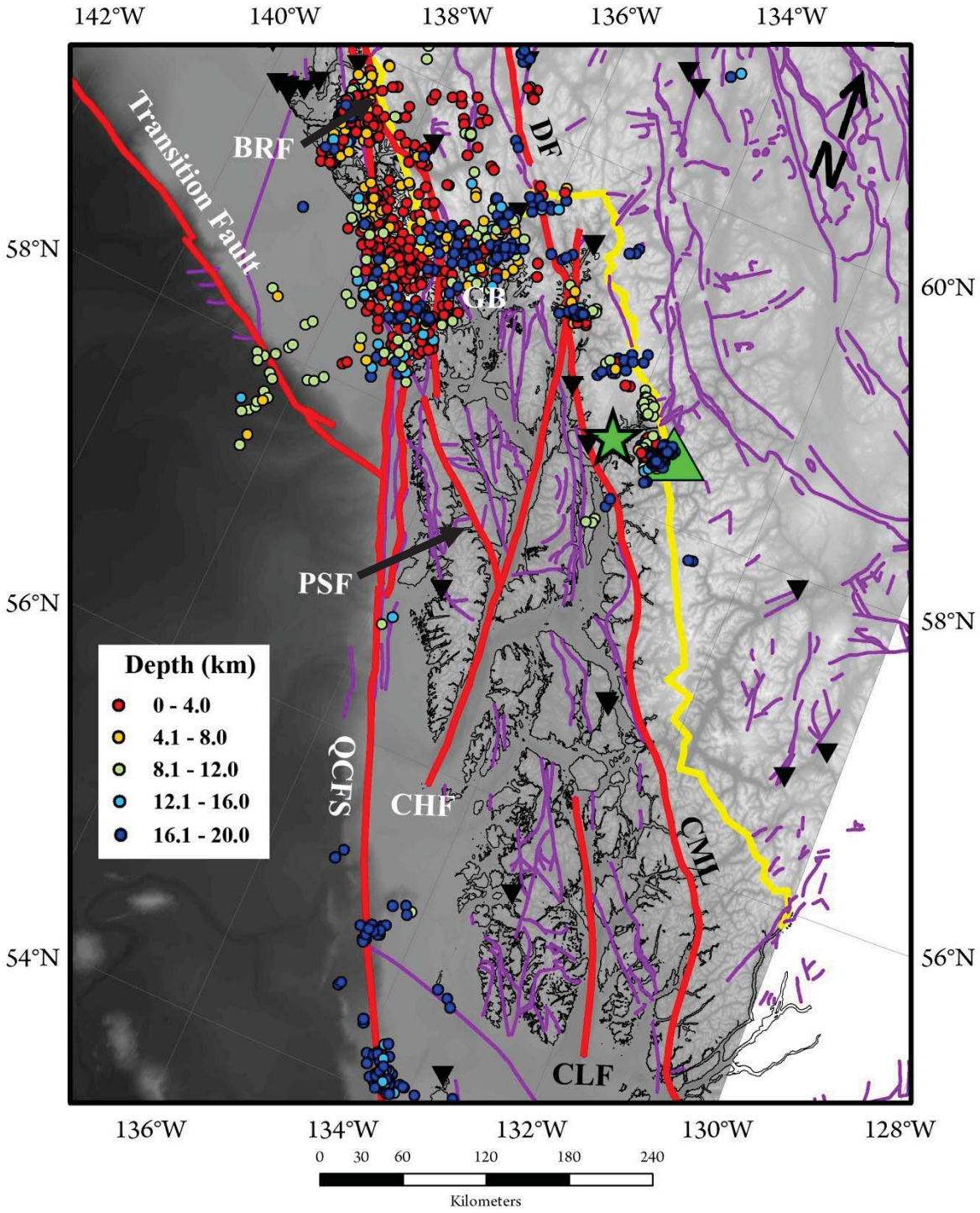

Figure 4-2. SEAK relocated earthquakes sorted by depth. Symbols same as Figure 4-1.

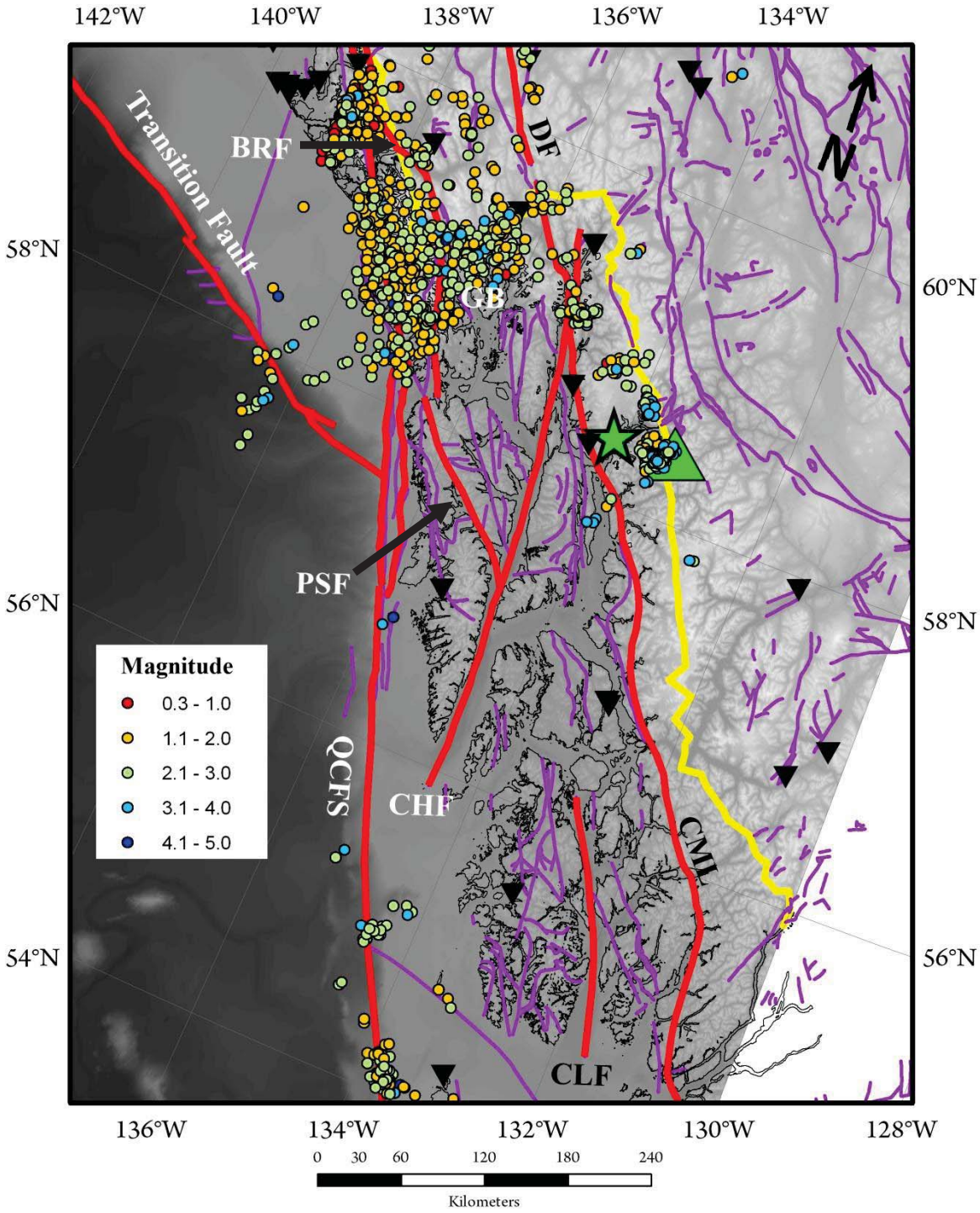

Figure 4-3. SEAK relocated earthquakes sorted by magnitude. Symbols same as Figure 4-1.

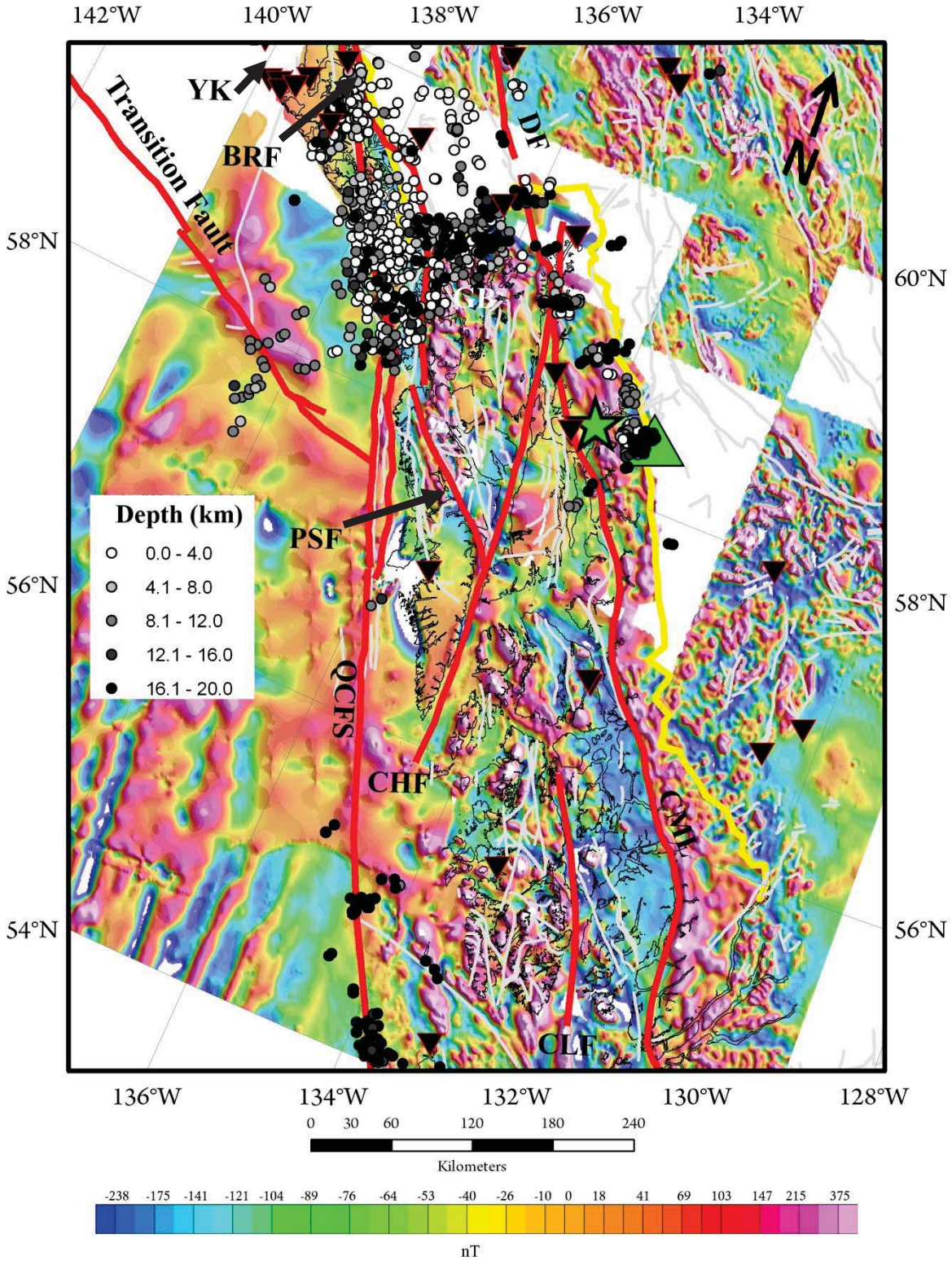

Figure 4-4. SEAK relocated earthquakes sorted by depth with total magnetic intensity map. Symbols same as Figure 4-1.

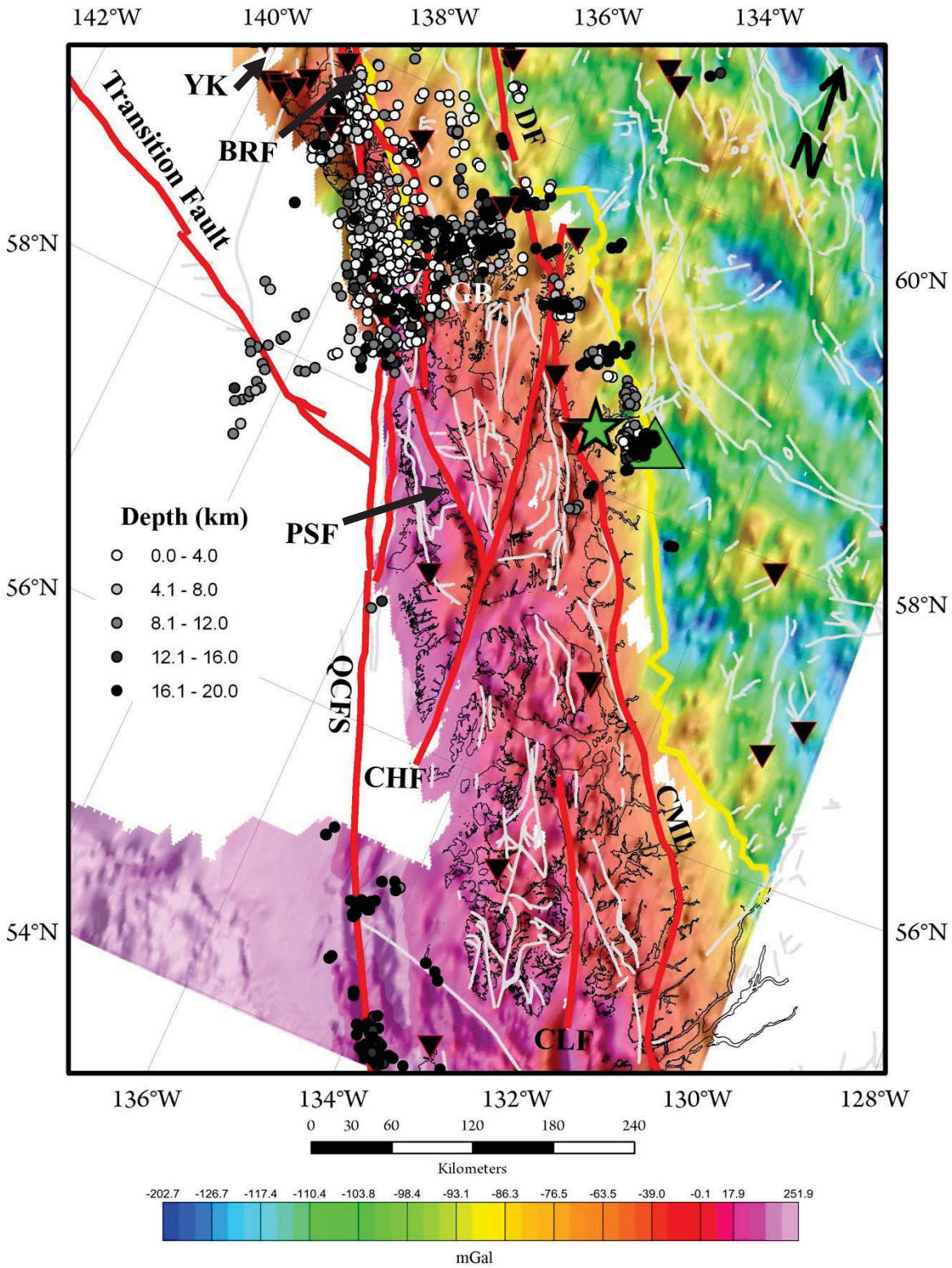

Figure 4-5. SEAK relocated earthquakes sorted by depth with Bouguer gravity anomaly map. Symbols same as Figure 4-1.

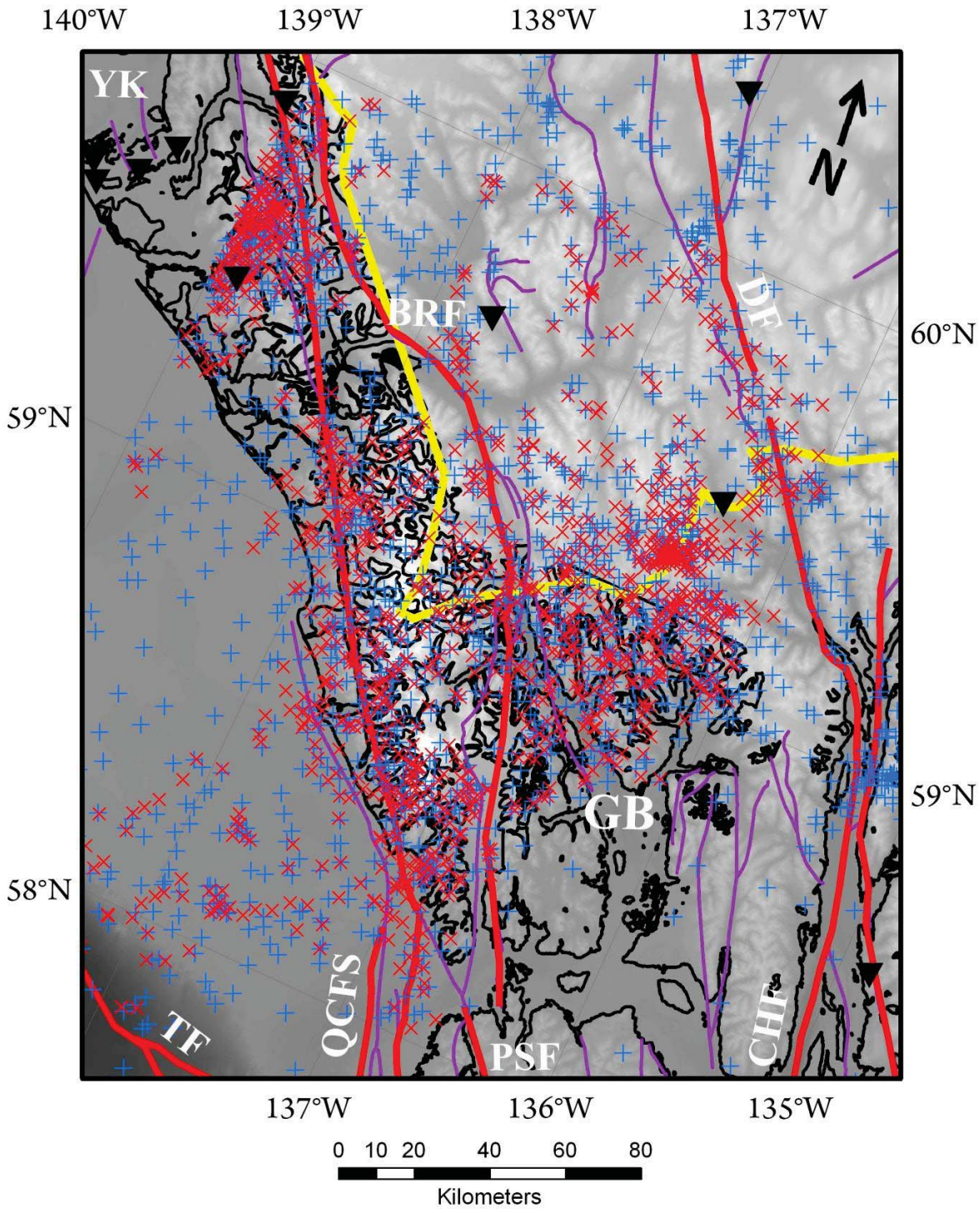

Figure 4-6. GBY plot comparison of catalog and relocated earthquakes. Blue crosses are catalog earthquakes locations, red X's are relocated; major faults are red lines; national boundary is yellow, black triangles are seismic stations; TF is Trasition fault; GB is Glacier Bay; YK is Yakutat; QCFS is Queen Charlotte-Fairweather Fault system; PSF is Peril Strait Fault; CHF is Chatham Strait Fault; BRF is Border Ranges Fault;. Faults from Plafker et al. (1994).

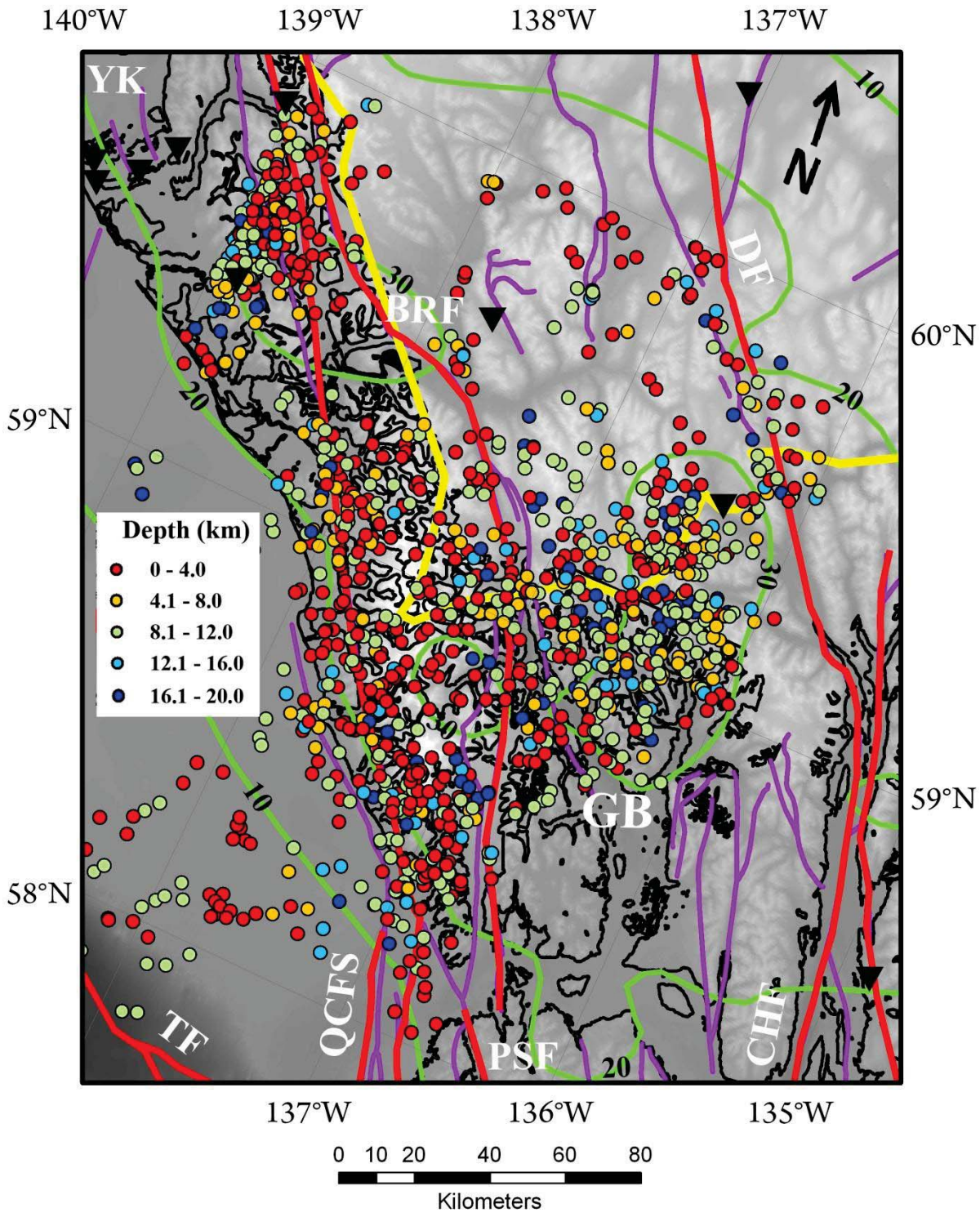

Figure 4-7. Map of GBY with relocated earthquakes sorted by depth. Green contours are uplift rates in mm/yr as reported by Freymueller (2008). Symbols same as Figure 4-6.

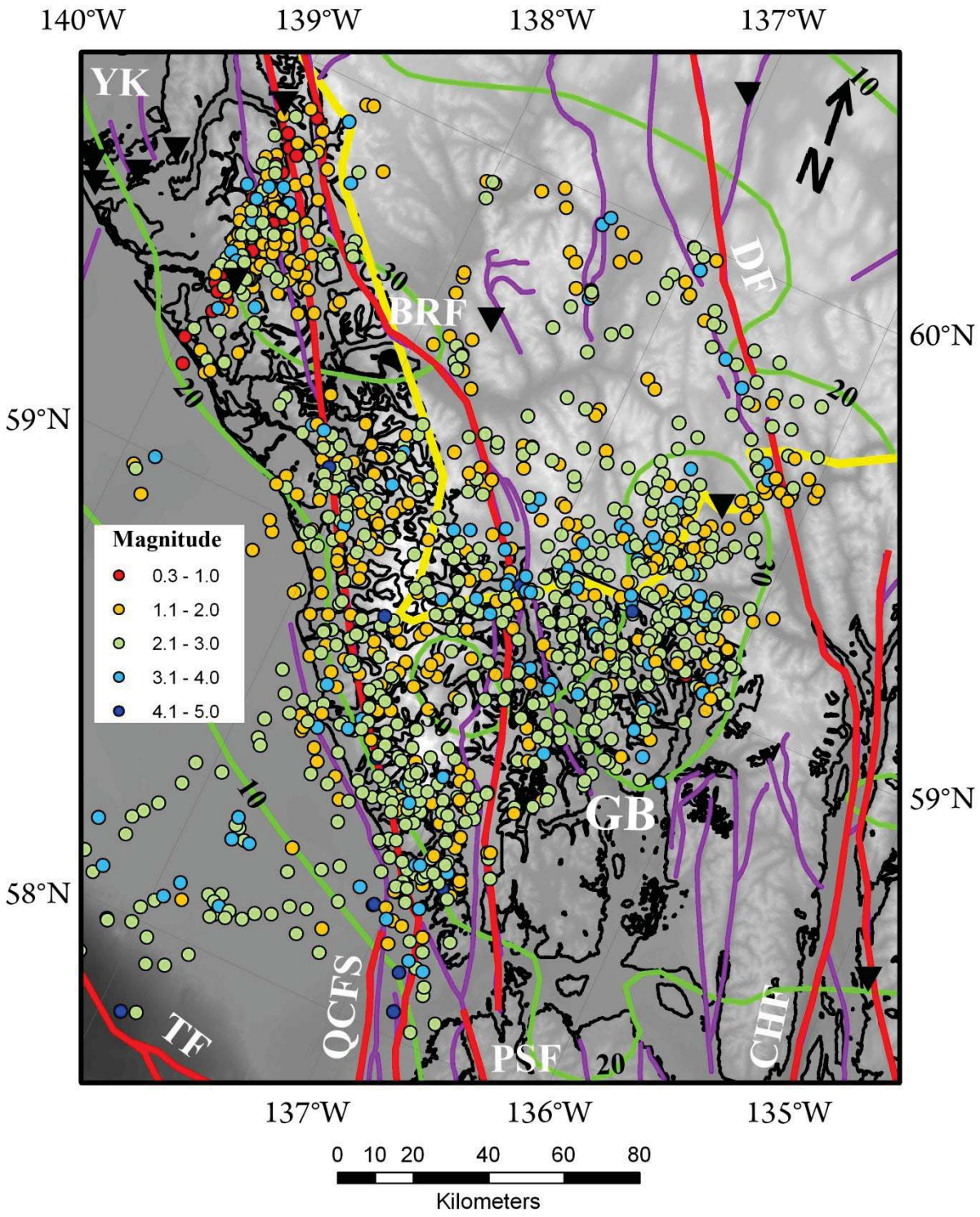

Figure 4-8. Map of GBY with relocated earthquakes sorted by magnitude. Green contours are uplift rates in mm/yr as reported by Freymueller (2008). Symbols same as Figure 4-6.

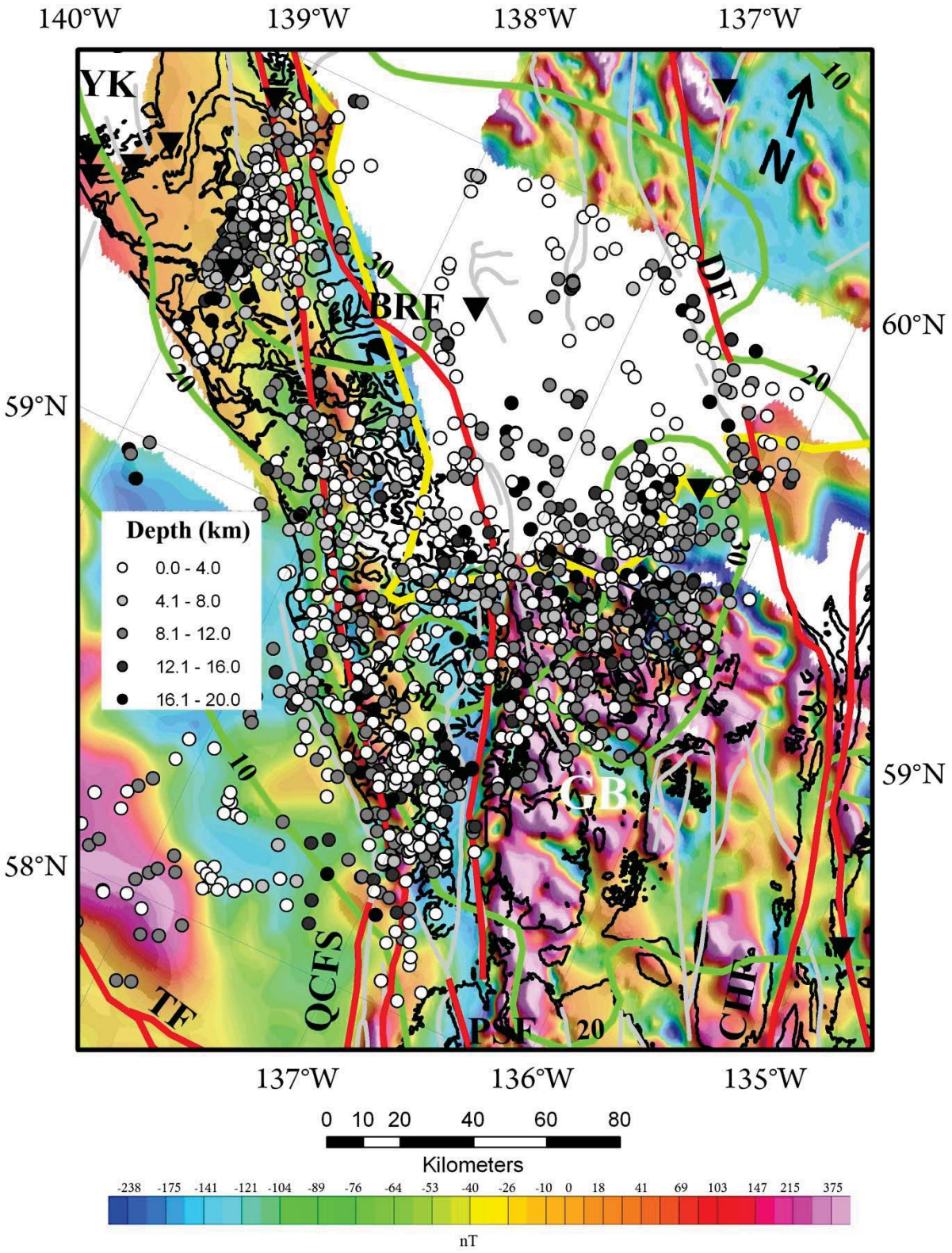

Figure 4-9. GBY total magnetic intensity map with relocated earthquakes sorted by depth. Green contours are uplift rates in mm/yr as reported by Freymueller (2008). Symbols are same as Figure 4-6.

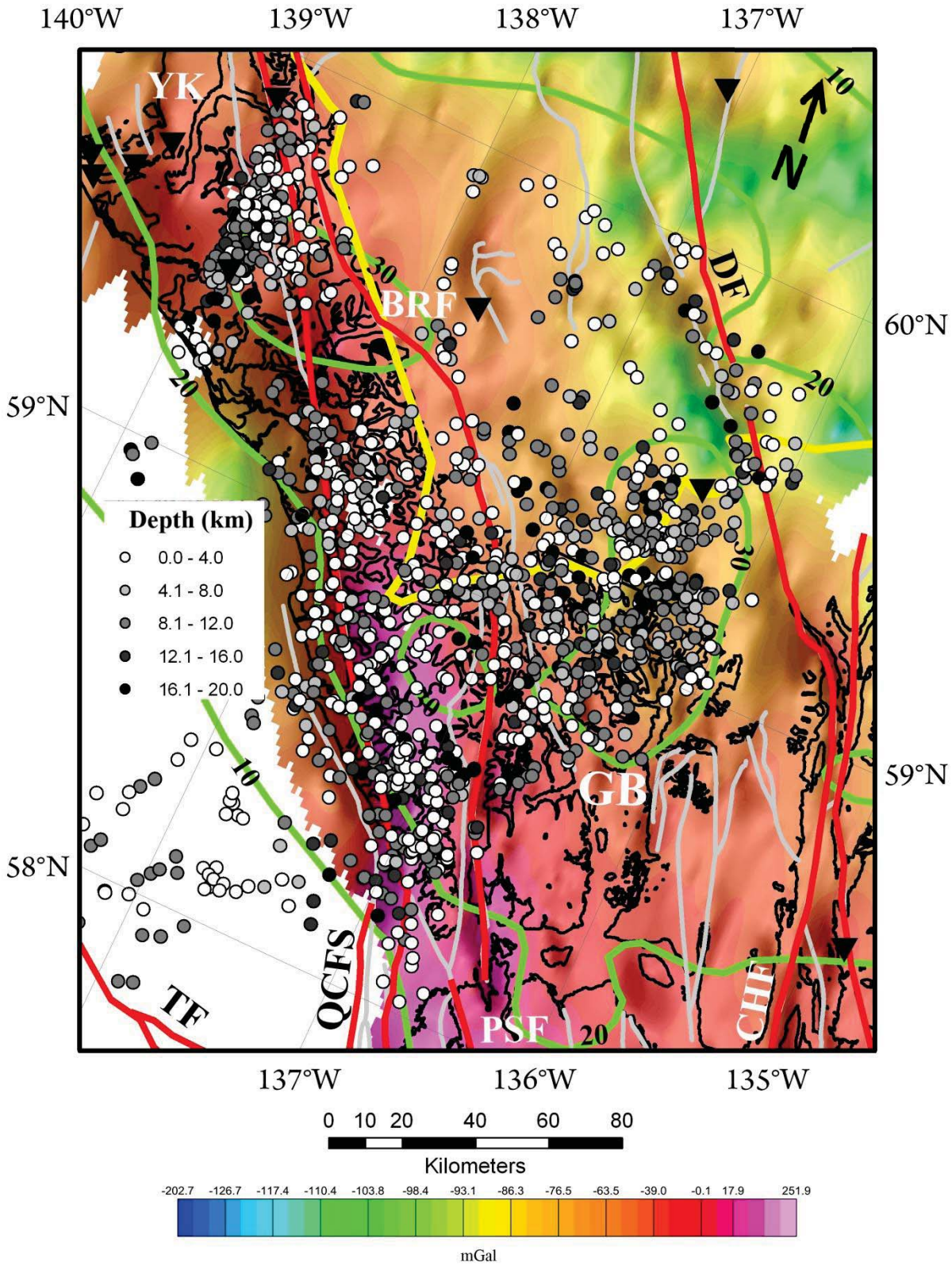

Figure 4-10. GBY Bouguer gravity anomaly map with relocated earthquakes sorted by depth. Green contours are uplift rates in mm/yr as reported by Freymueller (2008). Symbols are same as Figure 4-6.

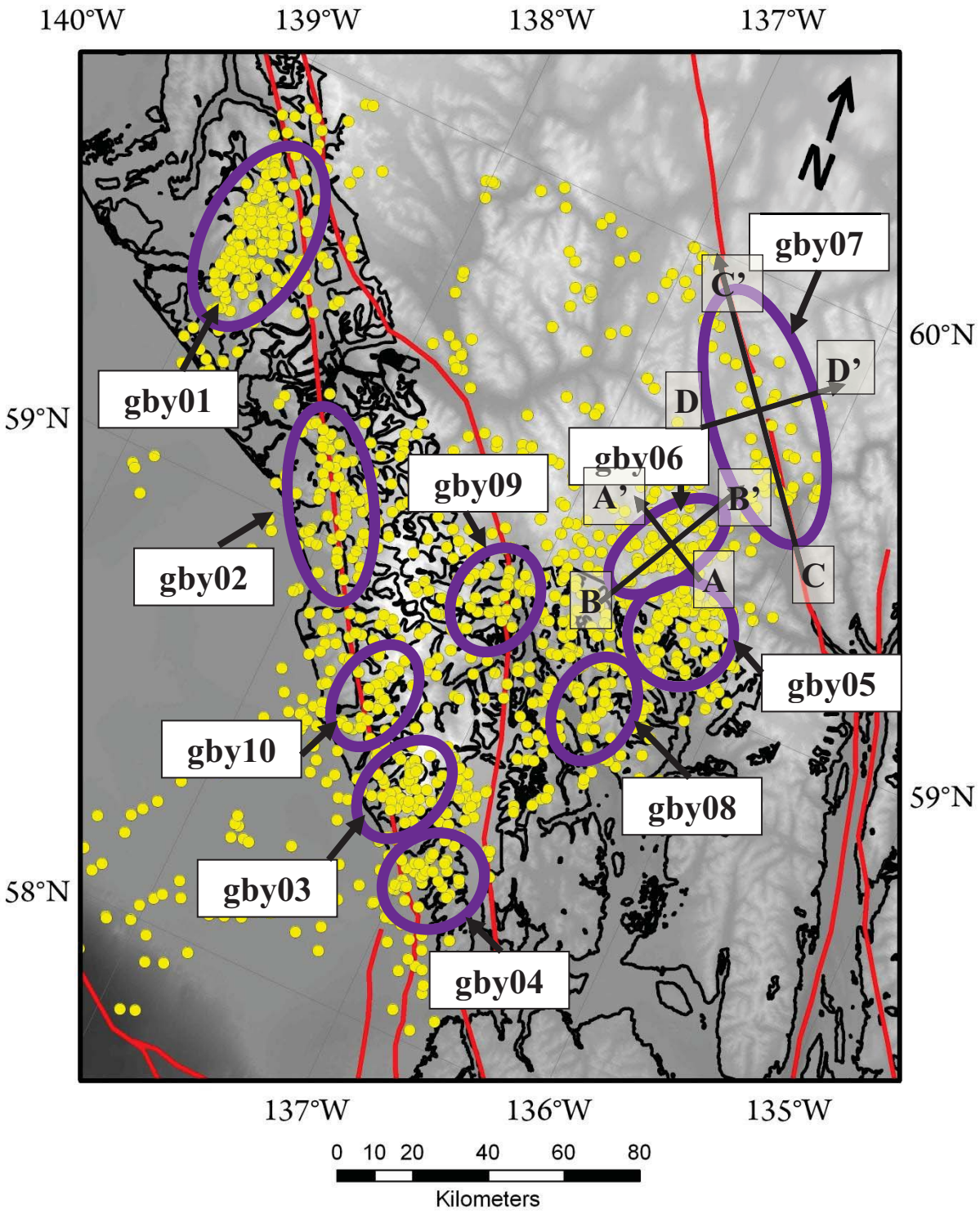

Figure 4-11. Simplified map showing selected clusters for cross-sections in GBY.

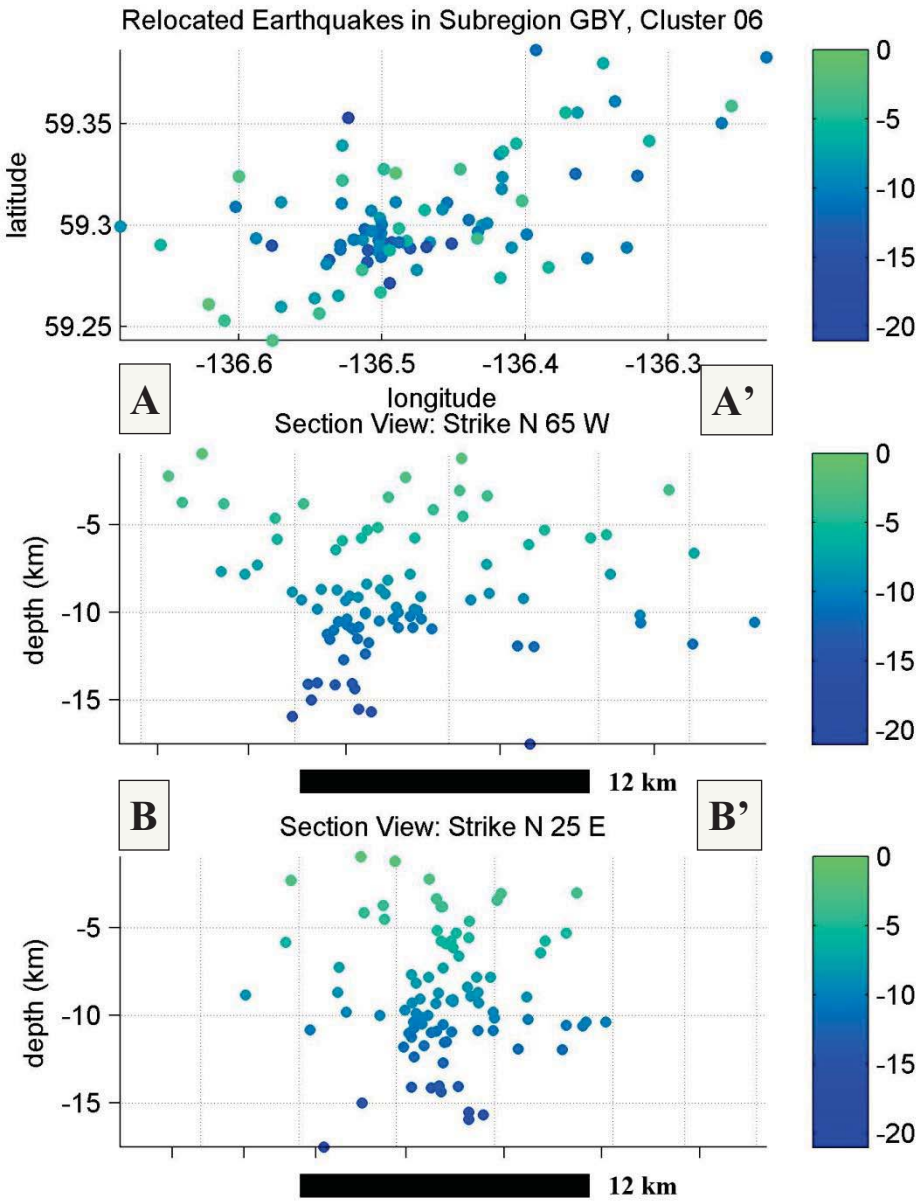

Figure 4-12. Depth cross section for *gby06*.

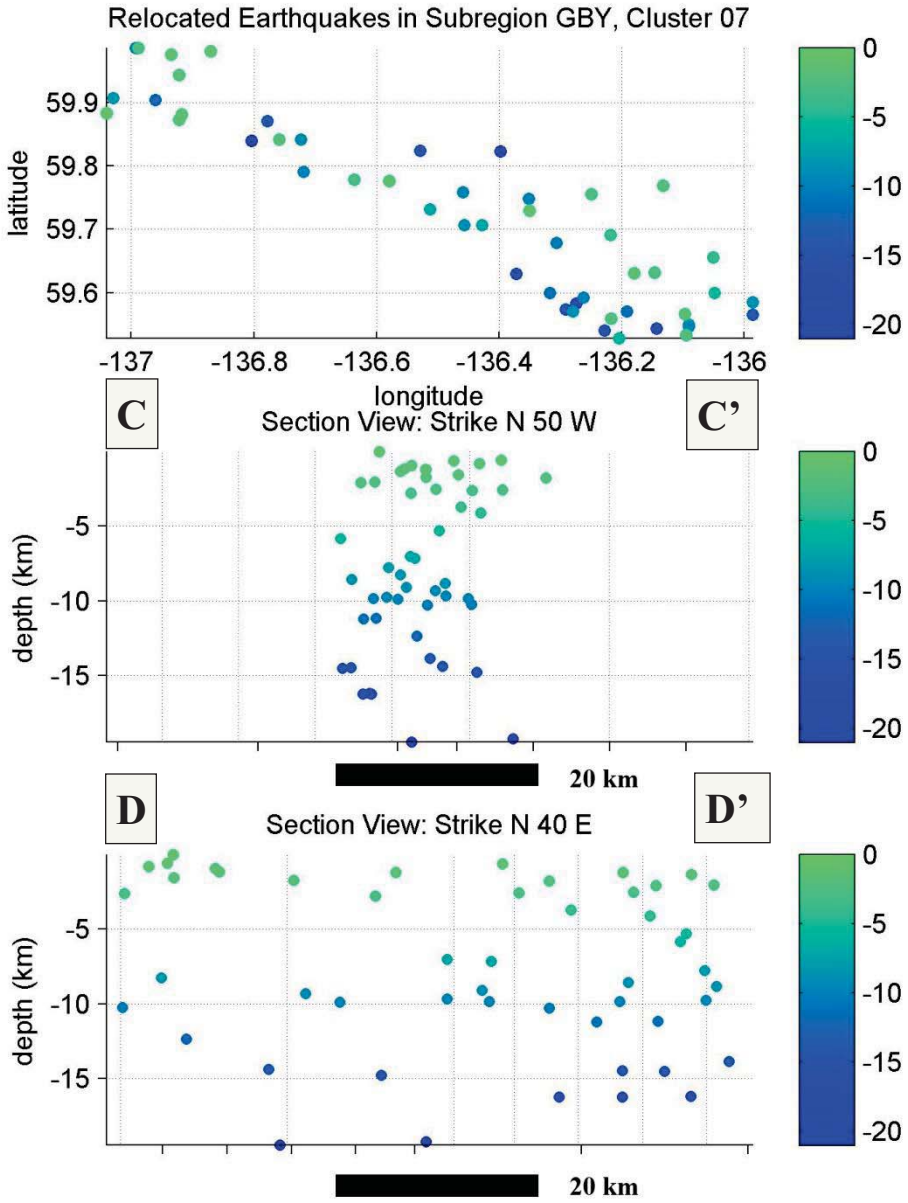

Figure 4-13. Depth cross section for *gby07*.

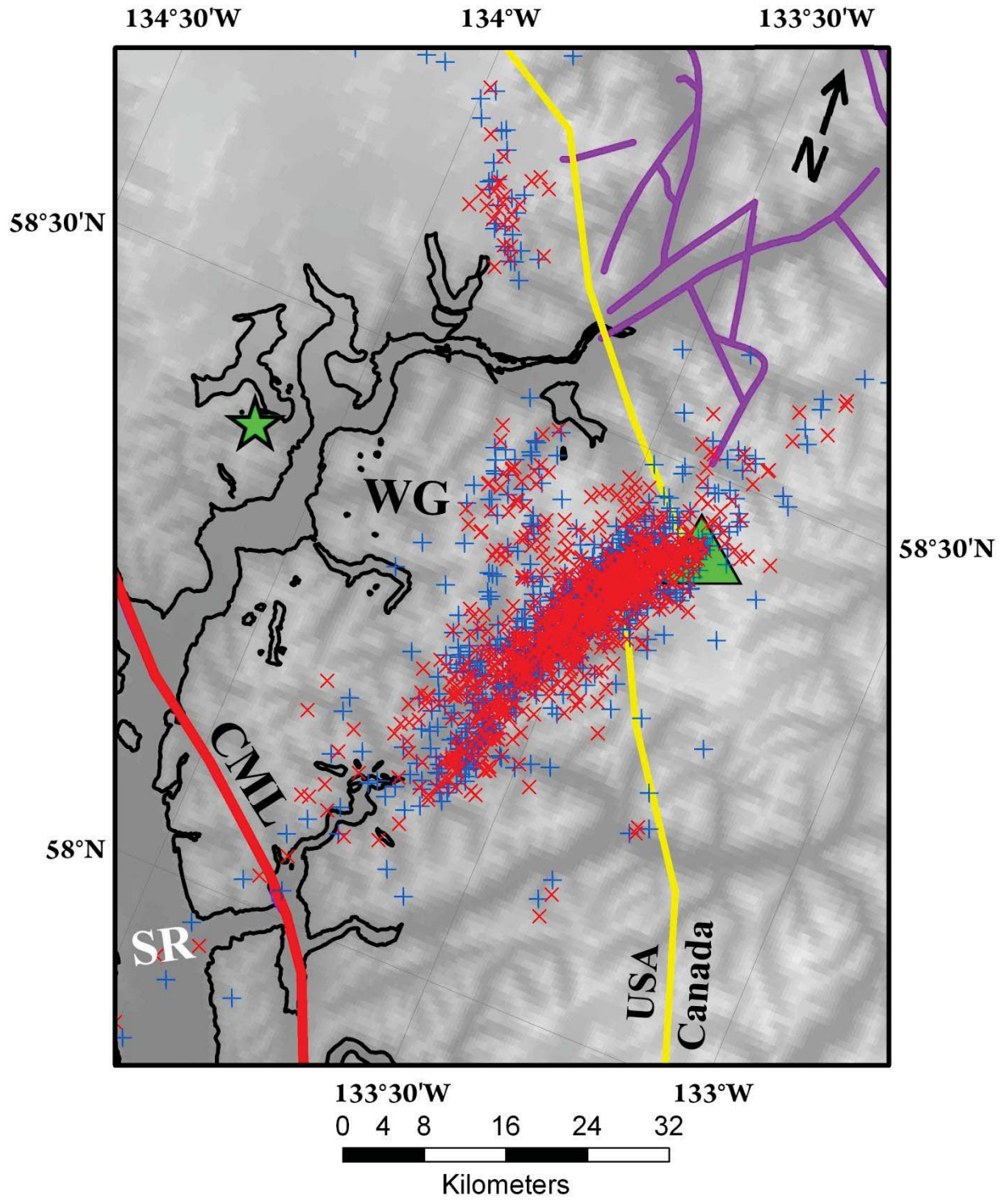

Figure 4-14. Map showing duplicates difference between catalog and relocated earthquakes in the MOG region. Blue crosses are catalog earthquake locations; red Xs are relocated earthquakes; green star is Juneau; green triangle is Mt. Ogden; purple lines are known faults; yellow is international boundary; SR is Speel River, WG is Wright Glacier; CML is Coast Mtns Megalineament.

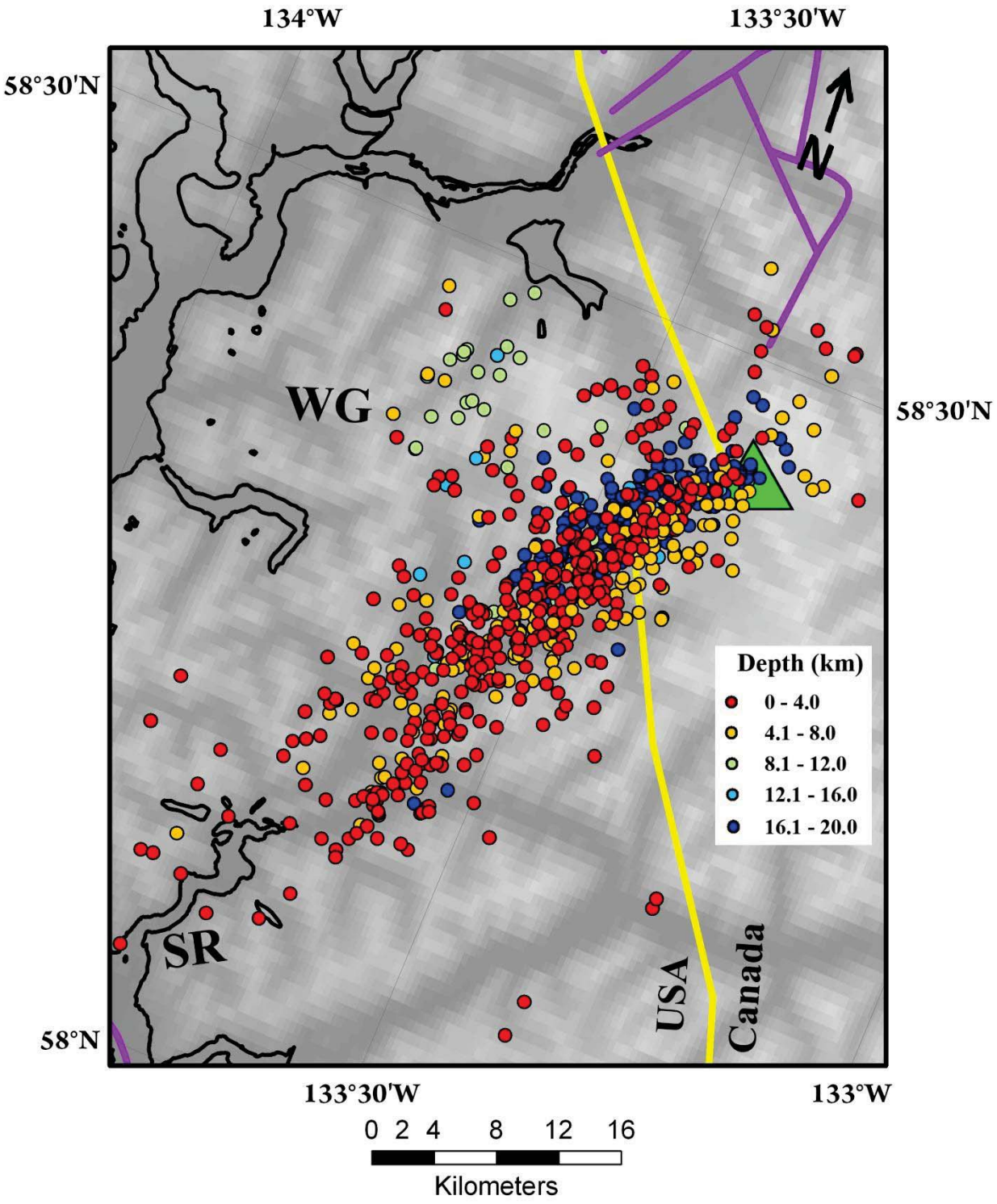

Figure 4-15. Map showing depth sorted relocated earthquakes in MOG area. Symbols same as Figure 4-14.

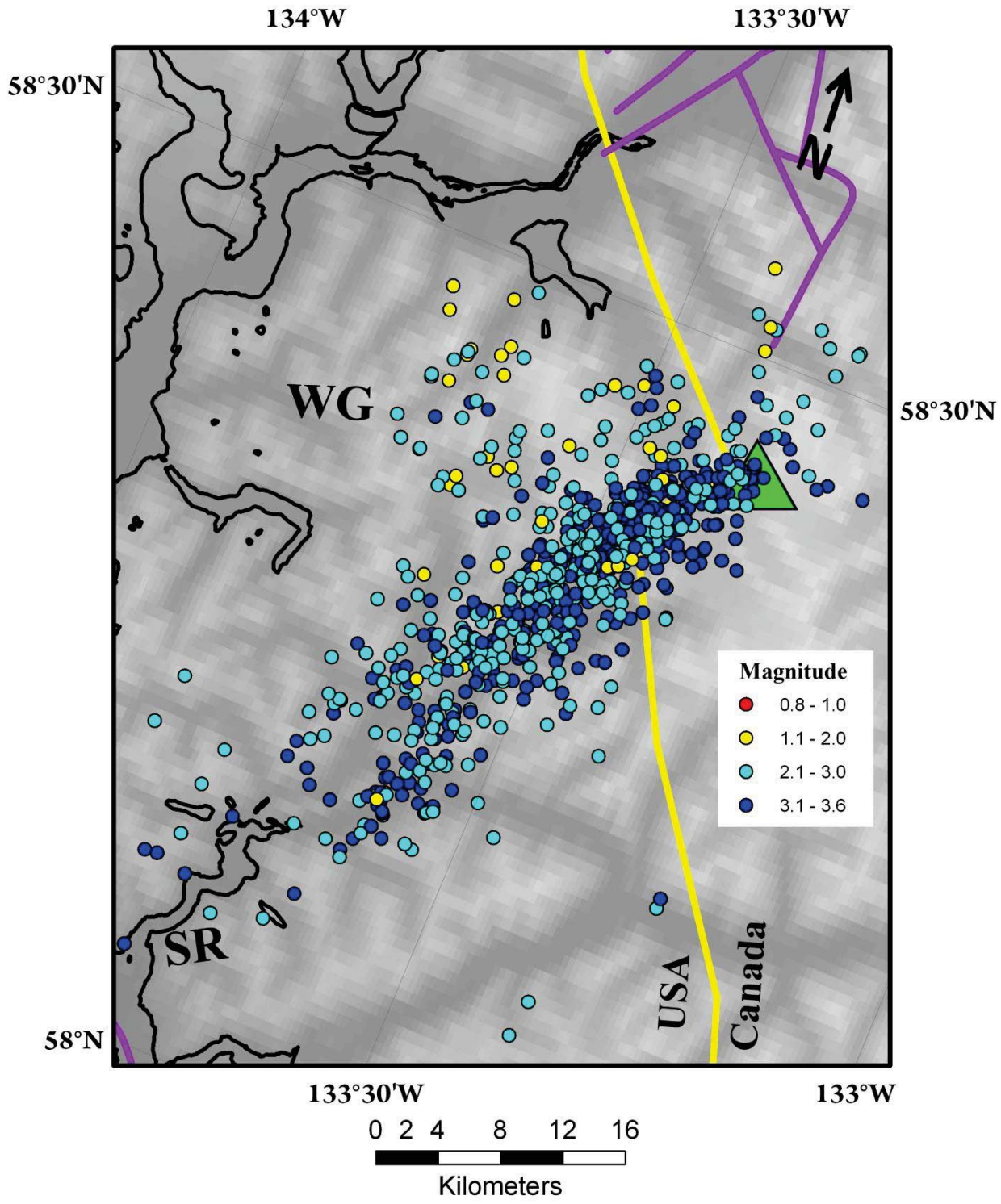

Figure 4-16. Map showing magnitude sorted relocated earthquakes in MOG area. Symbols same as Figure 4-14.

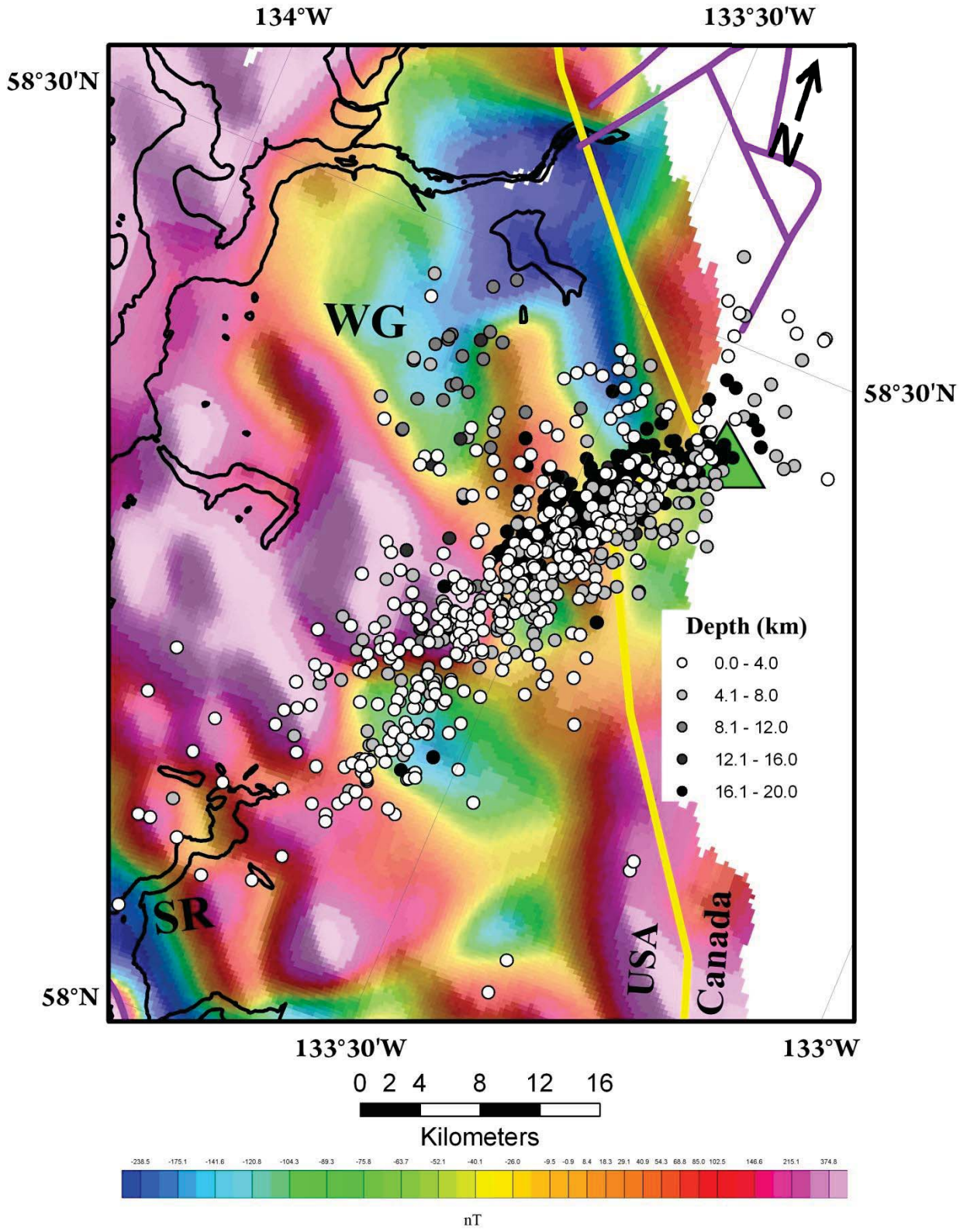

Figure 4-17. MOG total magnetic intensity map showing depth sorted earthquakes. Symbols same as Figure 4-14.

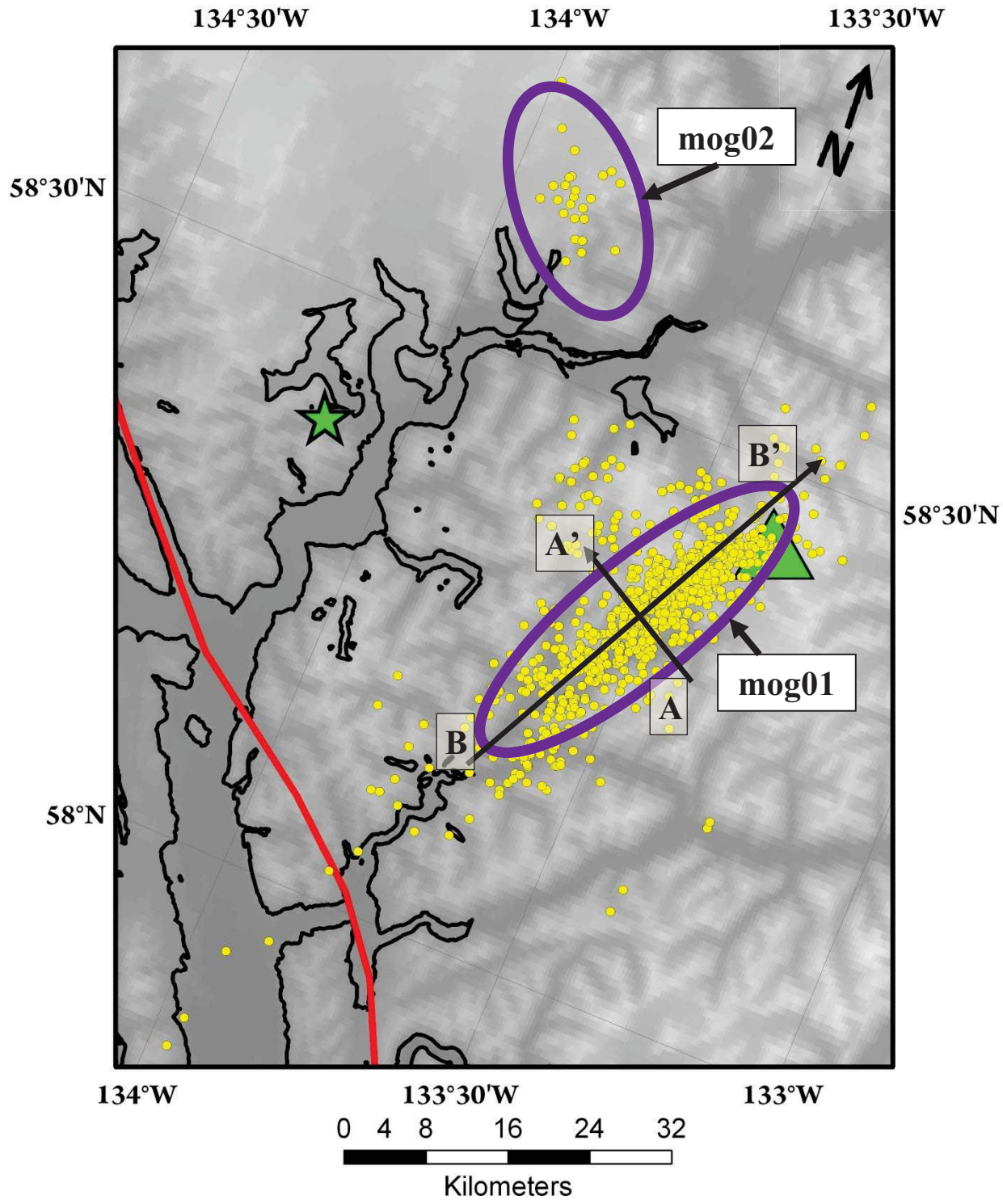

Figure 4-18. Simplified map showing selected clusters for MOG.

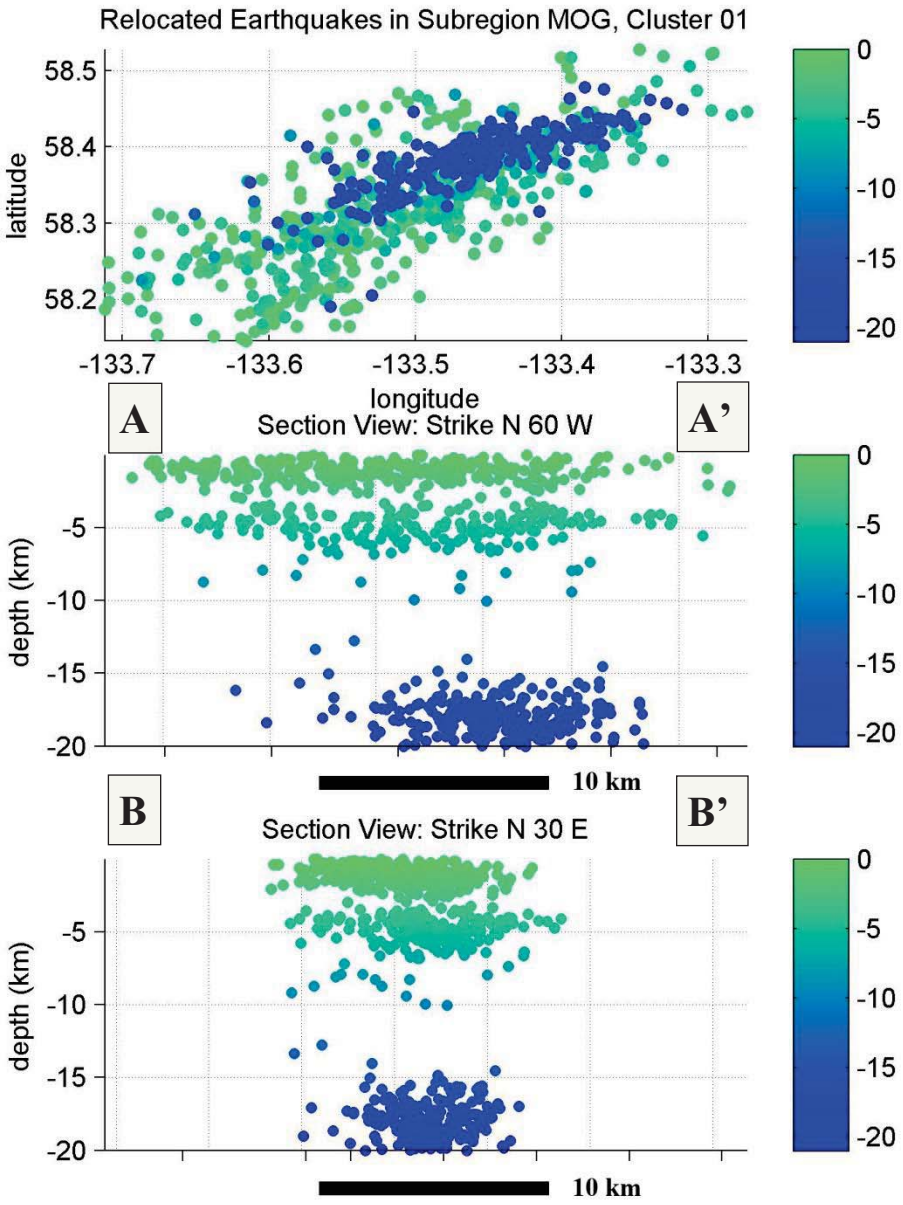

Figure 4-19. Cross section for MOG cluster 01.

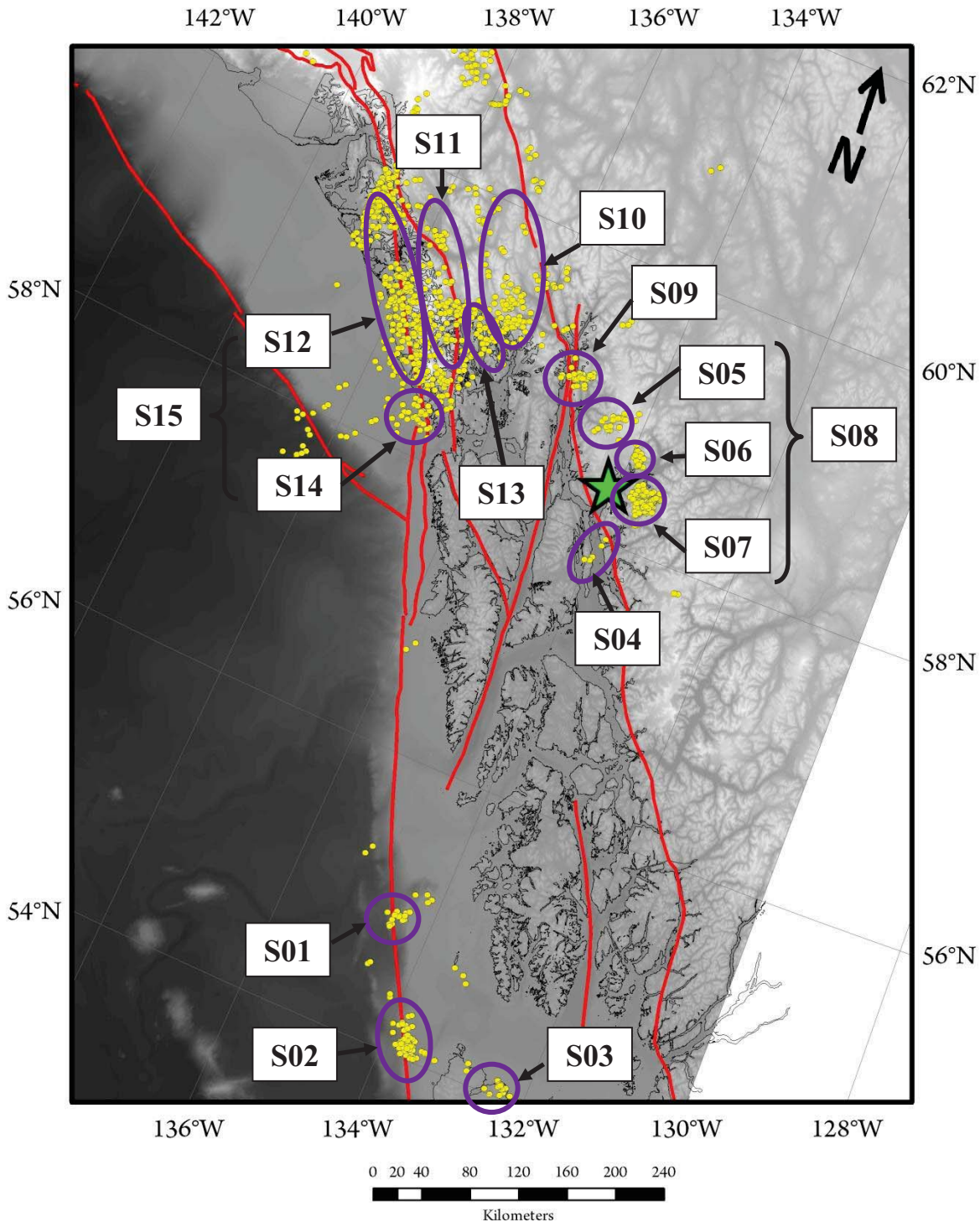

Figure 4-20. SEAK simplified map showing selected stress regions for calculations.

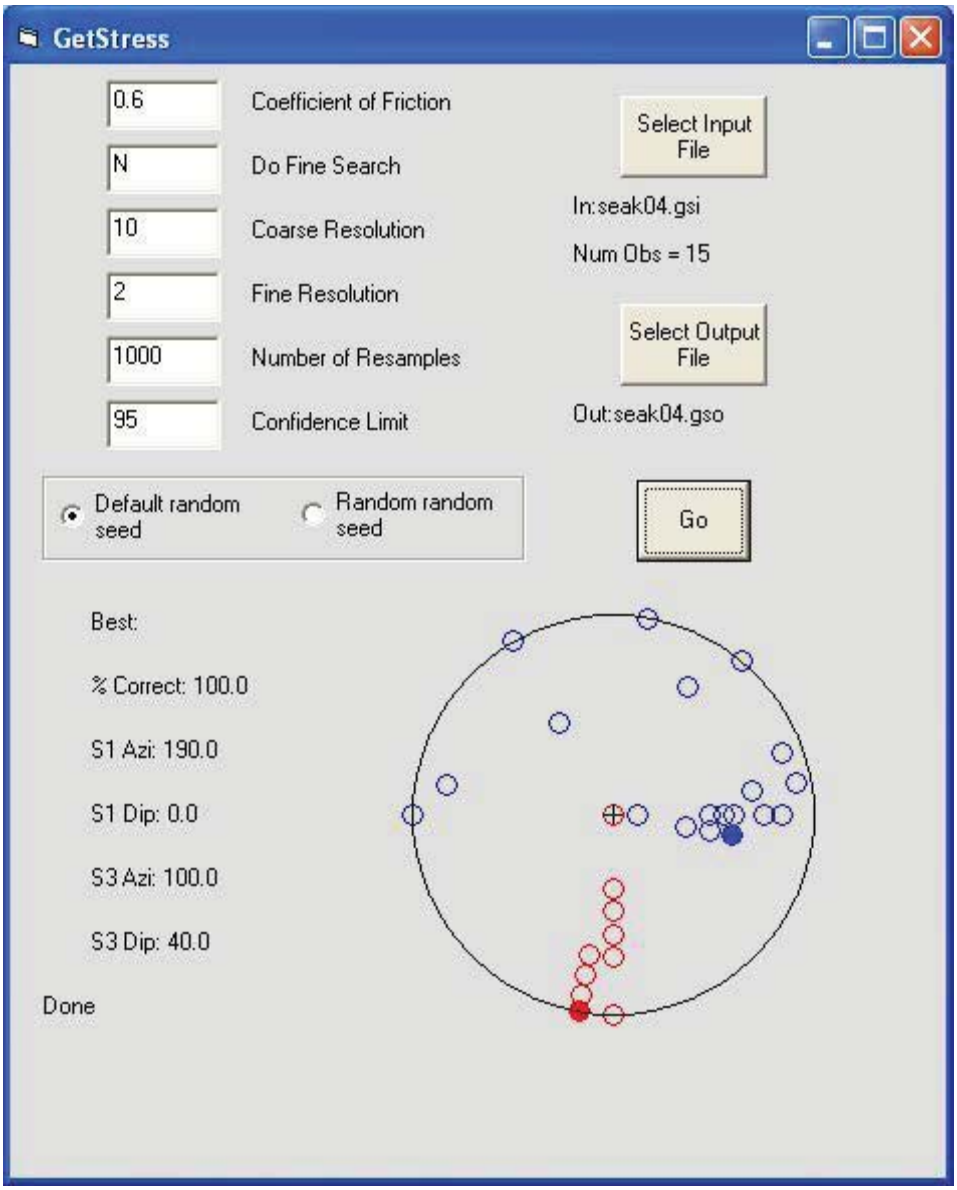

Figure 4-21: GetStress output window with stress tensor solution for seak04. Solid red circle is best fit for σ1; open red circles are σ1 results for 950 of 1000 inversions of randomly selected data for stress orientations (essentially showing the 95% confidence region); solid blue circle is best fit for σ3; open blue circles are σ3 95% confidence region.

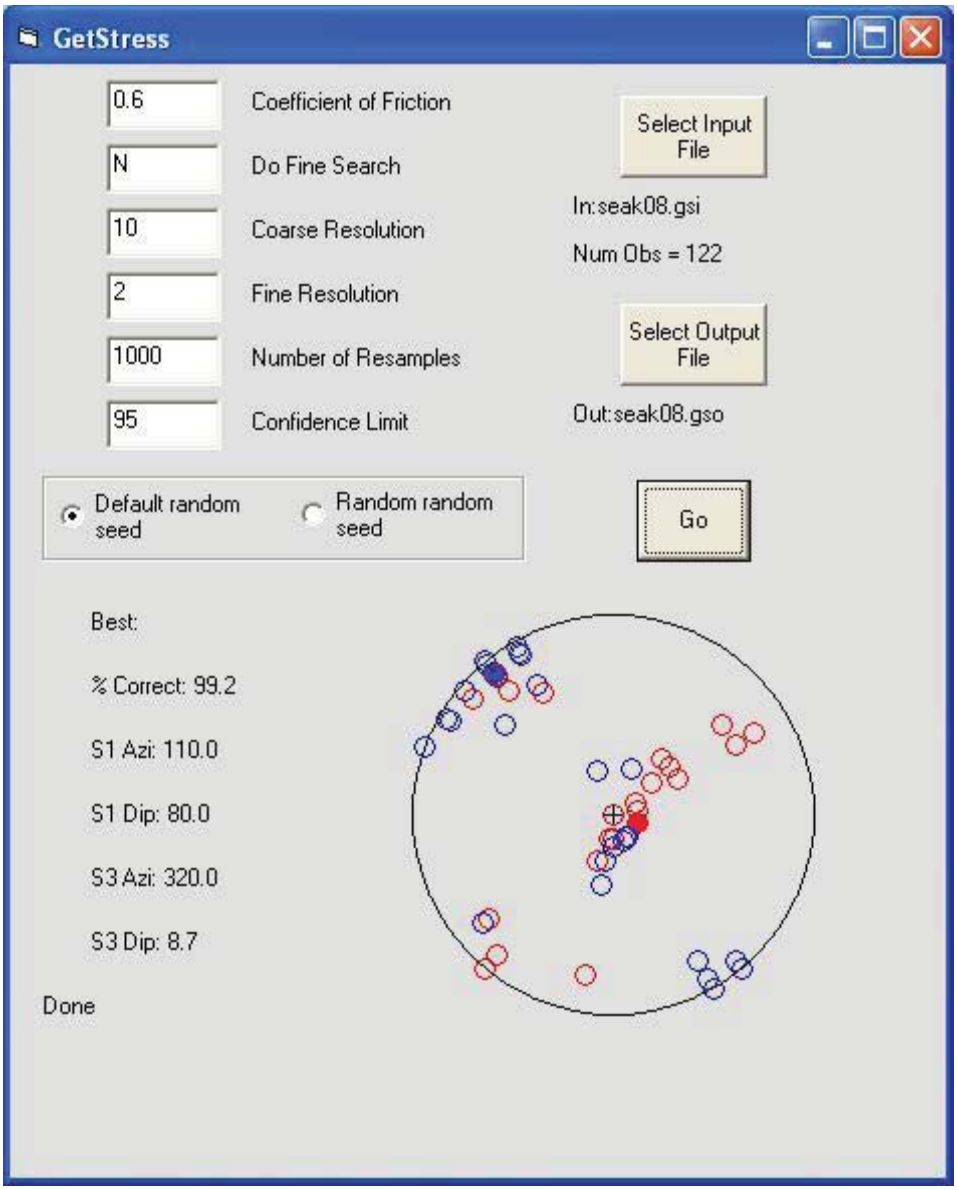

Figure 4-22. GetStress output window with stress tensor solution for *seak08.* Symbols are same as Figure 4-21.

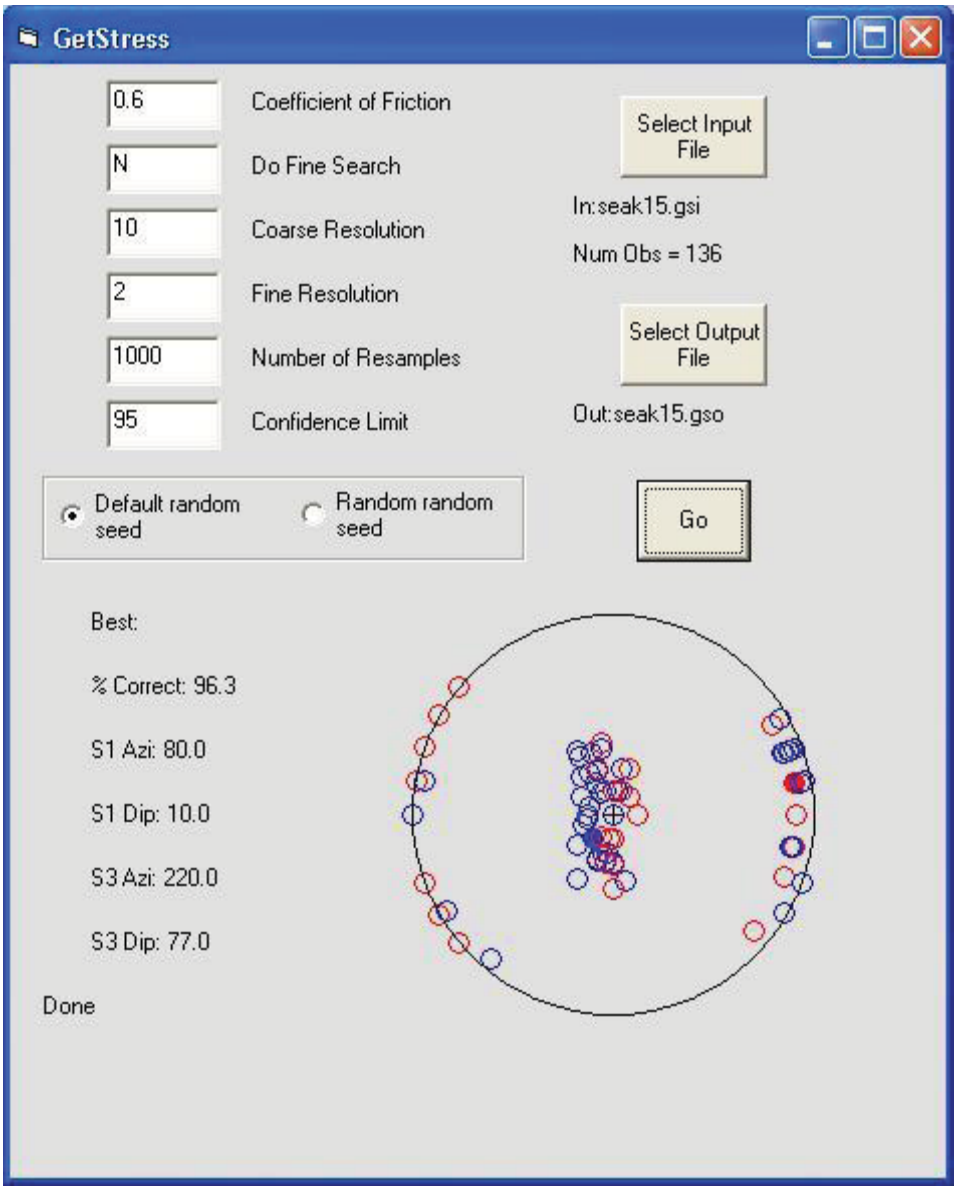

Figure 4-23. GetStress output window with stress tensor solution for *seak15*. Symbols same as Figure 4-21.

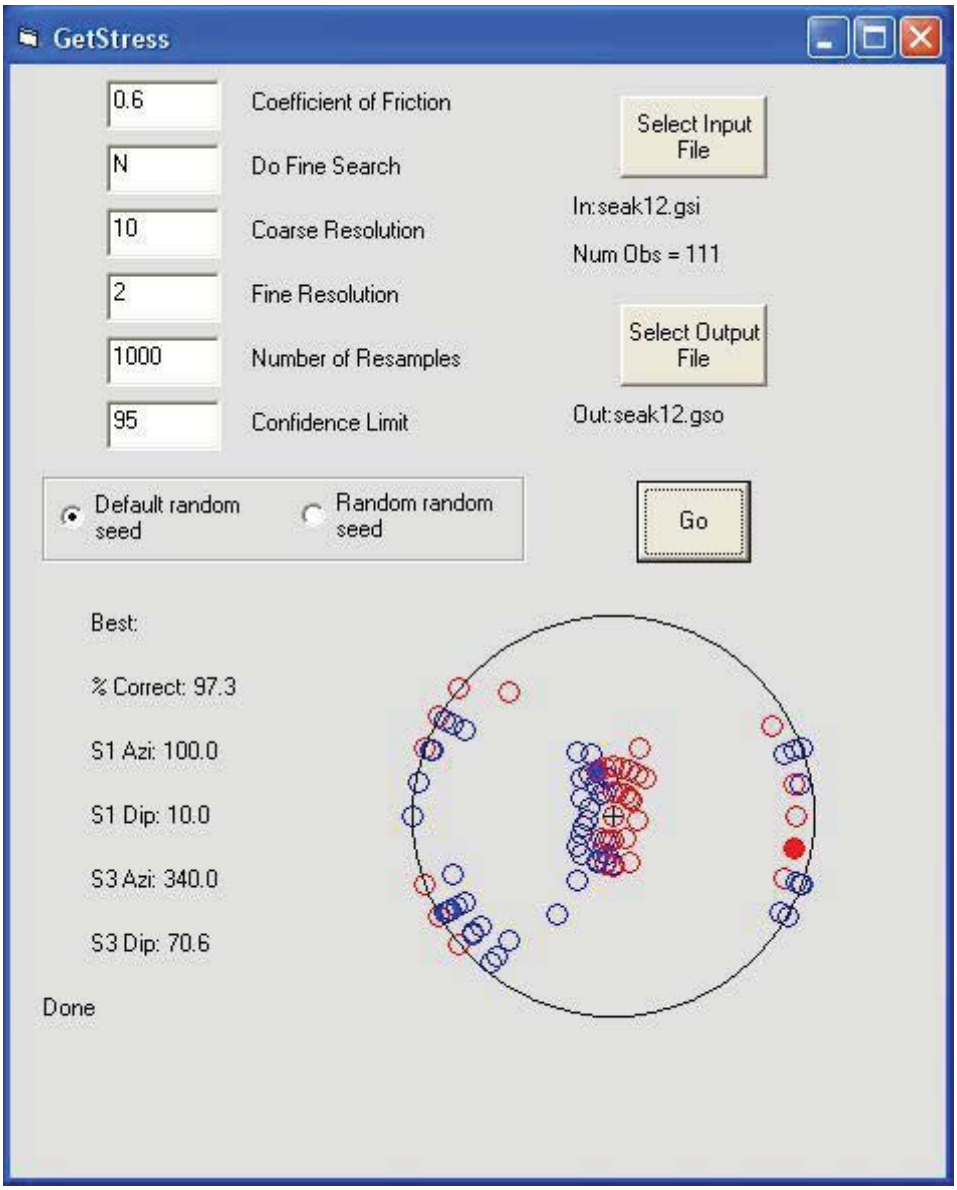

Figure 4-24. GetStress output window with stress tensor solution for *seak12*. Symbols same as Figure 4-21.

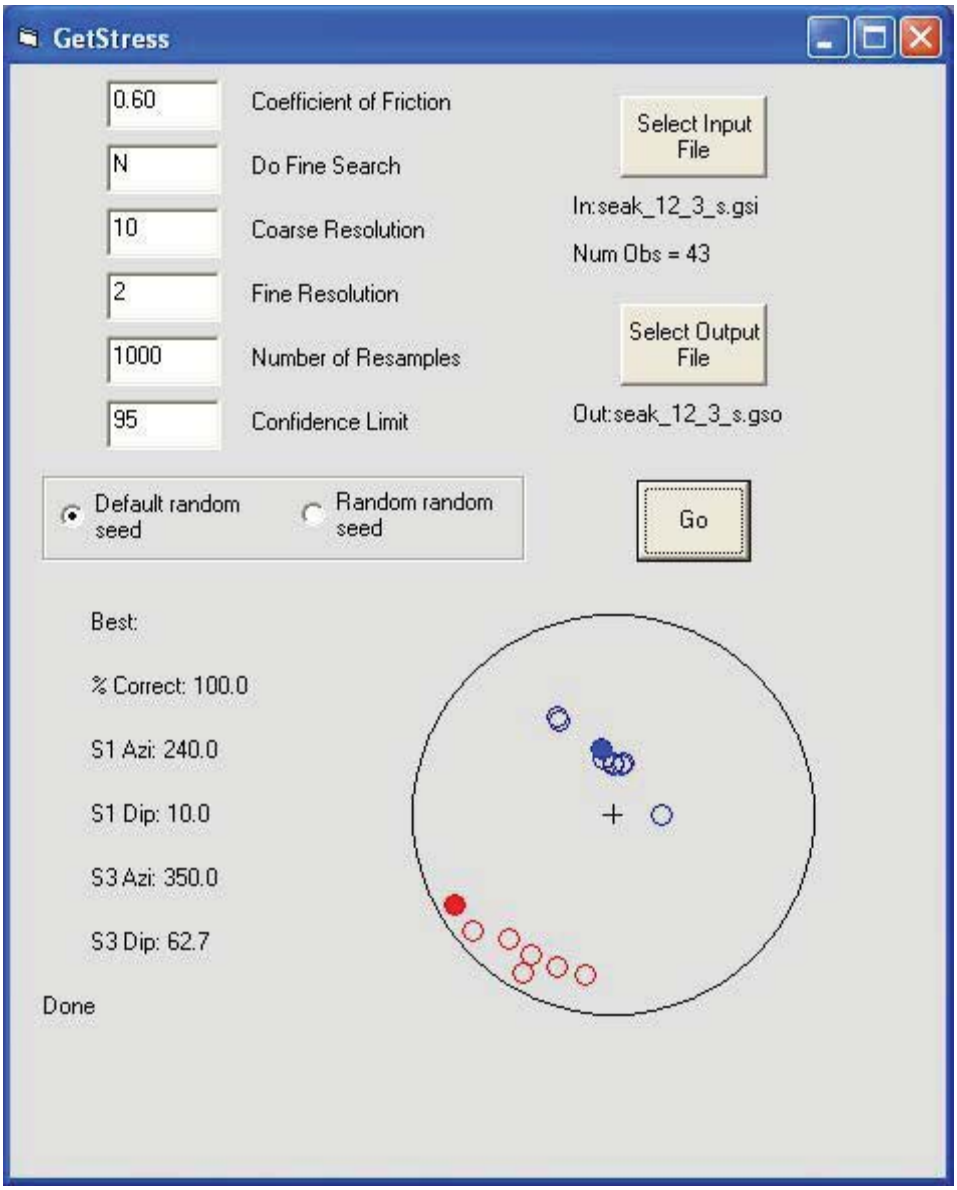

Figure 4-25. GetStress output window with stress tensor solution for *seak_12_3_s*. Symbols same as Figure 4-21.

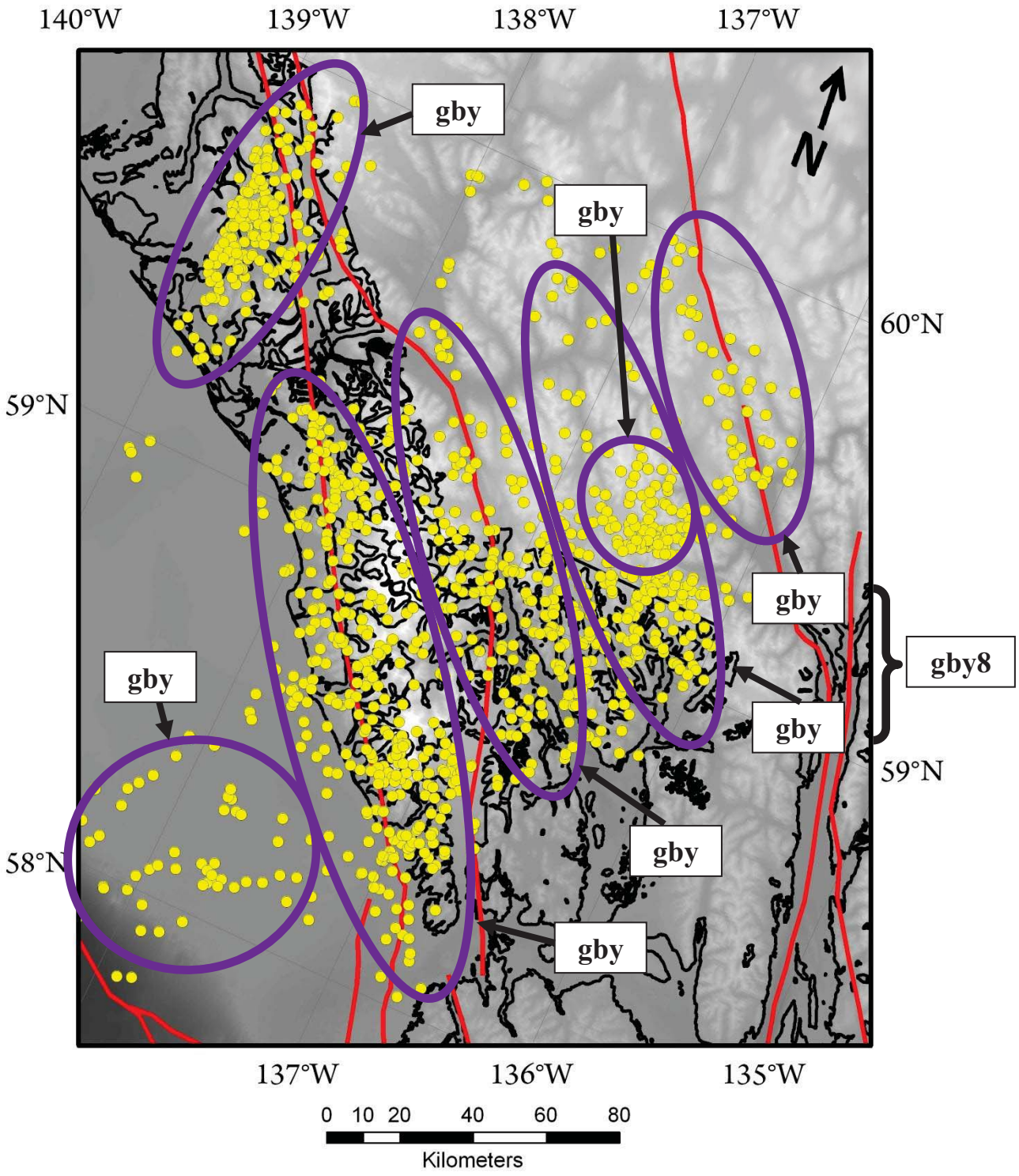

Figure 4-26. GBY simplified map showing selected stress regions for calculations.

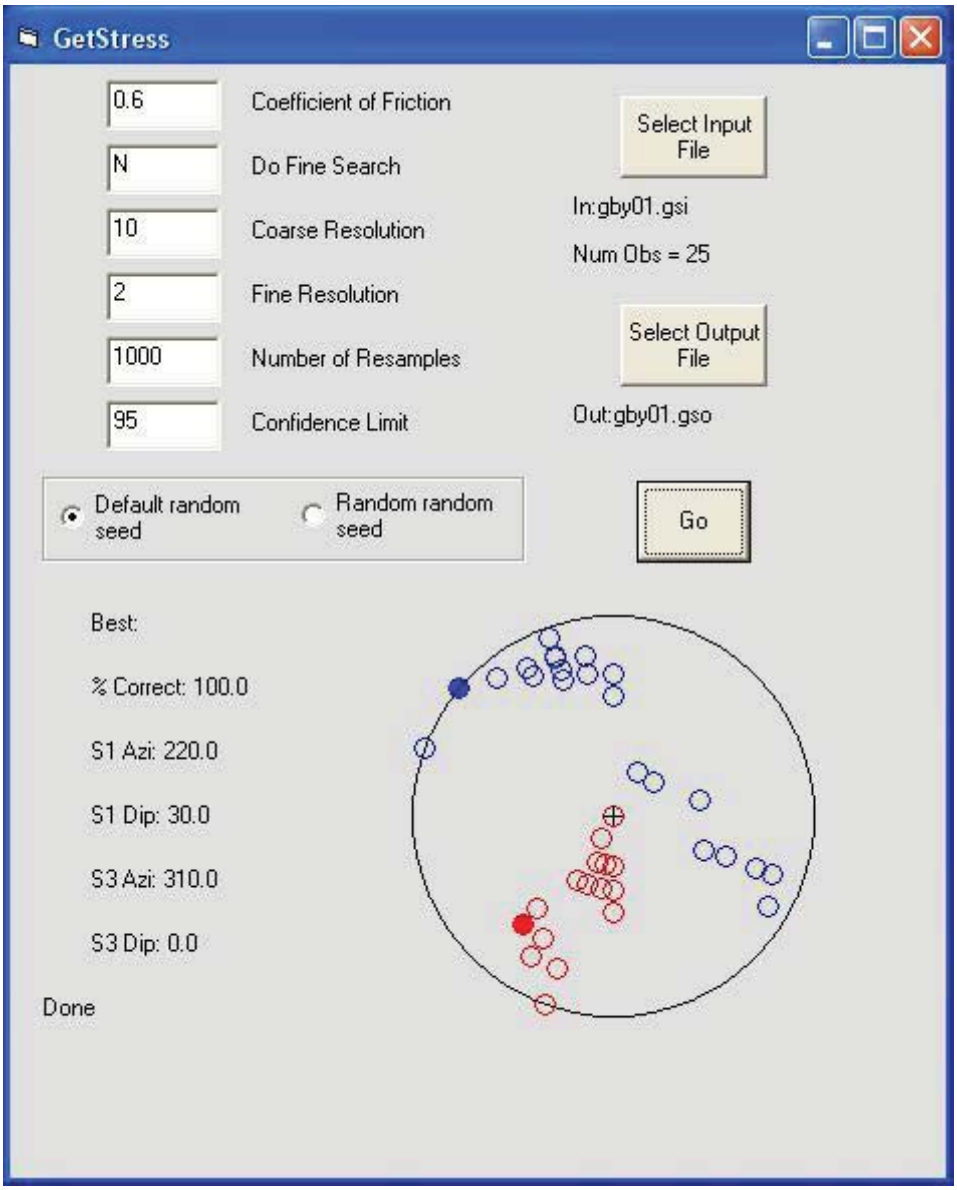

Figure 4-27. GetStress output window with stress tensor solution for *gby01*. Symbols same as Figure 4-21.

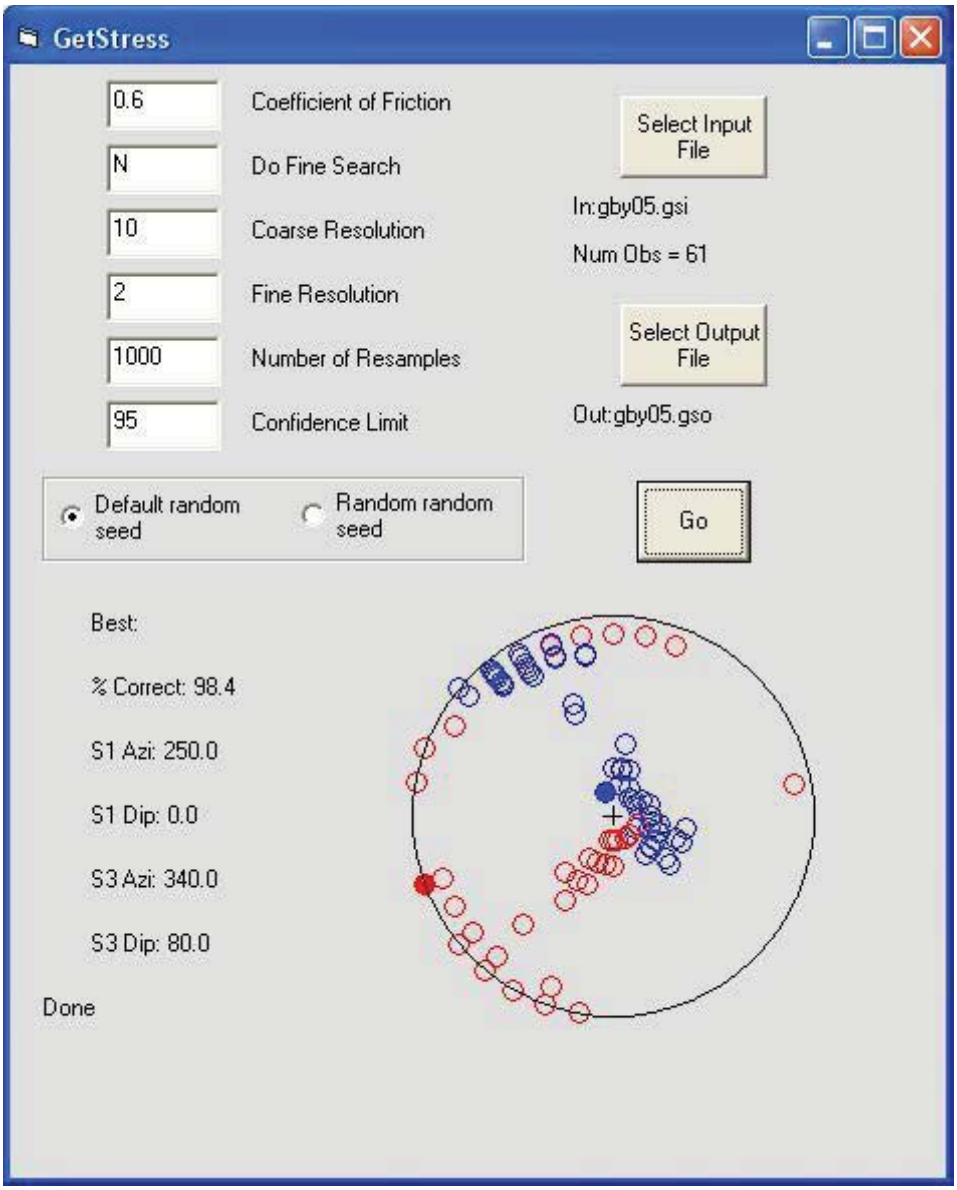

Figure 4-28. GetStress output window with stress tensor solution for *gby05*. Symbols same as Figure 4-21.

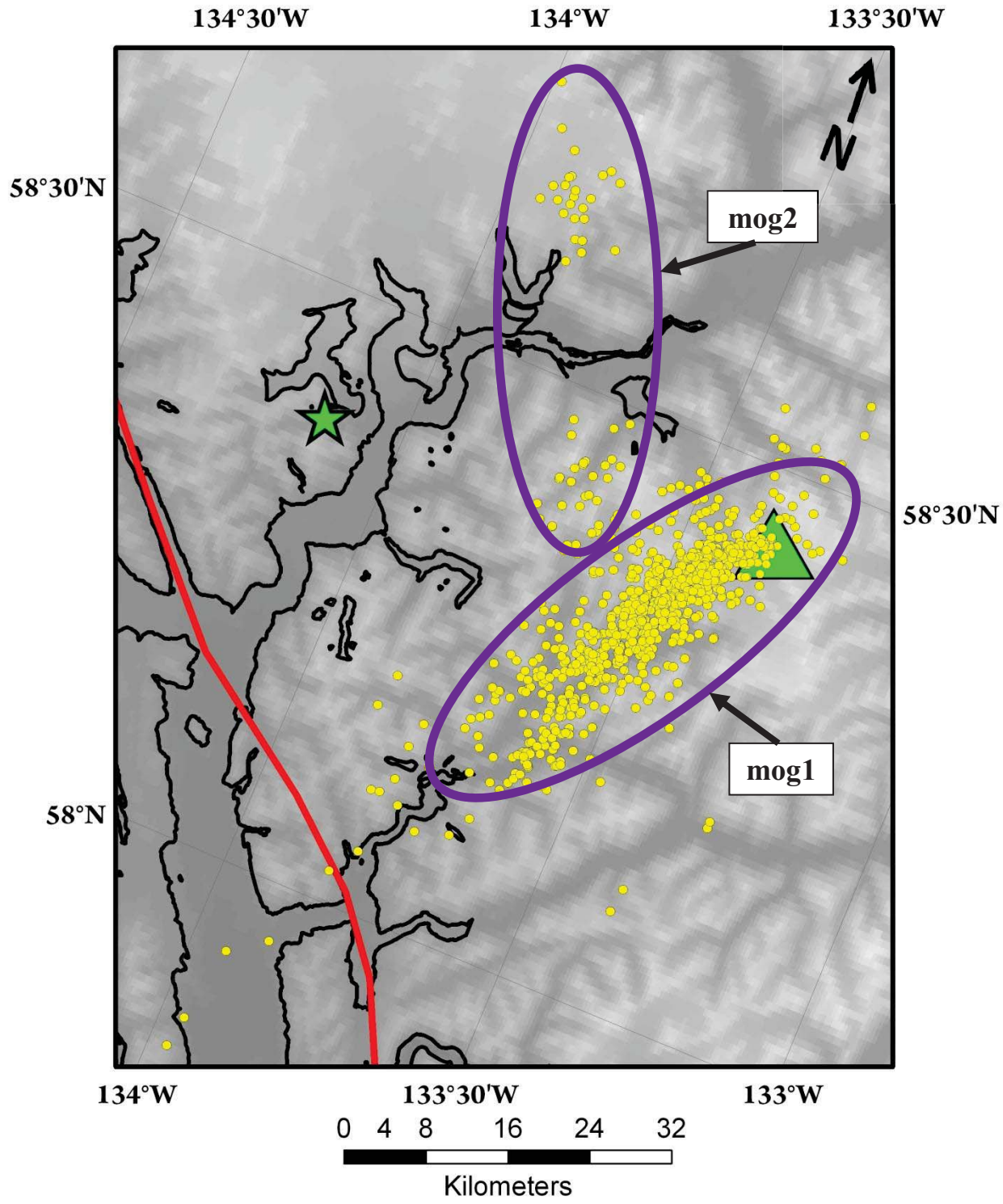

Figure 4-29. MOG simplified map showing selected stress regions for calculations.

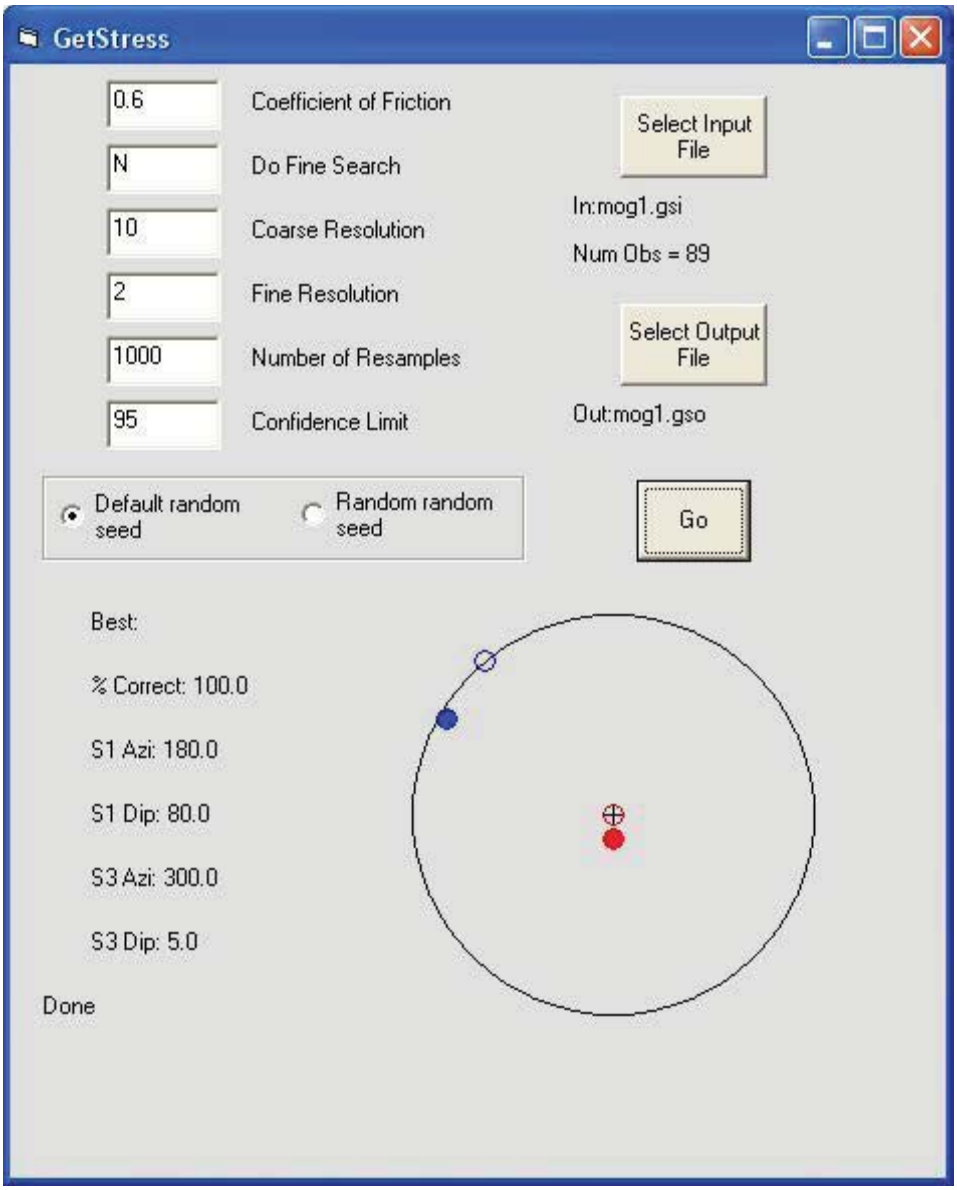

Figure 4-30. GetStress output window with stress tensor solution for mog1. Symbols same as Figure 4-21.

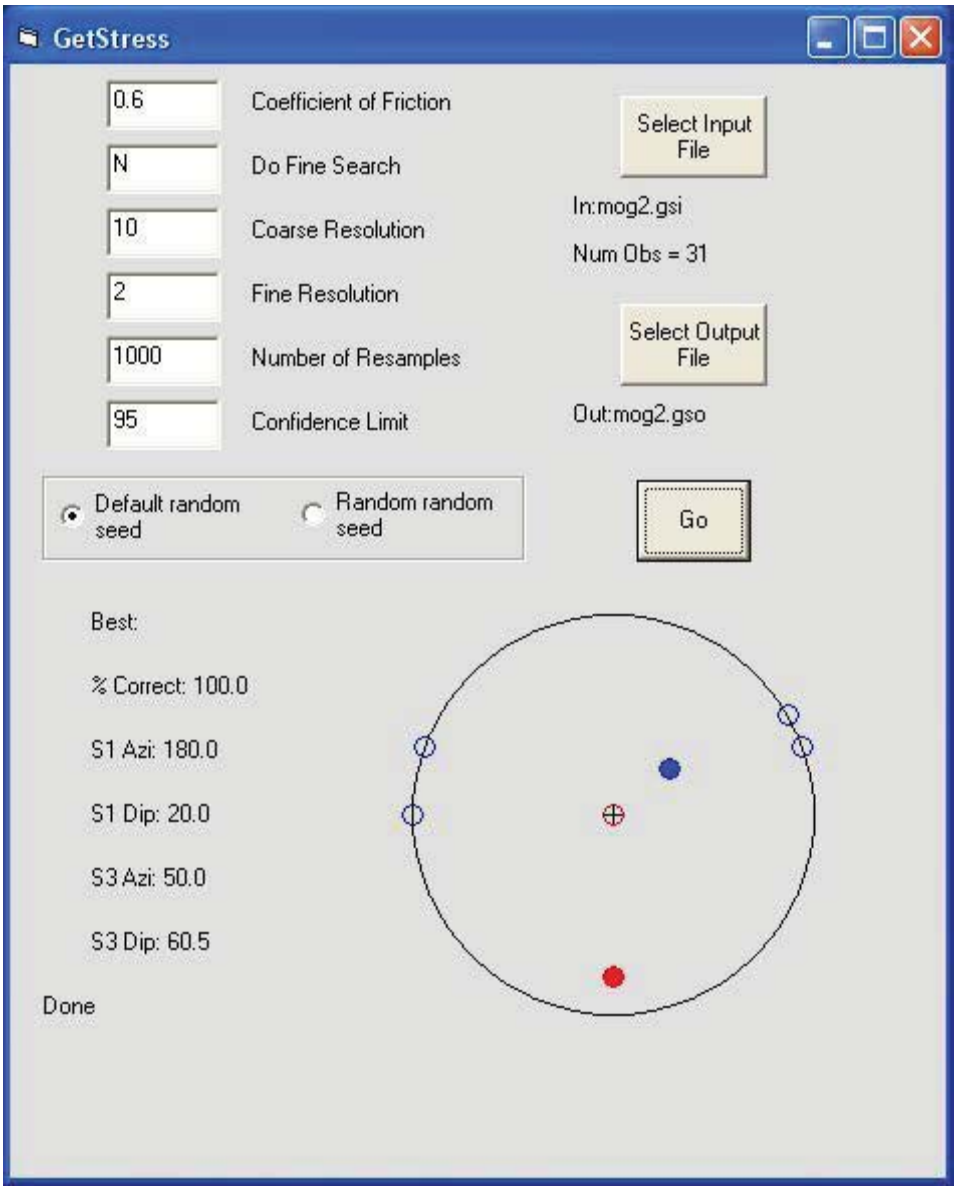

Figure 4-31. GetStress output window with stress tensor solution for mog2. Symbols same as Figure 4-21.

CHAPTER 5

CONCLUSIONS

The goal of this research was to study background seismicity to better understand the current state of stress in southeast Alaska. Previous studies focused on earthquakes of M≥3 and neglected the remainder of the region's earthquake catalog. For this reason seismicity in southeast Alaska is not fully understood. The geologic and geophysical complexities that make up southeast Alaska are the result of active tectonic deformation that continually abandons and activates faults as stresses are transferred throughout the study region.

Data was gathered for earthquakes that occurred between 1973-2005 from the Alaskan and Canadian databases. A total of 4,617 earthquakes with depths of depths <20 km and M<5 were used in this study. To obtain high resolution earthquake locations, the hypoDD program was used due to its ability to stably handle large datasets and allow earthquakes to migrate toward the structure in which they nucleated.

Relocation calculations were first done on the entire dataset, SEAK. At this scale, results show that large clusters are apparent at Glacier Bay, Mt. Ogden, near Yakutat Bay, and along major faults. Seismogenic features, were clearly delineated throughout the study region that were not mapped on the surface. Activity along the northern QCFS was dominated by shallow earthquakes with a quiet zone located within the southern Fairweather Range. A thick swath of seismicity represents an area of possible stress transfer that runs though northern Glacier Bay and connects the QCFS and Denali faults. Two subregions with high concentrations of seismicity were selected by observation of SEAK earthquake locations to study in more detail, Glacier Bay through Yakutat (GBY) and the area surrounding Mt. Ogden (MOG).

In general, earthquake locations in GBY are diffuse with some isolated clusters. The trend of shallow earthquakes along the northern QCFS was preserved as, well as the quiet zone that bisects the southern Fairweather Range. Much of the earthquakes that follow the QCFS are localized around a high amplitude Bouguer gravity anomaly that represents crystalline rocks related to Mt. Fairweather. The abrupt change in crustal material in this area appears to provide a suitable slip surface to generate earthquakes. The quiet zone to the north of the Fairweather gravity high is coincident with a drop in the gravity potential field possibly representing a change in crustal material that is accumulating strain and more likely to spawn earthquakes of M>5.

The northern most cluster on the QCFS, *gby01*, is cut off by the western extent of the study region. Using the GetStress program, earthquakes in *gby01*produced a stress tensor solution that indicated a strike slip system dominated the area. Previous stress field and focal mechanism studies determined that the same area had a more compressive regime. Both are plausible solutions in this tectonic environment where both reverse and oblique convergence occur. Differences could be due to the incomplete cluster in this study, the difference in magnitude cut-offs between studies, and the quality of picks for the lower magnitude earthquakes in this study.

The majority of this study's earthquakes in GBY were confined to areas of large crustal uplift with the Glacier Bay area. The southern edge of seismicity in Glacier Bay is defined by topographic features, gradual changes in the gravity field, and by the contoured edge of 25mm/yr of uplift as mapped by Freymueller, et al. (2008). Dense, isolated clusters occur within the 30mm/yr uplift contours.

Although earthquakes in this region are scattered, their locations are still accurate. hypoDD tends to draw earthquakes to their source structure, therefore the lack of clustering throughout the north Glacier Bay area shows that the crust is rupturing in small disjointed segments. The

diffuse nature of earthquake locations throughout the Glacier Bay area suggest that stress accommodation between the northern QCFS and the Denali fault is in part being relieved by a new fault system, or systems, that has not yet fully developed. It is plausible the high crustal uplift rates are allowing low magnitude earthquakes to occur at a much higher rate and are therefore slowly revealing the newly forming stress transfer system in Glacier Bay area. If such a phenomenon is occurring, it would have easily led to mixing of stress fields when selecting areas for stress tensor calculations and would serve as a partial explanation for the consistent overlapping confidence regions within the solutions.

The MOG subregion is dominated by a large northeast to southwest trending cluster, *mog1*, which trends along the Speel River as reported by Wolf *et al*. (1997). Gravity and aeromagnetic data show that the cluster clearly lies on a fault. Two parallel faults were identified that stem from the Wright Glacier toward the *mog1*. Stress tensor solutions for MOG were not favorable. The calculation for *mog1* indicates that the fault has a normal sense of motion, contradicting the region's overall tectonic signature. A second stress tensor was calculated for a pair of clusters north of *mog1* that resulted in a favorable solution, but had low confidence due to a limited number of observations.

Overall, the study was constrained by a lack of seismic station availability. The lack of coverage not only limited the number of available earthquakes, but it also affected the amount and quality of phase data that was observed. Background noise from the Pacific Ocean and glacial activity, coupled with low magnitude emergent earthquakes, could have contributed to the miscalculations. Still, hypoDD was very effective in obtaining the best possible earthquake locations needed to analyze southeastern Alaska's geologic complexity. Due to the large distances between earthquakes and stations, relocations had poor depth control. The GetStress

program was also limited by the quality of data. Calculated stress tensors were consistently incoherent or determined solutions that did not fit the region's overall stress regime.

REFERENCES

Angelier, J. 1979. Determination of the mean principal directions of stresses for a given fault population. Tectonophysics, 56: T17–T26.

Arendt, A. A., Echelmeyer, K. A., Harrison, W. D., Lingle, C. S., and Valentine, V. B., 2002. Rapid wastage of Alaska glaciers and their contribution to rising sea level. Science, v. 297, pp. 382-386.

Billings, S.D., Sambridge, M.S. and Kennett, B.L.N., 1994, Errors in hypocenter location: Picking, model, and magnitude dependence. Bulletin of the Seismological Society of America, v. 84, n. 6, pp. 1978-1990.

Bird, A. L., Rogers, G. C., and Spence, G. D., 1997, Earthquakes in the Queen Charlotte Islands region 1984-1996. Lithoprobe Seismic Processing Facility Newsletter, v. 10, n. 1. http://www.litho.ucalgary.ca/publications/newsletter10.1/bird.html

Bird, P. (1996). Computer simulations of Alaskan neotectonics, *Tectonics*15, 225–236.

Bruns, T.R., 1985, Tectonics of the Yakutat block, an allochthonous terrane in the northern Gulf of Alaska: U.S. Geological Survey Open-File Report 85–13, 112 p.

Bufe, C. G., 2005, Stress distribution along the Fairweather-Queen Charlotte transform fault system. Bulletin of the Seismological Society of America, v. 95, n. 5, pp. 2001-2008.

Canadian National Data Centre for Earthquake Seismology and Nuclear Explosion Monitoring home page, Geological Survey of Canada, 2008, http://earthquakescanada.nrcan.gc.ca/stnsdata/cndc/index_e.php

DeMets, C., Gordon, R.G., Argus, D.F., and Stein, S., 1990, Current plate motions. Geophysical Journal International, v. 101, pp. 425-478.

DeMets, C., Gordon, R.G., Argus, D.F., and Stein, S., 1994, Effect of recent revisions to the geomagnetic reversal time scale on estimates of current plate motions. Geophysical Research Letters, v. 21, pp. 2191-2194.

Doser, I.D. & Lomas, R., 2000, The transition from strike-slip to oblique subduction in southeastern Alaska from seismological studies: Tectonophysics. v. 316, pp. 45-65.

Doser, I.D., Pelton, J.R., and Veilleux A.M., 1997, Earthquakes in the Pamplona zone, Yakutat block, south central Alaska. Journal of Geophysical Research, v. 102, B11, pp. 24,499-24,511.

Eberhart-Phillips, D., Christensen, D. H., Brocher, T. M., Hansen, R., Ruppert, N. A., Haeussler, P. J., Abers, G. A., 2006, Imaging the transition from Aleutian subduction to Yakutat collsion in central Alaska, with local earthquakes and active source data. Journal of Geophysical Research, v. 111, B11303.

Ferris, A., Abers, G.A., Christensen, D.H., and Veenstra, E., 2003, High resolution image of the subducted Pacific plate beneath central Alaska, 50–150 km depth. Earth and Planetary Science Letters, v. 214, pp. 575–588.

Fletcher, H., and Freymueller, J. T., 1999, New GPS constraints on the motion of the Yakutat block, Geophysical Research Letters, v. 26, pp. 3029-3032.

Fletcher, H. J., and Freymueller, J. T., 2003, New constraints on the motion of the Fairweather fault, Alaska, from GPS observations, Geophysical Research Letters, v. 30, n. 3, 1139.

Fogleman, K.A., Lahr, J.C., Stephens, C.D. and Page, R.A., 1993, Earthquake locations determined by the southern Alaska Seismograph Network for October 1971 through May 1989. U.S. Geological Survey, Open-File Report 93-309, 54 p.

Ford, A.B. and Brew, D.A., 1987, The Wright Glacier volcanic plug and dike swarm, southeastern Alaska. Geologic Studies in Alaska by the U.S. Geological Survey during 1986, Hamilton T.D., and Galloway, J.P. (Editors), U.S. Geol. Surv. Circular 998, pp. 116-118.

Freymueller, J. T., Woodard, H., Cohen, S. C., Cross, R., Elliott, J., Larsen, C. F., Hreinsdottir, S., and Zweck, C., 2008, Active deformation processes in Alaska, based on 15 years of GPS measurements. Active Tectonics and Seismic Potential of Alaska, Geophysical Monograph Series, Volume 179, edited by Freymueller, J. T., Hauessler, P. J., Wesson, R. L., and Ekstrom, G., 350 p.

Gehrels, G. E., Saleeby, J. B., Berg, H. C., 1987, Geology of Annette, Gravina, and Duke islands, southeastern Alaska. Canadian Journal of Earth Sciences, v. 27, pp. 866-881.

Gehrels, G. E. and Berg, H. C., 1994, Geology of southeastern Alaska. *in* The Geology of Alaska: Boulder, Colorado, Geological Society of America, The Geology of North America v. G-1, edited by G. Plafker and H.C. Berg, pp. 451-467.

Geist, E. L., 1996, Relationship between the present-day stress field and plate boundary forces in the Pacific Northwest. Geophysical Research Letters, v. 23, n. 23, pp. 3381-3384.

Global Centroid Moment Tensor Project - National Science Foundation. http://www.globalcmt.org/

Gulick, S. P. S., Lowe, L. A., Pavlis, T. L., Gardner, J. V., Mayer, L. A., 2007, Geophysical insights into the Transition fault debate: Propagating strike slip in response to stalling Yakutat block subduction in the Gulf of Alaska. Geology, v. 35, n. 8, pp. 763-766.

Hamilton, T. D., 1994, Late Cenozoic glaciations of Alaska. *in* The Geology of Alaska: Boulder, Colorado, Geological Society of America, The Geology of North America v. G-1, edited by G. Plafker and H.C. Berg, pp. 813-844.

Horner, R. B., 1983, Seismicity in the St. Elias region of northwestern Canada and southeastern Alaska, Bulletin of the Seismological Society of America, v. 73, n. 4, pp. 1117-1137.

Johnston, A. C., 1987, Suppression of earthquakes by large continental ice sheets. Nature, v. 330, n. 3, pp. 467-469.

Lanphere, M. A., 1978, Displacement history of the Denali fault system, Alaska and Canada. Canadian Journal of Earth Sciences, v. 15, pp. 817-822.

Larsen, C. F., Motyka, R. J., Freymueller, J. T., Echelmeyer, K. A., and Ivins, E. R., 2004, Rapid uplift of southern Alaska caused by recent ice loss. Geophysical Journal International, v. 158, pp. 1118-1133.

Larsen, C. F., Motyka, R. J., Freymueller, J. T., Echelmeyer, K. A., and Ivins, E. R., 2005, Rapid viscoelastic uplift in southeast Alaska caused by post-Little Ice Age glacial retreat, Earth and Planetary Science Letters, v. 237, pp. 548-560.

Leonard, L. J., Hyndman, R. D., Mazzotti, S., Nykolaishen, L., Schmidt, M., and Hippchen, S., 2007, Current deformation in the northern Canadian Cordillera inferred from GPS measurements. Journal of Geophysical Research, v. 112, B08406.

Leonard, L. J., Mazzotti, S., and Hyndman, R. D.,2008, Deformation rates estimated from earthquakes in the northern cordillera of Canada and eastern Alaska. Journal of Geophysical Research, v. 113, B08406.

Li, H., Morozov, I. B., and Smithson, S. B., 2008, 3D seismic analysis of the Coast Shear Zone in SE Alaska and Western British Columbia: Broadside analysis of ACCRETE wide-angle data. Tectonophysics, v. 448, pp. 20-32.

Loney R. A., Brew D. A., Lanphere M. A., 1967, Post-Paleozoic Radiometric Ages and Their Relevance to Fault Movements, Northern Southeastern Alaska. Geological Society of America Bulletin, v. 78, n. 4, pp. 511–526.

Mazzotti, S., and Hyndman, R.D., 2002, Yakutat collision and strain transfer across the northern Canadian Cordillera. Geology, v. 30, p. 495–498.

Mazzotti, S., Hyndman, R.D., Flück, P., Smith, A.J., and Schmidt, M. 2003b. Distribution of the Pacific/North America motion in the Queen Charlotte Islands-S. Alaska plate boundary zone. Geophysical Research Letters, v. 30, n.14, 1762.

Matumoto, T. and Page, R. A., 1969, Microaftershocks following the Alaska earthquake of 28 March 1964: Determination of hypocenters and crustal velocities in the Kenai Peninsula-Prince William Sound area, in The Prince William Sound, Alaska, earthquake of 1964 and aftershocks, U.S. Coast and Geodetic Surv. Publ. 10–3 2B&C, U.S. Govt. Printing Office, Washington, D.C., pp. 157–173.

Morozov, I. B., Smithson, S. B., Hollister, L. S., and Diebold, J. B., 1998, Wide-angle seismic imaging across accreted terranes, southeastern Alaska and western British Columbia. Tectonophysics, v. 299, pp. 281-296.

Motyka, R.J., Larsen, C.F., Freymueller, J.T., & Echelmeyer, K.A., 2007, Post little ice age rebound in the Glacier Bay Region, in Piatt, J.F., and Gende, S.M., eds., Proceedings of the Fourth Glacier Bay Science Symposium, October 26–28, 2004: U.S. Geological Survey Scientific Investigations Report 2007-5047, p. 57-59.

Oldow, J. S., Bally, A. W. Lallemant, H. G. A., Leeman, W. P., 1989, Phanerozoic evolution of the North American Cordillera; United States and Canada. *in* The Geology of North America – An overview: Boulder, Colorado, Geological Society of America, v. A, edited by Bally, A. W., and Palmer, A. R., pp. 139-231.

Overshine, A. T., and Brew, D. A.,, 1972, Seperation history of the Chatam Strait fault, southeast Alaska, North America. 24th Proceedings of the International Geological Congress, Section 3, pp. 245-254.

Pavlis, G. and Booker, J., 1983, Progressive multiple event location (PMEL), Bulletin of the Seismological Society of America. 73, 1753–1777.

Pavlis, T.L., Picornell, C., Serpa, L., Bruhn, R.L., and Plafker, G., 2004, Tectonic processes during oblique collision: Insights from the St. Elias orogen, northern North American Cordillera: Tectonics, v. 23, p. TC3001.

Page, R.A., Stephens, C.D., and Lahr, J.C., 1989, Seismicity of the Wrangell and Aleutian Wadati-Benioff Zones and the North American Plate along the Trans-Alaska Crustal Transect, Chugach Mountains and Copper River Basin, southern Alaska. Journal of Geophysical Research, v. 94, pp. 16,059-16,082.

Page, R.A., Biswas, N.N., Lahr, J.C. and Pulpan, H., 1991, Seismicity of continental Alaska. *in* Neotectonics of North America: Boulder, Colorado, Geological Society of America, Decade Map V.1, edited by D.B. Slemmons, E.R. Engdahl, M.D. Zoback and D.D. Blackwell, pp. 47-68.

Perez, O., and K.H. Jacob, 1980, Tectonic model and seismic potential of the eastern Gulf of Alaska and Yakataga seismic gap. Journal of Geophysical Research, v. 85, pp. 7,132-7,150.

Plafker, G., Hudson, T., and Richter, D. H., 1977, Preliminary observations on late Cenozoic displacements along the Totshunda and Denali Fault systems; United States Geological Survey, Circular 733, pp. 67-69.

Plafker, G., Nocklberg, W. J., and Lull, J. S., 1989, Bedrock geology and tectonic evolution of the Wrangellia, Penninsular, and Chugach terranes along the Trans-Alaska Crustal Transect in the Chugach mountains and southern Copper River basin, Alaska. Journal of Geophysical Research, v. 94, n. B4, pp. 4255-4295.

Plafker, G. and Berg, H.C., 1994, Overview of the geology and tectonic evolution of Alaska. *in* The Geology of Alaska: Boulder, Colorado, Geological Society of America, The Geology of North America v. G-1, edited by G. Plafker and H.C. Berg, pp. 989-1021.

Plafker, G., Gilpin, L.M., and Lahr, J.C., 1994, Neotectonic map of Alaska, in Plafker, G., and Berg, H.C., eds., Geology of Alaska, Geology of North America, in Decade of North American Geology: Boulder, Geological Society of America, v. G-1, plate 12, 1sheet, 1:2,500,000 scale.

Plafker, G., Moore, J.C. and Winker, G.R., 1994, Geology of the southern Alaska margin. *In* The Geology of Alaska: Boulder, Colorado, Geological Society of America, The Geology of North America v. G-1, edited by G. Plafker and H.C. Berg, pp. 389-449.

Powell, R. D., 1984, Guide to the glacial geology of Glacier Bay, southeast Alaska. Alaska Geological Society, 85 p.

Power, M. A., 1988, Microearthquake seismicity on the Duke River, Denali Fault System. *In* Yukon Geology, v.2; Exploration and Geological Services Division, Yukon, Indian and Northern Affairs Canada, pp. 61-68.

Pujol, J., 2000, Joint Event Location – The JHD Technique and applications to data from local seismic networks. *In* Advances in Seismic Event Location, edited by C.H. Thurber and N. Rabinowitz, Kluwer Academic Publishers, Netherlands, pp. 163-204.

Ratchkovsky, N.A., Pujol, J. and Biswas, N.N., 1998, Relocation of shallow earthquakes in southern Alaska using Joint Hypocenter Determination Method. Journal of Seismology, v. 2, pp. 87-102.

Richter, D. H. and Matson, N. A., 1971, Quaternary faulting in the eastern Alaska Range, Alaska. Geological Society of America Bulletin, v. 82, pp. 1529-1540.

Ristau, J., Rogers, G. C., and Cassidy, J. F., 2007, Stress in western Canada from regional moment tensor analysis. Canadian Journal of Earth Sciences, v. 44, pp. 127-148.

Robinson, R., 1999, GetStess: A computer programme for inverting first motion observations to a regional stress tensor. Institute of Geological & Nuclear Sciences, Box 30368, Lower Hutt, New Zealand, 7 p.

Rogers, G.C., 1976, A microearthquake survey in northwest British Columbia and southeast Alaska: Seismological Society of America Bulletin, v. 66, pp. 1643-1655.

Ruppert, N. A., 2008, Stress map for Alaska from earthquake focal mechanisms. Active Tectonics and Seismic Potential of Alaska, Geophysical Monograph Series, Volume 179, edited by Freymueller, J. T., Hauessler, P. J., Wesson, R. L., and Ekstrom, G., 351 p.

Saltus, R.W., Connard, G.G., and Hill, P.L., Alaska Aeromagnetic Compilation – Digital Grids and Survey Data. U.S. Geological Survey, Open-File Report 99-502. 1999.

Saltus, R.W., Hudson, T.L., and Connard, G.G., 1999, A new magnetic view of Alaska. GSA Today, v. 9, n. 3, pp. 1-6.

Sauber, J. M., Ruppert, N. A., 2008, Rapid Ice Mass Loss: Does it have an influence on earthquake occurrence in southern Alaska? Active Tectonics and Seismic Potential of Alaska, Geophysical Monograph Series, Volume 179, edited by Freymueller, J. T., Hauessler, P. J., Wesson, R. L., and Ekstrom, G., 350 p.

Smith, B. and Sandwell, D., 2003, Coulomb stress accumulation along the San Andreas Fault system. Journal of Geophysical Research, v. 108, B6, 2296.

Stewart, I. S., Sauber, J., and Rose, J., 2000, Glacio-seismotectonics: ice sheets, crustal deformation and seismicity. Quaternary Science Reviews, v. 19, pp. 1367-1389.

University of Alaska at Fairbanks – UAF Seismology Laboratory home page, 2008, http://www.aeic.alaska.edu/

Waldhauser, F., 2001, HypoDD- A program to compute Double Difference Hypocenter Locations , *hypoDD* version 1.0 – 03/2001, . U.S. Geological Survey, Open-File Report 01-113, 25 p.

Waldhauser, F. and Ellsworth, W.L., 2000, A Double-Difference Earthquake Location Algorithm: Method and application to the Northern Hayward Fault, California. Bulleting of the Seismological Society of America, v. 90, n. 6, pp. 1353-1368.

Wilson, J. T., 1965, A new class of faults and their bearing on continental drift. Nature, v. 207, pp. 343-347.

Wolf, W.L., Rowe, C.A., Horner, R.B., 1997, Periodic seismicity near Mt. Ogden on the Alaska-British Columbia border: A case for hydrologically triggered earthquakes? Seismological Society of America Bulletin, v. 87, p. 1473-1483.

Wyss, M., Shimazaki, K., and Ito, A., 1999, Seismicity Patterns, Their Statistical Significance and Physical Meaning: Their Statistical Significance and Physical Meaning. *Published by* Birkhäuser, 530 p.

APPENDIX

hypoDD output parameter description for Table 4-3 pp. 48:

NITER: Number of iterations

WTCCP, WTCCS: Weight for cross-corr P-wave, S-wave data. –9 = data not used.

WRCC, WDCC: Max. event separation distance [km] for x-corr data, catalog data. -9 = not activated.

WTCTP, WTCTS: Weight for catalog P-wave, S-wave data. –9 = data not used.

WTCT, WDCT: Max. event separation distance [km] for x-corr data, catalog data. -9 = not activated.

DAMP: Damping (only for ISOLV= 2).

IT: First two columns indicate the iteration number. First column is numbers each iteration, second column numbers each successful iteration (those without airquakes).

EV: Indicates the percentage of events used in each iteration.

CT CC: Percentage of catalog and cross-correlation(if used) data used in each iteration.

RMSCT, RMSCC: Indicate RMS residual (in ms) and its percent change from the last iteration.

DX, DY, DZ, DT: Average absolute value of the change in hypocenter location and origin time during each iteration.

OS: Indicates absolute shift in cluster origin.

AQ: Indicates the number of airquakes detected and discarded.

CND: Condition number for the system of double difference equations; calculated ratio between the largest and smallest eigenvalue).

Table 4-1: ***seak run07 HypoDD output***

```
*       ---  CROSS DATA -----  ----CATALOG DATA ----
*  NITER   WTCCP  WTCCS  WRCC  WDCC  WTCTP   WTCTS  WRCT  WDCT  DAMP
   5       -9      -9     -9   -9     2.0     1.0    3.0   10    80
   5       -9      -9     -9   -9     0.5     0.1    0.5   10    40


Reading data ...   Wed Dec 10 00:48:40 2008
# events =  2025
# stations < maxdist =    688
# catalog P dtimes =   12914
# catalog S dtimes =    8032
# dtimes total =    20946
# events after dtime match =       1434
# stations =    126

no clustering performed.

RELOCATION OF CLUSTER: 1     Wed Dec 10 00:48:44 2008
----------------------
Initial trial sources =  1434

  IT   EV  CT    RMSCT   RMSST   DX   DY   DZ   DT   OS  AQ  CND
       %   %    ms     %    ms    m    m    m   ms    m
 1    100  94   310 -27.4     0  655  789  568   60    0  34   46
 2     97  88   293  -5.5     0  608  736  513   55    0  10   44
 3  1  96  86   286  -2.4  1175  599  714  497   53   26    0   42
 4     93  78   214 -25.1  1175  308  359  269   23   26   24   40
 5     91  72   195  -9.0  1175  286  330  238   21   26    1   38
 6  2  91  71   188  -3.7   756  278  323  230   21   15    0   37
 7     88  65   145 -22.6   756  160  183  119   11   15    8   35
 8  3  88  61   129 -11.6   573  150  172  110   10   20    0   33
 9     87  55    96 -25.0   573   90  105   77    6   20    6   31
10     86  51    82 -15.3   573   83   96   72    6   20    1   30
11  4  86  49    73 -10.2   330   79   90   69    5   23    0   29
12     86  43    51 -30.4   330   49   55   43    3   23    2   27
13     86  39    41 -20.1   330   45   50   39    3   23    1   25
14  5  86  37    35 -14.9   165   41   48   36    3   21    0   25
15     85  37    51  47.7   165   96  104   75    5   21    2   62
16  6  85  37    51  -0.2   147   96  104   74    5   20    0   62
17     85  37    49  -5.0   147   57   64  153    3   20    2   59
18  7  85  37    49  -0.1   151   57   64   49    3   22    0   59
19     85  37    47  -3.2   151   43   49   36    3   22    1   56
20  8  85  37    47  -0.3   153   43   49   37    3   23    0   56
21     85  37    46  -2.6   153   36   41   30    2   23    1   55
22  9  85  36    46  -0.1   165   36   41   30    2   27    0   55
23     84  36    45  -2.2   165   31   35   25    2   27    3   55
24 10  84  36    44  -0.7   156   31   35   25    2   26    0   54

writing out results ...
 Note: IEEE floating-point exception flags raised:
    Inexact;  Invalid Operation;
 See the Numerical Computation Guide, ieee_flags(3M)
```

Table 4-2: ***gby run03 HypoDD output***

```
*       ---  CROSS DATA -----  ----CATALOG DATA ----
*  NITER   WTCCP  WTCCS  WRCC  WDCC  WTCTP   WTCTS  WRCT  WDCT  DAMP
   5       -9      -9     -9   -9     2.0     1.0    3.0   10    50
   5       -9      -9     -9   -9     0.5     0.1    0.5   10    30
*


Reading data ...   Thu Dec 11 17:37:36 2008
# events =  1951
# stations < maxdist =    688
# catalog P dtimes =   13452
# catalog S dtimes =    8038
# dtimes total =    21490
# events after dtime match =       1557
# stations =    104

no clustering performed.

RELOCATION OF CLUSTER: 1     Thu Dec 11 17:37:38 2008
----------------------
Initial trial sources =  1557

  IT   EV  CT    RMSCT   RMSST   DX   DY   DZ   DT   OS  AQ  CND
        %   %   ms     %    ms    m    m    m   ms    m
 1    100  95  374 -32.4     0 1445 1282 1046  108    0  94   87
 2     93  81  357  -4.6     0 1324 1136  748   94    0  24   78
 3     92  78  350  -2.0     0 1284 1109  729   91    0   6   77
 4     91  78  347  -0.8     0 1275 1098  726   90    0   1   77
 5     91  77  346  -0.4     0 1272 1095  727   89    0   2   75
 6     91  77  345  -0.1     0 1272 1087  727   89    0   1   75
 7  1  91  77  345  -0.1  1550 1268 1087  727   89   46   0   75
 8     85  62  259 -24.9  1550  612  493  384   37   46  31   65
 9     82  56  223 -14.0  1550  548  432  322   33   46   5   62
10     82  54  205  -7.9  1550  526  410  300   31   46   1   59
11  2  82  54  196  -4.4   873  514  395  288   30   23   0   59
12     80  46  140 -28.8   873  263  211  142   14   23   6   52
13     79  42  112 -19.6   873  232  184  123   13   23   1   50
14     79  40   98 -13.1   873  216  171  114   12   23   1   49
15  3  79  39   89  -9.2   452  206  164  113   11   33   0   47
16     78  33   57 -35.9   452  104   86   57    5   33   3   42
17  4  77  29   43 -24.5   279   90   77   49    5   32   0   40
18  5  77  25   22 -49.0    87   45   36   26    2   38   0   35
19     77  25   34  55.7    87   76   68   43    4   38   2   70
20  6  77  24   34  -0.2   105   76   69   43    4   42   0   70
21  7  77  24   32  -6.2   109   43   41   27    2   50   0   66
22  8  77  24   31  -3.8   110   32   31   19    2   53   0   64
23  9  77  24   30  -2.7   110   26   25   16    1   55   0   61
24 10  77  24   29  -2.1   110   23   22   14    1   57   0   61

writing out results ...
 Note: IEEE floating-point exception flags raised:
    Inexact;  Invalid Operation;
 See the Numerical Computation Guide, ieee_flags(3M)
```

Table 4-3: ***ogden run07 HypoDD output***

```
*       ---  CROSS DATA -----  ----CATALOG DATA ----
*  NITER   WTCCP  WTCCS  WRCC  WDCC  WTCTP   WTCTS  WRCT  WDCT  DAMP
   5       -9      -9     -9   -9     2.0     1.0    3.0   10    70
   5       -9      -9     -9   -9     0.5     0.1    0.5    5    60
*

Reading data ...   Thu Dec 11 21:29:37 2008
# events =  1098
# stations < maxdist =    688
# catalog P dtimes =   14274
# catalog S dtimes =   12158
# dtimes total =    26432
# events after dtime match =        998
# stations =     34

no clustering performed.

RELOCATION OF CLUSTER: 1     Thu Dec 11 21:29:39 2008
----------------------
Initial trial sources =   998

  IT   EV  CT    RMSCT   RMSST   DX   DY   DZ   DT   OS  AQ  CND
        %   %   ms     %    ms    m    m    m   ms    m
 1    100  96  291 -26.2     0  814  784  395   63    0   4   57
 2  1 100  95  285  -2.2   883  784  755  377   61   53   0   56
 3     99  90  217 -23.7   883  440  446  198   28   53  11   55
 4  2  98  87  207  -4.5   673  422  421  184   27   60   0   55
 5     98  81  170 -18.1   673  234  287  119   15   60   5   51
 6  3  98  78  157  -7.3   575  220  270  109   14   80   0   49
 7     97  73  134 -15.0   575  147  193   78    9   80   7   46
 8     97  70  123  -8.3   575  136  181   73    9   80   1   44
 9  4  97  69  117  -4.8   435  132  174   71    8   92   0   44
10     97  64   97 -16.8   435   93  127   52    6   92   2   42
11  5  96  61   88 -10.0   241   87  120   49    5   90   0   41
12     90  48  109  24.3   241  104  150   57    6   90   2   44
13  6  89  48  109  -0.1   236  104  150   57    6   63   0   44
14     89  47  104  -4.4   236   75  108   41    4   63   7   42
15  7  89  46  104   0.3   236   76  108   41    4   55   0   42
16     88  45  101  -3.0   236   59   82   33    3   55   3   40
17  8  88  45  101   0.0   237   59   82   33    3   55   0   40
18     88  44   99  -2.2   237   51   69   29    3   55   1   40
19  9  88  44   99   0.0   237   51   69   29    3   63   0   40
20     88  43   97  -1.9   237   44   60   25    3   63   5   39
21 10  87  43   97   0.1   235   44   60   25    3   70   0   39

writing out results ...
 Note: IEEE floating-point exception flags raised:
    Inexact;  Invalid Operation;
 See the Numerical Computation Guide, ieee_flags(3M)
```

CURRICULUM VITAE

Hugo Rodriguez was born on January 19, 1978 in El Paso, Texas. He is from a family of five children, with parents Neil and Delfina R. Fisher; four of which have at least a bachelors' degree. He graduated from Irvin High School, El Paso, Texas in May of 1996. Hugo enlisted in the U.S. Air Force after a couple of years of engineering college and decided to return school after his honorable discharge to achieve a higher degree of education. Upon returning to UTEP, he changed majors and became a geology student in the UTEP Geosciences Department. While an undergraduate, he was involved with various organizations, but is most proud of helping Dr. Jose M. Hurtado start the UTEP Geology Club. His undergraduate research allowed him various opportunities to travel, including an internship in New York City where he studied meteors and their relationship to the origins our galaxy. Research at UTEP also took him north to Alaska as a field assistant and to present his research in San Jose, Costa Rica.

Hugo entered the University of Texas at El Paso's Master of Science program in geophysics in August of 2007 where he was able to succeed under the guidance of his advisor, Dr. Diane I. Doser. His studies focused on earthquakes in southeastern Alaska and completed all requirements in November of 2009. He is now in the oil and gas industry as an exploration geophysicist for SandRidge Energy, Inc in Oklahoma City.

Permanent address: 515 ½ NW 19th St.
Oklahoma City, OK 73103

This thesis was typed by Hugo Rodriguez